

Trace metals and REY in shells of *Mytilus edulis* as possible proxies for carbonate ion concentration in seawater

Bachelors Thesis

By

Jeroen Mesman



University of Applied Sciences Leiden

Chemistry, Analytical Chemistry

Supervisor:
Dr. Karsten Kaspers



Alfred-Wegener-Institut
Helmholtz-Zentrum Für Polar- und
Meeresforschung

Bremerhaven, Marine Biogeosciences

Supervisor:
Prof. Dr. Jelle Bijma

Bremerhaven, 14.09.2015 – 17.06.2016

Abbreviations

Contents

Abbreviations	5
Samenvatting	7
Abstract	9
1 – General Introduction	11
1.1 Ocean acidification	11
1.2 The carbonate chemistry	14
1.3 CO ₂ in the past	15
1.4 Reconstruction of the carbonate chemistry and the ocean pH using proxies	20
1.4.1 δ ¹¹ B for pH	20
1.4.2 B/Ca for Δ[CO ₃ ²⁻]	23
1.4.3 U/Ca for Δ[CO ₃ ²⁻]	25
1.4.4 REY for Δ[CO ₃ ²⁻]	25
1.4.5 Other proxies for the carbonate system	26
1.5 The bivalve <i>Mytilus edulis</i>	27
1.5.1 Samples	27
1.5.2 Shell structure	27
1.6 Analytical techniques	31
2 – Effect of bleaching on organic matrix of a <i>Mytilus edulis</i> shell	32
2.1 Introduction	32
2.2 Materials and methods	32
2.3 Results	35
2.4 Discussion	39
2.5 Conclusion	43
3 – Effects of bleaching times on a single size fraction	44
3.1 Introduction	44
3.2 Materials and methods	44
3.3 Results	46
3.4 Discussion	48
3.5 Conclusion	51
4 – Effects of size fractionation on a single bleaching method	52
4.1 Introduction	52
4.2 Materials and methods	52
4.3 Results	53

Abbreviations

4.4 Discussion..... 55

4.5 Conclusion..... 55

5 – Stability of dissolved samples and inter-/intra-variability between valves and bivalves 56

5.1 Introduction 56

5.2 Materials and methods..... 56

5.3 Results..... 58

5.4 Discussion..... 61

5.5 Conclusion..... 61

6 – Analysis of valves cultured at four different pCO₂ atmospheres 62

6.1 Introduction 62

6.2 Materials and methods..... 62

6.3 Results..... 64

6.4 Discussion..... 70

6.5 Conclusion..... 71

7 – Acknowledgements..... 72

8 – References..... 74

Appendix 1: exact concentrations of standards used for all experiments 82

Appendix 2: individual graphs showing change of Me/Ca ratios after 99 days of storage 86

Appendix 3: graphs for Me/Ca versus parameters of the carbonate system..... 90

Appendix 4: experimental conditions of salinity, temperature and pH over 1 year 94

Abbreviations

CCD – Carbonate Compensation Depth
C.I. – Confidence Interval
DIC – Dissolved Inorganic Carbon
EPF – Extrapallial Fluid
FAO – Food and Agriculture Organization of the United Nations
GLODAP – Global Ocean Data Analysis Project
(LA)-ICP-MS – (Laser Ablation) Inductively Coupled Plasma Mass Spectrometer
IPCC – Intergovernmental Panel on Climate Change
MQ – Milli-Q water
Me/Ca – Metal-calcium ratio.
NBS – Natural Bureau of Standards
NIST – National Institute of Standards and Technology
OA – Ocean Acidification
PETM – Paleocene-Eocene Thermal Maximum
REY – Rare Earth Yttrium elements
SD – Standard Deviation
TA – Total Alkalinity
TE – Trace Elements
THC – Thermohaline Circulation

Abbreviations

Samenvatting

De recente grote hoeveelheid CO₂ uitstoot heeft ervoor gezorgd dat de pH van de oceaan langzaam daalt. CO₂ reageert met water en vormt zo bicarbonaat-, carbonaat- en waterstof-ionen. Kleine veranderingen in de pH van de oceaan kan grote gevolgen veroorzaken voor het klimaat. Om de gevolgen voor het klimaat beter te kunnen begrijpen, kunnen zogenaamde proxies worden gebruikt om te kijken naar het verleden. Tijden in de geschiedenis van de aarde met een vergelijkbare, grote hoeveelheid CO₂ uitstoot kunnen dan gebruikt worden om voorspellingen te doen voor de toekomst. Om de chemie van het carbonaatsysteem in de oceaan uit te kunnen rekenen, moeten twee van de zes variabelen bekend zijn (DIC, TA, [CO₂], [HCO₃⁻], [CO₃²⁻] en [H⁺]). Het doel van de experimenten was om een proxy voor [CO₃²⁻] in zeewater te vinden. Eerst was er een schoonmaakmethode opgezet voor *Mytilus edulis* schelpen. Daarna waren monsters, gekweekt bij vier verschillende pCO₂ atmosferen (390, 1120, 2400, 4000 µatm) geanalyseerd met een ICP-MS. Sporelementen en zeldzame aardmetalen waren bepaald Calciumverhoudingen van de elementen werden uitgezet tegen verschillende parameters van het carbonaatsysteem om te kijken welke ratio het beste correleert met [CO₃²⁻]. Maar, zodra CO₂ reageert met water om het zuurder te maken, zorgt dit er ook voor dat alle andere parameters van het carbonaatsysteem ook verschuiven. Dit zorgt er dan voor dat een element vergelijkbare correlaties heeft met parameters van het carbonaatsysteem. Om beter te kunnen begrijpen hoe losse componenten van het carbonaatsysteem effect uitoefenen op elementen die in de schelp worden ingebouwd, moet er meer experimenten worden gedaan met een ontkoppelde carbonaatchemie.

Abstract

The recent large-scale anthropogenic CO₂ emissions has caused a steadily decreasing ocean pH. CO₂ reacts with water, forming bicarbonate-, carbonate- and hydrogen-ions. Small changes in pH can result in a major impact on the climate. To better understand exact changes on the climate, so-called proxies are being established to help understand the consequences of previous carbon perturbations. To calculate seawater chemistry, 2 out of 6 variables need to be known (DIC, TA, [CO₂], [HCO₃⁻], [CO₃²⁻] and [H⁺]). The goal of the experiments done was to find a proxy for [CO₃²⁻] in seawater. First, a cleaning method for *Mytilus edulis* shells was established. Then, samples cultured at four different pCO₂ atmospheres (390, 1120, 2400 and 4000 μatm) were analyzed for trace- and rare earth yttrium elements. Calcium-ratios of trace elements were plotted versus various parameters of the carbonate system to see which element correlates best to [CO₃²⁻]. When CO₂ reacts with water and lowers the pH, all parameters of the carbonate system change as well. This causes single elements to have similar correlations for all carbonate system parameters. However, to understand how single components of the carbonate chemistry interact with element incorporation into the shell, more work should be done with decoupled carbonate chemistry.

Abstract

1 – General Introduction

1.1 Ocean acidification

During the last 800 000 years the amount of carbon dioxide (CO₂) in the atmosphere has fluctuated between 180 and 260-280 ppm during glacial and interglacial periods ([Sigman and Boyle, 2000](#)). These values have been determined by the analyses of CO₂ in ice-cores. Since the industrial revolution (ca. 1800) there has been a massive increase in CO₂ emission resulting from human activity (anthropogenic). The main sources of CO₂ emissions are the burning of fossil fuels and deforestation ([Etheridge et al., 1996](#)). The average CO₂ concentration in the atmosphere has been steadily rising with no sign of stopping or slowing down. In 2015, the average amount of CO₂ in the atmosphere has breached the 400 ppm mark, figure 1. By the year 2100 the concentrations are expected to range between 550 ppm to 1000 ppm depending on the emission scenario used, (IPCC).

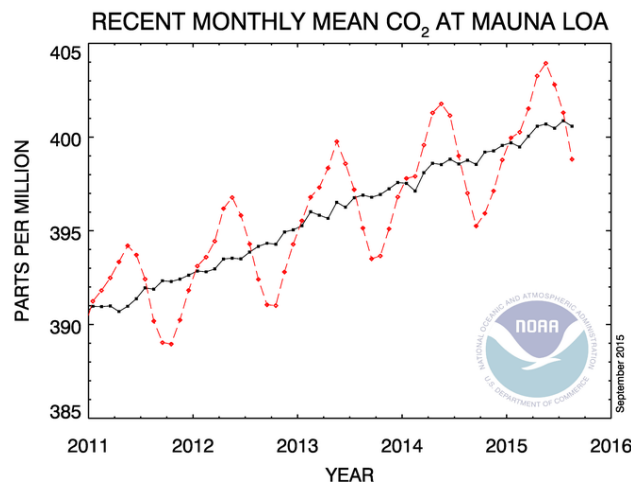
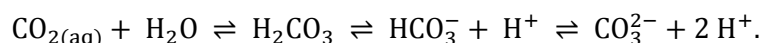


Figure 1 – Monthly mean CO₂ concentrations measured at the Mauna Loa Observatory (Hawaii), NOAA-ESRL ([Team, 2005](#)).

The variation in the red line in figure 1 is caused by seasonal cycles. In spring the vegetation of the northern hemisphere starts growing. By doing so it takes up enough CO₂ to decrease the concentration in the atmosphere by several ppm. After that, in fall, evergreens reduce their photosynthetic rate whilst deciduous plants and trees lose their foliage and photosynthesis comes to a complete halt. Hence, CO₂ uptake is much reduced and dead leaves and vegetation decay releasing CO₂ ([Bacastow et al., 1985](#)).

The recent rapid increase of CO₂ emissions has caused the Earth's global temperature to rise thereby melting ice-caps and warming oceans ([Hartmann et al., 2013](#)). Another, relatively recent discovered, effect of CO₂ is ocean acidification (OA, coined in 2001 by Broecker and Clark). OA is the term for the process involving a change in the carbonate system, releasing protons and hence decreasing ocean pH. This is caused by the uptake of CO₂ from the atmosphere by the ocean. For a while it was thought that the ocean was just a big carbon sink, storing excess CO₂ and slowing down the increase of CO₂ in the atmosphere. But unlike other gases in the atmosphere, CO₂ reacts with sea water making it more acidic (i.e. less alkaline). It is estimated that since the industrial revolution the pH of the oceans has been lowered by 0.1 units on the total pH scale, representing a 29 percent increase of acidity ([Mora et al., 2013](#)). The mechanism for the pH decrease by CO₂ is described below:



1 – General Introduction

The combined concentrations of $[\text{CO}_2]$, $[\text{HCO}_3^-]$ and $[\text{CO}_3^{2-}]$ form the total Dissolved Inorganic Carbon (DIC). True carbonic acid $[\text{H}_2\text{CO}_3]$ is also a part of the DIC however its concentration in seawater is negligible as it is almost completely dissociated. The DIC along with the total alkalinity (TA) and the temperature (T) form the key parameters determining the ocean pH. The TA is defined as the number of moles of hydrogen ion equivalent to the excess of proton acceptors (i.e. all negative ions and some neutral species such as NH_3 or H_3PO_4) over proton donors ([Wolf-Gladrow et al., 2007](#)). The TA in seawater slows down, or buffers, changes in ocean pH because of the different acid-base pairs. When the seawater is too basic, H_2CO_3 and HCO_3^- dissociate, releasing protons and decreasing the pH or vice versa, so the pH increases. The temperature influences the pH by controlling the amount of CO_2 that can be dissolved. Colder regions are able to take up more CO_2 than warmer regions. Figure 2 shows the effect of temperature on the solubility of CO_2 . A small difference in temperature can have a large effect on the amount of CO_2 that can be dissolved. This effect can also be seen in figure 3A and B. The pH of colder ocean surface waters has changed relatively more than warmer surface waters. (Figure 3B: no data is available for the arctic and the reduced decrease at the Antarctic is most likely due to shelf ice which prevents CO_2 from the atmosphere reaching the ocean). As a consequence, warmer regions tend to have higher $[\text{CO}_3^{2-}]$ and are more saturated with respect to carbonate minerals ([Zeebe, 2012](#)).

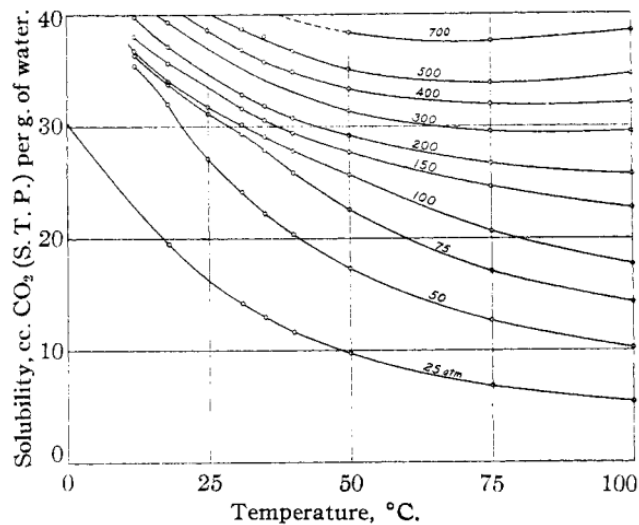


Figure 2 – Solubility of CO_2 at different pressures (atm) in water as a function of the water temperature ($^{\circ}\text{C}$) ([Wiebe and Gaddy, 1940](#)).

1 – General Introduction

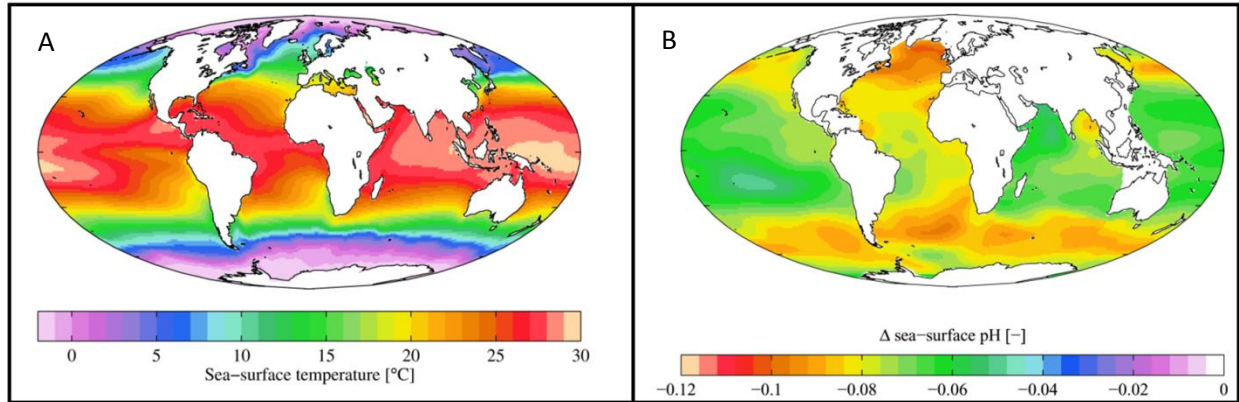


Figure 3 – A) Annual mean sea surface temperature from the World Ocean Atlas 2009 (Locarnini et al., 2010). B) Estimated change in sea water pH caused by human created CO₂ between the 1700s and 1990s, from the Global Ocean Data Analysis Project (GLODAP) (Key et al., 2004) and the World Ocean Atlas (Antonov et al., 2010; Locarnini et al., 2010).

Because the pH scale is logarithmic, even minor changes can have great impacts on ocean life. Especially in combination with overfishing and pollution, a great loss of biodiversity can be expected. An acidified ocean will intensify bleaching in corals and can reduce growth in other calcifying organisms. But these are just some of the known/better understood consequences. A lower pH also has adverse effects on the physiology of organisms and even ecosystems (Bijma et al., 2013; Ries et al., 2009). However, until these issues are better understood it is difficult to make predictions about the impacts on our future. Besides the direct effects on marine life, an acidified ocean is likely to have adverse effects on society. According to an estimate by the FAO in 2007, fish supplies over 20 percent of proteins to about 2.6 billion people. So a loss of biodiversity and changing of migration routes of organisms can have major impacts on cities/villages that are mostly dependent on services from the ocean such as e.g. fishing. So it is clear that more research needs to be done on ocean acidification, its effects and methods of prevention.

At this moment the global average pH of the surface ocean is about 8.1, it varies about 0.3 pH units because of local, regional and seasonal variations. This means that relative DIC concentrations for [CO₂], [HCO₃⁻] and [CO₃²⁻] are <1%, ≈90% and ≈9%, respectively. When pH decreases – i.e. when the ocean gets more acidic – the amount of dissolved [CO₂] and [HCO₃⁻] increase while [CO₃²⁻] decreases. This is illustrated in a Bjerrum plot, figure 4. When more CO₂ dissolves in the ocean, thus shifting the pH to the left of the plot, the equilibrium ratios of the carbonate chemistry are also shifted. As shown in figure 4 minor changes of pH mostly affect [CO₃²⁻], this is also demonstrated in table 1.

1 – General Introduction

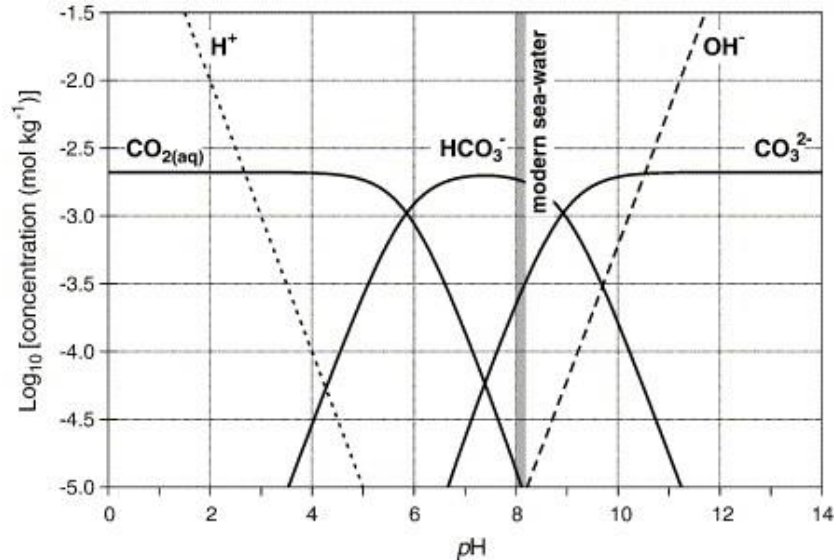


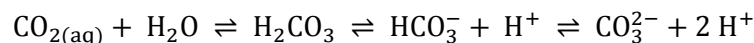
Figure 4 – Bjerrum plot showing the DIC concentration's dependence on the pH (Ridgwell and Zeebe, 2005).

Table 1 – Relative concentrations of DIC in the ocean for the past and the future.

pH	Relative DIC concentrations		
	[CO ₂]	[HCO ₃ ⁻]	[CO ₃ ²⁻]
8.2 (pre-industrial)	<1 %	≈90 %	≈9 %
7.9 (predicted for the year 2050, 560 ppm CO ₂) (Orr et al., 2005)	<2 %	≈92 %	≈5 %

1.2 The carbonate chemistry

As described above, when CO₂ dissolves in water it can react with water forming bicarbonate and carbonate ions:



Two different dissociation constants belong to this reaction:

$$K_1 = \frac{[\text{HCO}_3^-][\text{H}^+]}{[\text{CO}_2]} \quad K_2 = \frac{[\text{CO}_3^{2-}][\text{H}^+]}{[\text{HCO}_3^-]}$$

As stated before: TA is defined as the number of moles of hydrogen ion equivalent to the excess of proton acceptors. In seawater it is usually described as (Zeebe, 2012):

$$\text{TA} = [\text{HCO}_3^-] + 2 [\text{CO}_3^{2-}] + [\text{B}(\text{OH})_4^-] + [\text{OH}^-] - [\text{H}^+] + \text{minor compounds}$$

The carbonate system can be described by six variables: DIC, TA, [CO₂], [HCO₃⁻], [CO₃²⁻] and [H⁺]. This means there are four equations to describe the carbonate system: for the DIC, TA and the two dissociation constants. If two of these parameters are known, the carbonate system can be solved. The calcite saturation state (Ω) describes whether the calcite dissolves or forms in water. With a value above 1, calcite is not readily dissolved and below 1, calcite will completely dissolve if the production rate is lower than the dissolution rate. In the ocean a boundary at certain depths can form where the saturation state is 1.

1 – General Introduction

This boundary is called the lysocline or saturation horizon and is a result of the *in situ* $[\text{CO}_3^{2-}]$, depth (pressure) and temperature, $[\text{Ca}]$ is conservative and equal to ca. 10 mmol/kg throughout the world oceans). Above the lysocline the ocean is supersaturated with respect to calcite or aragonite and below it, it is under saturated. However this does not mean no calcite or aragonite exists below their respective lysocline (which has a higher elevation for aragonite – it is less stable). If the precipitation rate of calcifying organisms exceeds that of the dissolution rate then CaCO_3 can still be formed. The point where the settling rate is exceeded by the dissolution rate, thus the mineral completely dissolves, is called the carbonate compensation depth (CCD) ([Thurman and Trujillo, 2004](#)). The saturation state can be calculated by:

$$\Omega_c = \frac{[\text{Ca}^{2+}][\text{CO}_3^{2-}]}{K_{sp}}$$

Where Ω_c is the saturation state; $[\text{Ca}^{2+}]$ and $[\text{CO}_3^{2-}]$ are the *in situ* concentrations of the ions in seawater and K_{sp} is the solubility constant of calcite or aragonite ([Zeebe et al., 2001](#)). Now an example from [Zeebe \(2012\)](#) shows how the carbonate system affects the saturation state and why it is important to know the value of two parameters to describe the carbonate system. (TCO_2 is the same as DIC). “For instance, future atmospheric CO_2 concentrations have been compared with pCO_2 levels during the Cretaceous (~145 to ~65 Mya), which may have been as high as 2 000 parts per million by volume (ppmv). Although at some point in the future, atmospheric CO_2 levels might approach values similar to those during the Cretaceous, this by no means implies similar surface-ocean chemistry. A surface ocean with $\text{TCO}_2 = 2.4 \text{ mmol kg}^{-1}$ in equilibrium with an atmosphere at $\text{pCO}_2 = 2\,000 \text{ ppmv}$ would have a calcite saturation state (Ω_c) of 1.1 [$T_c = 15^\circ\text{C}$ (T_c denotes temperature in $^\circ\text{C}$), $S = 35$]. However, at a higher TCO_2 value of 4.9 mmol kg^{-1} , the calcite saturation state Ω_c would be 4.5 (same T_c and S).”

1.3 CO_2 in the past

CO_2 concentrations measured in ice-cores from the last 800 000 years have varied between 180 and 260-280 ppm during glacial and interglacials, respectively (figure 5). Although the cause for this cyclic variation and the reasons for the upper and lower limits are not known, a lot of processes have been proposed. Suggestions include ([Fischer et al., 2015](#)):

- Southern Ocean ventilation by wind or buoyancy feedbacks
- Iron fertilization of the marine biosphere in the Southern Ocean
- Changes in the re-mineralization depth of organic carbon
- Release of permafrost carbon during the deglaciation
- Decreased solubility due to ocean warming
- Changes in air/sea gas exchange due to changing sea ice cover
- Marine carbonate feedbacks

1 – General Introduction

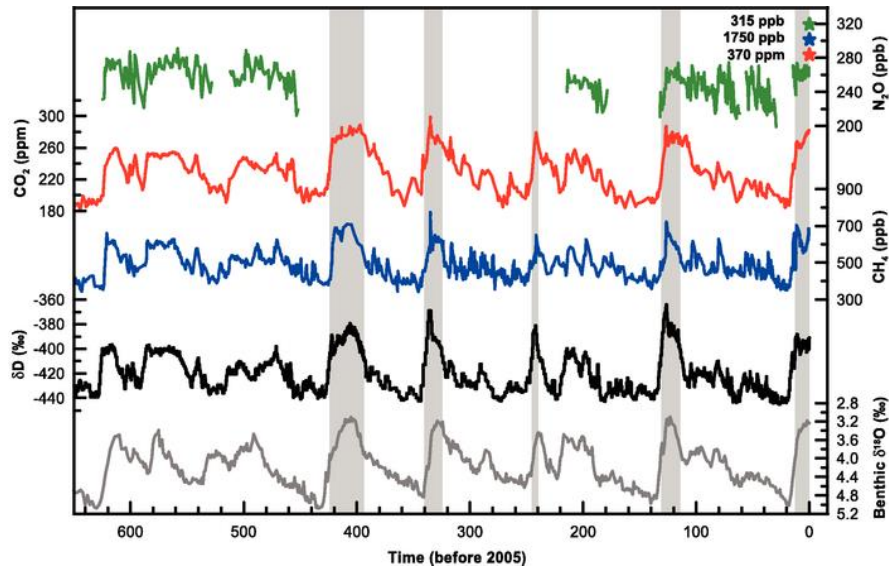


Figure 5 –The variation of some greenhouse gasses over the last 650 ka, Green: N₂O, Red: CO₂ and blue: CH₄. The black and grey lines show the variation in isotopic composition (ratios) of Hydrogen (deuterium, D) and oxygen (¹⁸O) respectively. These ratios can be measured in ice-cores and be used to determine temperature or ice-sheet coverage (can be used as a proxy). All the lines show a similar pattern caused by glacial-interglacial periods. Interglacial, relatively warmer periods, are marked by grey vertical lines. The top right corner shows the atmospheric conditions in 2007 ([Solomon et al., 2007](#)).

But according to [Berner and Kothavala \(2001\)](#); [Bergman et al. \(2004\)](#) and [Rothman \(2002\)](#) CO₂ concentrations have been a lot higher in Earth's history, figure 6. Exceeding 700 ppm during the Paleocene-Eocene Thermal maximum (PETM, 56 Ma) and 4 000 ppm during the Ordovician-Silurian (447 – 443 Ma). The best analogue to today's rapid change in ocean chemistry is probably the PETM. It started with an increase of global surface temperature by 5 – 9 °C over a period of a few thousand years ([Kennett and Stott, 1991](#)). Bottom water temperatures also increased, leading to a destabilization of so called methane hydrates (clathrates) and the release of large amounts of methane. As methane oxidizes very quickly (atmospheric residence time of ca. 12 years), this is equivalent to the release of a large amount of carbondioxide to the ocean-atmosphere system causing a drop in the ¹³C/¹²C ratios. This release led to ocean acidification which subsequently dissolved deep-sea carbonates ([Zachos et al., 2005](#); [Zeebe et al., 2009](#)). However, it is not known what started this chain reaction of global warming.

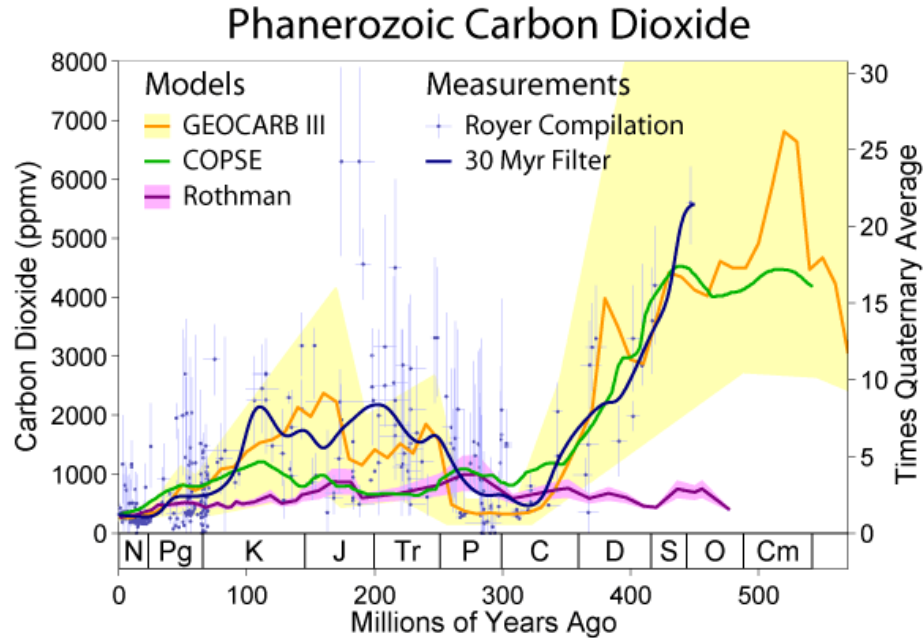


Figure 6 – Estimates of the changes in atmospheric carbon dioxide concentrations during the Phanerozoic. Three estimates are based on geochemical modeling: GEOCARB III (Berner and Kothavala, 2001), COPSE (Bergman et al., 2004; Rothman, 2002). These are compared to the carbon dioxide measurement database of Royer et al. (2004) and a 30 Myr filtered average of those data. Error envelopes are shown when they were available. The right hand scale shows the ratio of these measurements to the estimated average for the last several million years (the Quaternary). Customary labels for the periods of geologic time appear at the bottom. Image and text from Rohde, 2005. N: Neogene; Pg: Paleogene; K: Cretaceous; J: Jurassic; Tr: Triassic; P: Permian; C: Carboniferous; D: Devonian; S: Silurian; O: Ordovician and Cm: Cambrian.

In contrast to other ocean acidification events, the PETM happened over a relatively short timescale and it is also related to a fast and massive input of carbon. So by studying the past it may be possible to gain insights into the geochemical consequences, rates and timescales of change and to make predictions about our future (although it should be noted that during the PETM the climate, ocean chemistry and timescale were different than today's). Figure 7A shows the difference in timescale of the carbon perturbation. During all of the ocean acidification events, the ocean and marine life had more time to adapt/react to changing a changing environment. Rocks and minerals have a longer time to react/dissolve and counteract/buffer the lowering of the pH. Because today the change in ocean chemistry is so fast now, there may not be enough time for the environment to adapt. This can be seen in Figure 7B. The huge amount of carbon and rapid input results in a significant drop in the calcite saturation state (Ω_c). When compared to the still large but slower carbon input during the PETM it can be seen that the ocean had more time to counteract and mitigate a drop in saturation state.

The atmospheric CO₂ concentration is effectively controlled by the ocean carbon reservoir, over a time scale of millennia (Broecker, 1982). It has by far the largest carbon reservoir apart from (much less dynamic) sedimentary rocks and is an essential component of the long-term stabilization of atmospheric CO₂ (figure 8). It does so by controlling a dynamic balance of carbon in the atmosphere and ocean, this is the marine carbon cycle. This cycle is again split into a solubility pump and biological pump. Together they maintain a downward gradient of increasing DIC concentrations, keeping the surface ocean relative to the deep ocean, depleted in DIC (Gehlen et al., 2011). The solubility pump transports CO₂ downwards and along with the large-scale ocean circulation (also known as the conveyor belt or thermohaline circulation (THC), a global current caused by differences in density). CO₂ dissolves more readily under higher pressure and lower temperature, both characteristics of the deep ocean. This increased CO₂ in the bottom waters

1 – General Introduction

subsequently increase DIC concentrations. The biological pump consists of two parts, the carbonate pump and the soft tissue pump.

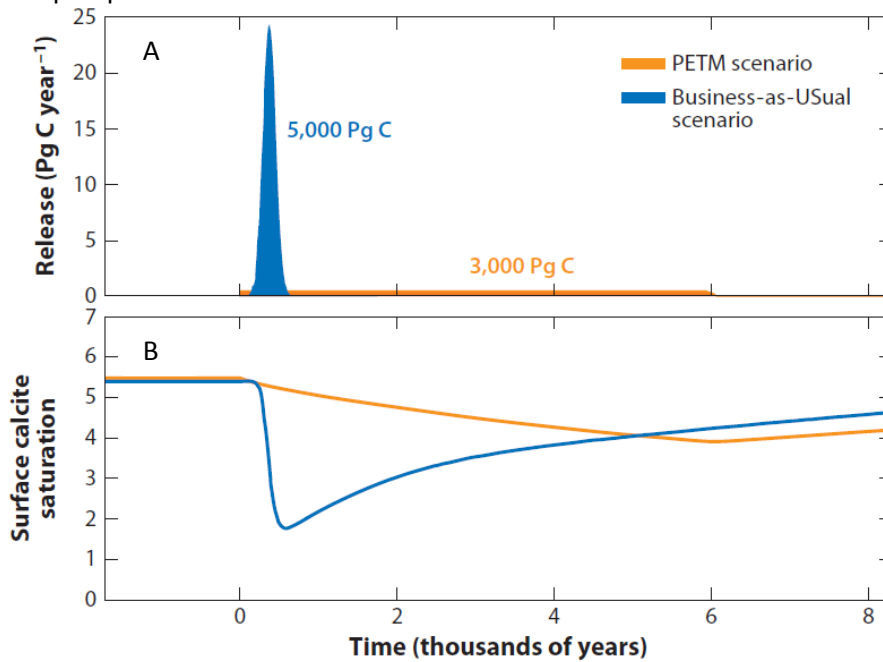


Figure 7 – A) The difference in timescale of the carbon perturbation of the present to the future (≈ 500 years) versus the perturbation from the PETM. B) This shows the expected change in the calcite saturation state for the future versus the change that happened during the PETM (Zeebe, 2012).

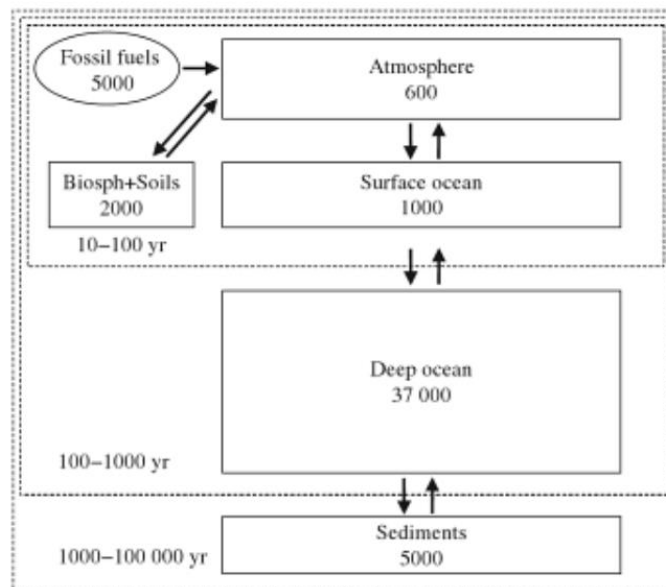
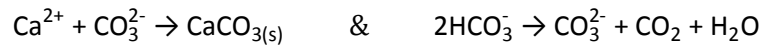


Figure 8 – The carbon cycle with approximate sizes of the reservoirs in Pg C ($1 \text{ Pg} = 10^{15} \text{ g}$). The dashed boxes indicate exchanges between reservoirs and their corresponding time scales (Gehlen et al., 2011).

1 – General Introduction

The carbonate pump has three main processes that affect the carbon cycle and operates counter intuitively in that carbonate precipitation produces CO₂. When CaCO₃ precipitates it reduces total alkalinity more than DIC (ratio of 2 to 1), causing an increase of dissolved CO₂ in near surface waters. This in turn equilibrates with the atmosphere and raises pCO₂. Ca²⁺ reacts with CO₃²⁻ to form CaCO₃. This removes carbonate ions from the water resulting in shift in relative DIC concentrations. To compensate for lost CO₃²⁻, bicarbonate ions (HCO₃⁻) dissociate to replenish CO₃²⁻ while also forming CO₂ (Gehlen et al., 2011). The reactions for this process are shown here:



Secondly there is the dissolution of CaCO₃ which affects the carbon content of the ocean. Dissolution rate/depth is simply a result of the saturation state of the ambient water. Saturation state in turn is governed by temperature, pressure, depth and biological activity. Lastly there is the response of carbonate sediment to changing ocean conditions. When the pH of the ocean changes too much, sediment dissolves and resupplies lost carbonate ions. This process provides a perfect buffer against ocean acidification. However the dissolution rate and the time it takes for CO₂ to interact with CO₃²⁻ are very slow and on the order of thousands of years.

The soft-tissue pump consists of carbon being cycled in the ocean through organic matter from phytoplankton. Particles either, stay in the surface waters and continue being recycled or they slowly sink down, forming larger aggregates. These pumps effectively control the atmospheric pCO₂ and carbon cycling throughout the ocean. An overview of the pumps can be found in figure 9.

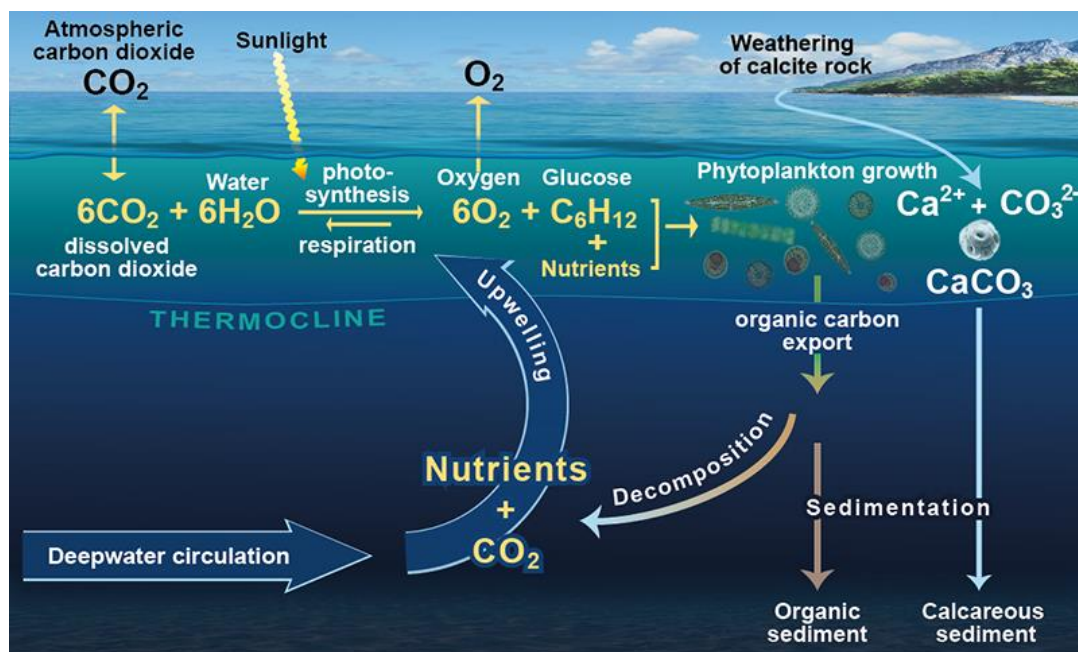


Figure 9 – Overview of the biological pump showing the carbonate and soft-tissue pump

Collapse or halting of the biological pump by a major perturbation such as a mass extinction can result in a “Strangelove ocean” (Birch et al., 2016). Collapse of the pump leads to increased DIC concentrations in surface waters. This carbon is subsequently outgassed and contributes greatly to global atmospheric pCO₂ concentrations (Rampino and Caldeira, 2005). This in turn amplifies global warming and ocean acidification.

1.4 Reconstruction of the carbonate chemistry and the ocean pH using proxies

1.4.1 $\delta^{11}\text{B}$ for pH

To help predict the effects of a lower pH and different carbonate chemistry it can be very useful to look into the past. However since the pH in the past can't be measured directly anymore, a so-called 'proxy' is used. Climate proxies are natural recorders of climate variability such as ice-cores, tree-rings, ocean sediments or carbonate from calcifying organisms. These recorders slowly accumulate/grow over time. And while growing they incorporate different amounts of elements or isotopes which are controlled by the ambient environment. The $\delta^{18}\text{O}$ in water for example (ratio of oxygen isotopes) is dependent on the $\delta^{18}\text{O}$ of the water and its temperature. By measuring the $\delta^{18}\text{O}$ in corals, a calcifying organism, and knowing the $\delta^{18}\text{O}$ of the water in which it grew, the temperature can be calculated.

To determine the pH of the ocean in past times, the isotopic composition of boron in a calcifying organism can be used. In seawater boron exists mainly in two forms: boric acid, $\text{B}(\text{OH})_3$ and borate, $\text{B}(\text{OH})_4^-$. These two molecules are in equilibrium with each other:



In figure 10A (Rae et al., 2011) can be seen that the equilibrium changes with pH, at a lower pH boric acid is the more dominant species. Because of different vibrational energy's and molecular geometry, ^{10}B is preferentially fractionated into borate and ^{11}B into boric acid, figure 10B. The fractionation between the two species is constant and independent of pH. This causes borate ($\text{B}(\text{OH})_4^-$) to be 27.2‰ more depleted in ^{11}B than boric acid. The reaction for this fractionation can be seen below:

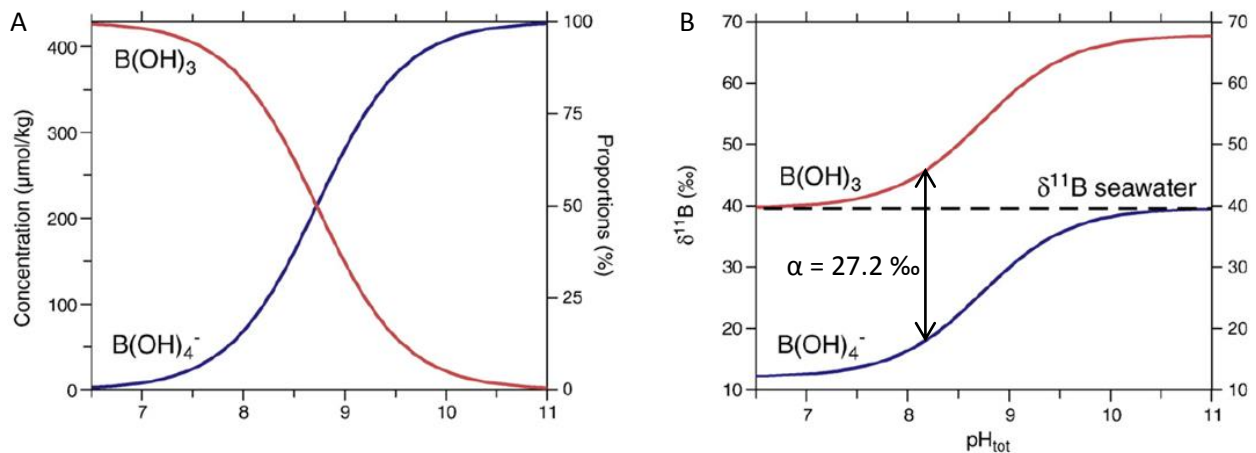
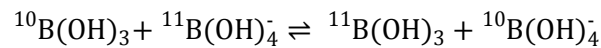


Figure 10 – These graphs were made with typical deep ocean conditions: $T = 2^\circ\text{C}$, $S = 34.7$ and $P = 3000$ dbar resulting in a $pK_B^* \approx 8.7$. And with $\alpha_{\text{B}(\text{OH})_3-\text{B}(\text{OH})_4^-} = 1.0272$, $\delta^{11}\text{B}$ of seawater = 39.61‰ (Foster et al., 2010) and $B_T = 432.6 \times (S/35)$ μmol/kg (Lee et al., 2010). The graphs show the varying concentrations and isotopic compositions of boric acid and borate as a function of the pH. Image modified from Rae et al. (2011).

1 – General Introduction

Because the partitioning of the two species is pH dependent, a lower pH will result in more of the relative heavier boric acid in water. By analyzing modern marine calcifiers, ([Hemming and Hanson, 1992](#)) concluded that only the charged boron species is included into the carbonate shells or skeletons. For example, when *Amphistegina lessonii* (a benthic foraminifer, figure 11) calcifies, it incorporates trace amounts of boron from the surrounding seawater in the form of borate ([Kaczmarek et al., 2015a](#)).

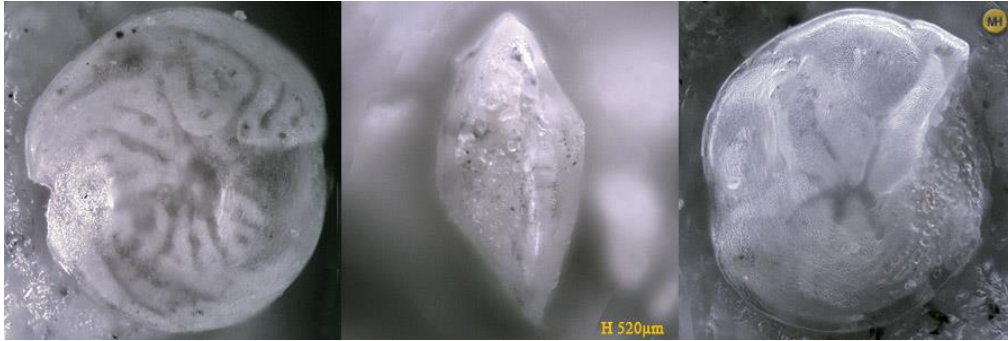
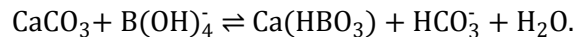


Figure 11 – View of a specimen of *Amphistegina lessonii* ([Hesemann, 2016a](#)).

It is still a matter of debate, whether also a small fraction of the boron included into the crystal lattice may be due to boric acid ([Klochko et al., 2009](#)). [Noireaux et al. \(2015\)](#) recently suggested this is only true for aragonite, incorporation into calcite is more complex. [Hemming and Hanson \(1992\)](#) proposed the following mechanism for the addition of boron into the carbonate



This results in a carbonate structure that has logged the isotopic composition for borate of the ambient seawater (thus the pH). Hence, under equilibrium conditions, the incorporated $\delta^{11}\text{B}$ should follow the same trend as the $\delta^{11}\text{B}$ of the seawater. However, calibration studies have demonstrated that this is not always the case as can be seen in figure 12. The $\delta^{11}\text{B}$ from the corals and foraminifera are offset from the $\delta^{11}\text{B}$ of seawater. This is due to so called “vital effects” of the organisms. In short, this means that the organisms alter the pH of their micro-environment by photosynthesis, respiration and calcification. This changes the concentration and the isotopic of the boron species causing an offset in $\delta^{11}\text{B}$ from that of the bulk seawater. These vital effects also explain why a proxy is species-specific and cannot be directly used on other species.

1 – General Introduction

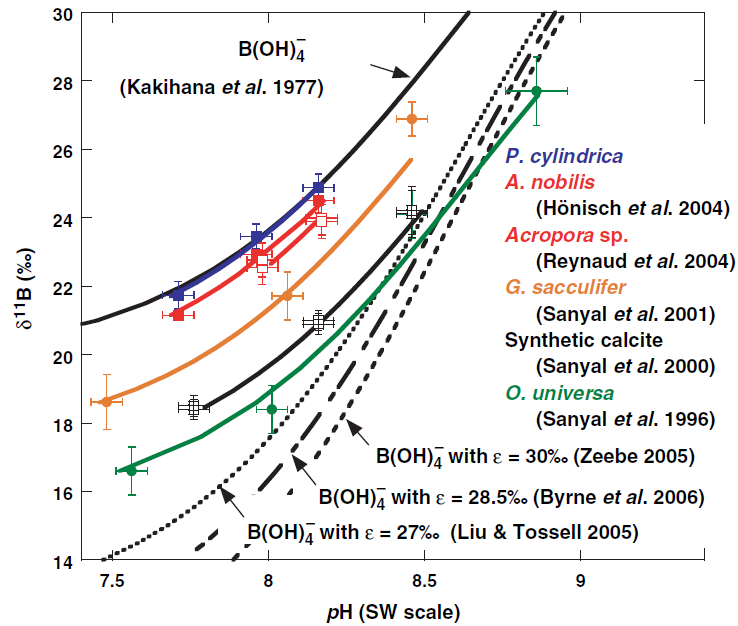


Figure 12 – This graph shows the relationship between $\delta^{11}\text{B}$ and the pH of seawater. The red and purple lines represent $\delta^{11}\text{B}$ in three coral species; the orange and green lines are foraminifera. The upper solid black, dotted and dashed black line are the $\delta^{11}\text{B}$ of $\text{B}(\text{OH})_4^-$ using for $\alpha_{\text{B}(\text{OH})_3-\text{B}(\text{OH})_4^-}$: 1.019, 1.027 and 1.030 ((Kakihana and Kotaka, 1977; Liu and Tossell, 2005; Zeebe, 2005). The dot-dashed line has an experimentally determined $\alpha_{\text{B}(\text{OH})_3-\text{B}(\text{OH})_4^-}$ of 1.0285 (Byrne et al., 2006). As can be seen the $\delta^{11}\text{B}$ of the organisms are offset from the seawater $\delta^{11}\text{B}$. (Zeebe et al., 2008).

To calculate the isotopic composition of a sample, the equation below can be used

$$\delta^{11}\text{B}(\text{‰}) = \left[\left(\frac{{}^{11}\text{B}/{}^{10}\text{B}_{\text{sample}}}{{}^{11}\text{B}/{}^{10}\text{B}_{\text{NIST951}}} \right) - 1 \right] \times 1000.$$

In this formula the ratio of the isotopic concentration of a sample is divided by that of a standard and converted to permil (‰). The isotopic composition of a sample is expressed relative to a standard (NIST951, boric acid isotopic standard). A standard is used, because mass spectrometers are very good in determining the relative differences in isotopic compositions but cannot measure the absolute ratio of the heavy versus the light isotope. In addition, different measurements and or different laboratories can be compared by looking at the relative shifts from a standard with a certified composition. Both borate and boric acid are shifted positively from - are heavier than - the standard. When pH increases so does the $\delta^{11}\text{B}$ of borate and therefore the $\delta^{11}\text{B}$ of the carbonate. Figure 12 also shows how the $\delta^{11}\text{B}$ shifts when the pH changes. Boron isotopes are now routinely used to reconstruct sea water pH (Foster, 2008; Hönisch et al., 2008; Rae et al., 2011; Raitzsch and Honisch, 2013). However, to fully reconstruct the carbonate chemistry, a second, independent, proxy is required.

1.4.2 B/Ca for $\Delta[\text{CO}_3^{2-}]$

Numerous studies have been carried out to try to reconstruct past $[\text{CO}_3^{2-}]$ using for example: foraminiferal shell weight, dissolution rates, shell formation rates and boron isotopes. However many studies have conflicting results and each proxy has its disadvantages due to other (specific) interfering parameters (e.g. S, T, pH, P and vital effects). Concentrations of past carbonate ions remain uncertain ([Brown et al., 2011](#); [Yu and Elderfield, 2007](#)). This is why it is necessary to try to develop new proxies for different species. New proxies may help resolve conflicting results and eventually lead to a more accurate estimation of $[\text{CO}_3^{2-}]$ in the past. When the $[\text{CO}_3^{2-}]$ is known for the past, it can be combined with a proxy for the pH to reconstruct the entire carbonate chemistry of the ocean. Since only two parameters are necessary to calculate the other four: DIC, TA, $[\text{CO}_2]$ and $[\text{HCO}_3^-]$.

B/Ca in benthic foraminifers (bottom-dwellers) as well as in the bivalve *Mytilus californianus* have been shown to reflect the $\Delta[\text{CO}_3^{2-}]$ of the ocean, figure 13A ([Hönisch et al., 2008](#); [McCoy et al., 2011](#); [Rae et al., 2011](#); [Raitzsch et al., 2011a](#); [Yu and Elderfield, 2007](#)). $\Delta[\text{CO}_3^{2-}]$ is not the same as $[\text{CO}_3^{2-}]$ but it can be calculated from it. $\Delta[\text{CO}_3^{2-}]$ is the difference between $[\text{CO}_3^{2-}]_{\text{in situ}}$ and $[\text{CO}_3^{2-}]_{\text{at saturation}}$. This relationship can be seen in Figure 13B and in the equation below.

$$\Delta[\text{CO}_3^{2-}] = [\text{CO}_3^{2-}]_{\text{in situ}} - [\text{CO}_3^{2-}]_{\text{sat}}$$

So with regard to paleoceanography, a proxy can be used to define $\Delta[\text{CO}_3^{2-}]$ and $[\text{CO}_3^{2-}]_{\text{sat}}$ can be modelled when the relevant parameters are known (e.g. pH, T, P and S). Which means $[\text{CO}_3^{2-}]_{\text{in situ}}$ can be calculated.

$$[\text{CO}_3^{2-}]_{\text{in situ}} = [\text{CO}_3^{2-}]_{\text{sat}} + \Delta[\text{CO}_3^{2-}]$$

However, for planktonic foraminifers (sub-surface species) this relationship seems to be more complicated. This may be due to pH, salinity ([Foster, 2008](#); [Henehan et al., 2015](#)) or temperature effects on the incorporation of borate ([Allen and Hönisch, 2012](#); [Hönisch et al., 2008](#)). Although B/Ca of benthic species are also affected by this, the effect is much less pronounced. This is likely due to the fact that the conditions at the bottom of the ocean are more stable than that of the surface waters.

In natural ocean water the different parameters of the carbonate chemistry are not independent. For instance when pH goes up, $[\text{CO}_3^{2-}]$ goes up as well. To decipher the controls of the various proxies requires to decouple the carbonate chemistry. This was done before to investigate the impact of the carbonate chemistry on $\delta^{18}\text{O}$ and $\delta^{13}\text{C}$ ([Bijma et al., 1999](#); [Spero et al., 1997](#)). Very recently this was also done by [Kaczmarek et al. \(2015b\)](#) and [Howes et al. \(2016\)](#). In the study by [Kaczmarek et al. \(2015\)](#) benthic foraminifers have been grown under a decoupled carbonate chemistry. This allows either pH or $[\text{CO}_3^{2-}]$ to be changed while keeping the other constant. For example, when nitrogen is bubbled through the water, CO_2 is being removed from the solution which causes the pH to shift. The Bjerrum plot, figure 4, shows that a changing pH also changes DIC concentrations, so the relative concentrations change. Then a strong base is added to return the pH to its original value. The result is water with the same pH but lower $[\text{CO}_3^{2-}]$. [Howes et al. \(2016\)](#) did a similar study with the planktonic foraminifer *Orbulina universa*. Both studies concluded that B/Ca of the foraminifer shells had a positive correlation with $\text{B}(\text{OH})_4^-/\text{HCO}_3^-$, suggesting a competition between the two ions for incorporation into the lattice.

1 – General Introduction

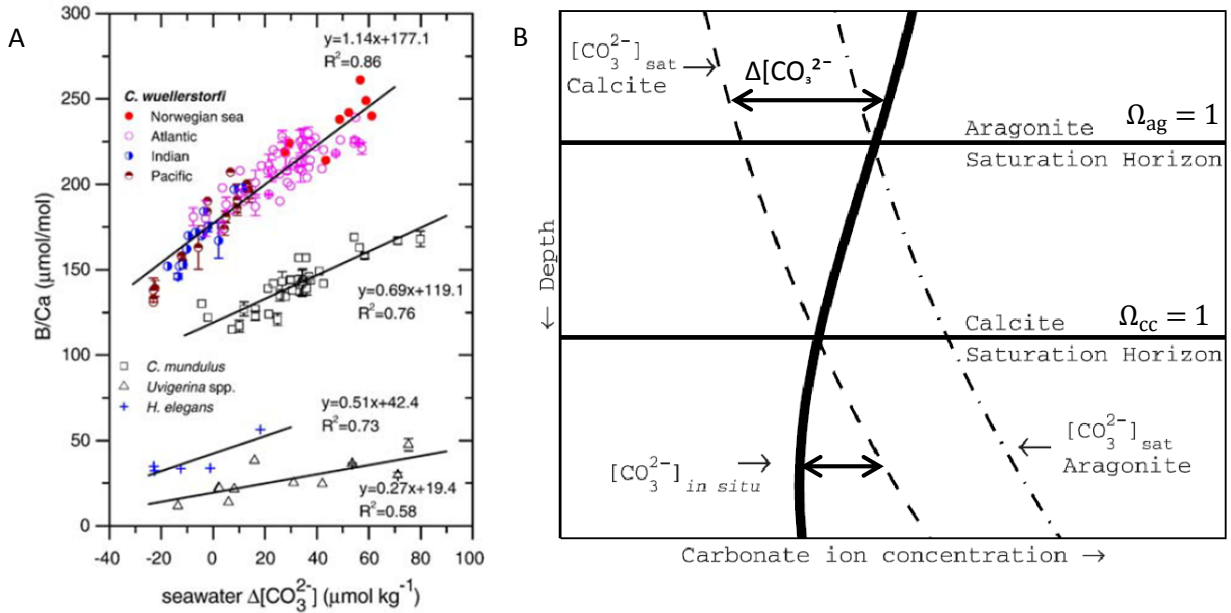


Figure 13 – A) Bottom water $\Delta[\text{CO}_3^{2-}]$ vs. B/Ca ratios in four different benthic species found in Holocene (present) sediments over the world. This graph shows the correlation of *C. mundulus*, *Uvigerina spp.*, *H. elegans* and four different locations for *C. wuellerstorfi* (Yu and Elderfield, 2007). B) When pressure increases, so does the solubility of calcite and aragonite. The point where the carbonate ion concentration is in equilibrium with the carbonate of calcite or aragonite is the saturation horizon. Below this horizon the respective mineral starts dissolving (lysocline). Note that aragonite dissolves more readily than calcite. $\Delta[\text{CO}_3^{2-}]$ is also shown by the two arrows. Image is modified from Zeebe and Westbroek (2003).

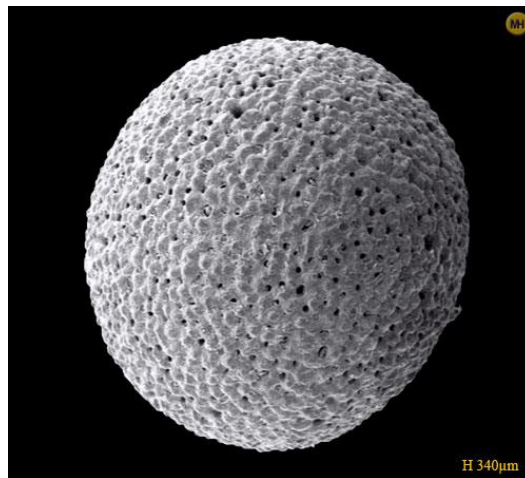


Figure 14 – View of a specimen of *Orbulina universa* (Hesemann, 2016b).

1.4.3 U/Ca for $\Delta[\text{CO}_3^{2-}]$

The U/Ca proxy for $\Delta[\text{CO}_3^{2-}]$ is relatively new and has not yet been well studied. It is assumed that uranium is incorporated in the form of $\text{UO}_2(\text{CO}_3)_3^{4-}$. The concentration of this ion in seawater decreases as pH rises and the incorporation onto test surfaces is slowed by $[\text{CO}_3^{2-}]$, Figure 15 (Levin et al., 2015). Although U/Ca is correlated to $[\text{CO}_3^{2-}]$ in both benthic and planktonic foraminifera (Raitzsch et al., 2011b; Russell et al., 2004), Yu et al. (2008) and Gussone et al. (2010) showed that temperature affects the correlation and it is potentially the dominant control of U/Ca for some coral species (Felis et al., 2009). It is also prone to partial dissolution in corrosive bottom waters and it changes over time limiting its use as a paleoproxy (Broecker, 1963; Kaufmann et al., 1971; Yu et al., 2008). Keul et al. (2013) experimentally decoupled the carbonate chemistry, they varied the pH and $[\text{CO}_3^{2-}]$ both independently and simultaneously. The conclusion for the foraminifer *Ammonia sp.* was that B/Ca is, in fact, correlated to $[\text{CO}_3^{2-}]$ and has a strong potential for use as a proxy.

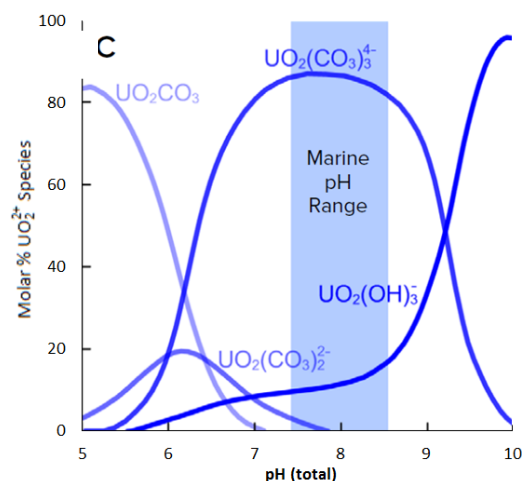


Figure 15 – The relative amounts of uranium species in seawater are affected by the pH. The presumably incorporated $\text{UO}_2(\text{CO}_3)_3^{4-}$ increases in concentration when water gets more acidic (Levin et al., 2015).

1.4.4 REY for $\Delta[\text{CO}_3^{2-}]$

The inorganic behaviour of REY is controlled by carbonate complexation (e.g. Cantrell and Byrne (1987 1987)). Depending on pH Lanthanides (Ln) exist as free ions, as a mono- or as a di-carbonate complex. Two equilibrium constants control the relative concentrations of each of the species. At a pH below pK_1 (i.e. the log value of the first equilibrium constant), the dominant form is the free lanthanide ion (Ln^{3+}). Between pK_1 and pK_2 the dominant species is a carbonate complex (LnCO_3^+). Above pK_2 the dominant species is a dicarbonate complex ($\text{Ln}(\text{CO}_3)_2^-$). The pK_1 values are below ca. 7.4 and below normal sea water pH values. The pK_2 values cover a smoothly declining range between pH 8.47 for La to pH 7.42 for Lu. This makes REY-carbonate speciation very sensitive to small variations in seawater carbonate ion concentration (Byrne, 2002).

Organic complexation of REY complicates a straight forward interpretation of free Ln^{3+} available for biomineralisation. However, at the end the seawater carbonate remains the primary control of dissolved REE as with decreasing pH (and $[\text{CO}_3^{2-}]$) and increasing $[\text{H}^+]$ both the organic and inorganic speciation result in a greater proportion of free Ln^{3+} . A study of REY in *Mytilus edulis* has already been done by Ponnurangam et al. (2015). Speciation had been modelled there, and they confirmed the correlation of REY incorporated into the carbonate of shells.

1.4.5 Other proxies for the carbonate system

It is thought that Li/Ca ratio represents the saturation state which is linked to growth rate ([Bryan and Marchitto, 2008](#); [Hall and Chan, 2004](#)). However an effect of temperature and salinity has also been noticed ([Marriott et al., 2004](#)). Sr/Ca has been proven for some marine calcifiers including the aragonite of corals has been shown to reflect temperature of the seawater ([de Villiers et al., 1994](#); [Weber, 1973](#)). Mg/Ca has, like strontium, also been identified as a proxy for seawater temperature. Incorporation of Mg requires energy, therefore, Mg/Ca ratio is directly correlated to an increase of temperature in seawater ([de Villiers et al., 1994](#)). The Ba/Ca in corals has been shown to reflect the Ba/Ca of seawater, which in turns is related to the nutrient Si ([LaVigne et al., 2011](#)). So it is expected that lithium would decrease with pH/saturation state and Mg, Sr and Ba to stay constant over the different pH ranges.

1.5 The bivalve *Mytilus edulis*

1.5.1 Samples

The focus of this research is on the bivalve *Mytilus edulis* also known as the common/blue mussel (in this paper both terms are used interchangeably). For this research, empty shells of juvenile *M. edulis*, cultured under controlled conditions were supplied. They had been grown under varying CO₂ atmospheres, resulting in a different pH and different DIC concentrations. The next paragraph will, in short, explain the culturing setup. For more details about the setup and conditions please refer to [Hahn et al. \(2014\)](#).

“*Mytilus edulis* were harvested on 5 × 5 cm PVC plates that had been suspended for 10 days in 1 m water depth in Kiel Fjord in July 2010. The plates with freshly settled juveniles attached (shell length of 400 to 500 μm) attached, were transferred to an experimental setup identical to that described in Thomsen & Melzner (2010). Plates with settled mussels (one plate per aquarium) were incubated in 16 aquaria with a volume of 16 l each. (...) A constant food supply was established by perfusing the header tank with a *Rhodomonas* (algae) suspension.” Four different pCO₂ atmospheres were chosen for the tanks with each four replicates: 380 μatm (39 Pa, control, pH 8.0), 1 120 μatm (113 Pa, pH 7.7), 2 400 (243 Pa, pH 7.5) and 4 000 μatm (405 Pa, pH 7.2). Minimum and maximum saturation states for the lowest pH setting were: Ω_{arag} = 0.1 and Ω_{calc} = 0.2. For the highest pH (control) they were: Ω_{arag} = 0.9 and Ω_{calc} = 1.5. Temperature (11.6 °C), salinity (15.7), pH_{NBS}, DIC (C_T) were kept constant and were measured daily except for DIC which was measured biweekly. Detailed values can be found in table 2 and table 3 on the next page, data was supplied by Prof. Frank Melzner (GEOMAR, Kiel).

The focus of their research was on the shell ultrastructure and isotope ratios of δ¹³C, δ¹⁸O and δ²⁶Mg. Whereas this research focuses on different element ratios and isotopic composition of the shell.

1.5.2 Shell structure

The shell of a mussel consists of calcium carbonate (CaCO₃), about 95 to 99% and the rest is organic matrix. CaCO₃ in a shell has two polymorphs (crystal structures) called calcite and aragonite. The inner nacreous part of the shell is made up of the more soluble aragonite. On top of the aragonite is a prismatic calcite layer which in turn is covered by an organic layer called the periostracum. See also figure 16.

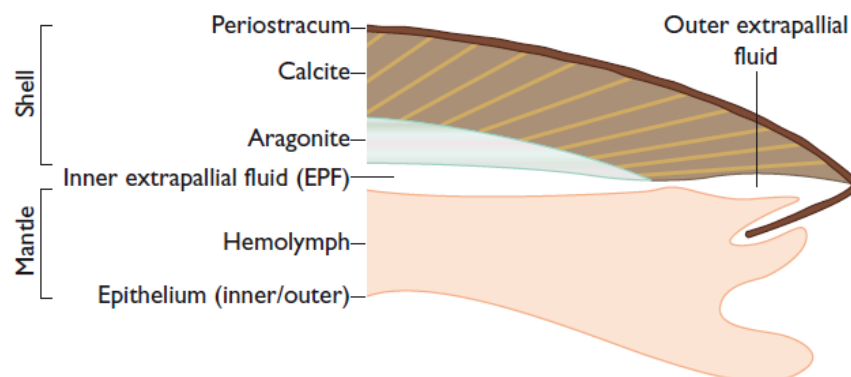


Figure 16 – Section through the margin of shell and mantle of a *Mytilus edulis*. The crystalline shell consists of two separate layers: a prismatic layer of calcite and an aragonitic layer of nacre. The outermost layer is secreted in growth increments in the area between the shell and the mantle. Image and text from [Klunder et al. \(2008\)](#).

Table 2 – Parameters of the living conditions and of experimental setups. Carbonate system speciation August 2010 to August 2011, N=53 determinations per treatment. Mean values over the entire one year cycle and standard deviations (SD), *calculated from C_T and pH_{NBS} measurements using CO2SYS.

Treatment	Salinity (psu)	Temperature (°C)	pH_{NBS}	C_T ($\mu\text{mol/kg}$)	A_T^* ($\mu\text{mol/kg}$)	pCO_2^* (μatm)	$\Omega_{\text{calcite}}^*$	$\Omega_{\text{aragonite}}^*$
380 μatm (N=53)	15.7	11.8	8.03	1 894.1	1 938.4	612	1.47	0.86
SD	± 1.1	± 5.0	± 0.06	± 84.6	± 82.7	± 87	± 0.28	± 0.17
1 120 μatm (N=53)	15.7	11.6	7.73	1 953.6	1 932.2	1 254	0.76	0.45
SD	± 1.0	± 5.1	± 0.05	± 93.9	± 88.0	± 146	± 0.18	± 0.11
2 400 μatm (N=53)	15.7	11.6	7.46	2 025.0	1 934.5	2 360	0.42	0.25
SD	± 1.1	± 5.2	± 0.07	± 101.7	± 88.9	± 343	± 0.11	± 0.07
4 000 μatm (N=53)	15.7	11.7	7.21	2 112.5	1 922.6	4 237	0.24	0.14
SD	± 1.0	± 5.2	± 0.06	± 109.8	± 84.0	± 461	± 0.07	± 0.04

Table 3 – Final shell masses and shell lengths after 1 year experimental duration and average *Rhodomonas sp.* food algae concentrations during 1 year incubation. *Rhodomonas* solution was supplied continuously to experimental aquaria. N=166-177 mussels for each treatment.

Treatment	shell length (mm)	shell mass (mg)	<i>Rhodomonas</i> (cells/ml)
380 μatm	22.3	273.4	1 967
SD	± 3.6	± 103.1	± 92
1120 μatm	22.2	252.1	2 388
SD	± 3.3	± 96.0	± 313
2400 μatm	22.7	271.9	2 359
SD	± 3.2	± 93.6	± 505
4000 μatm	20.8	207.3	2 245
SD	± 2.5	± 64.7	± 157

CO2sys is a program used to calculate different parameters of the carbonate system and more based on 2 or more input variables. In this case, the variables were temperature, salinity, pH and DIC. The settings used for CO2SYS were: K1 and K2 from [Millero \(2010\)](#) ; Seawater on NBS scale and $[B]_T$ from [Lee et al. \(2010\)](#) . Data showing the variations of salinity, temperature and pH over the 1 year culturing experiment are shown in Appendix 4.

The crystal lattice of aragonite is less well organized than calcite, this is the reason calcite is more stable and is less prone to dissolution. Aragonite is also susceptible to recrystallization under conditions found on Earth. The process of changing the crystal structure from aragonite to the more stable calcite is called diagenesis. Although this transformation is very slow, it can change the initial elemental and isotopic composition. Thus aragonite is less suited as a paleoproxy ([Gordillo et al., 2014](#); [Groeneveld et al., 2008](#)). A different crystal structure also affects element incorporation during calcification. Calcite and aragonite discriminate differently against some elements which causes concentrations to differ between the two layers ([Furst et al., 1976](#)). Boron for example can be 1.5 to 2 times more concentrated in aragonite. This can overprint the possible proxy signal. Vital effects, which were discussed earlier, are another mechanism that can cause an offset of element ratios. When a shell grows, it precipitates CaCO_3 and incorporates metals (Me) from the extrapallial fluid (EPF). Precipitation therefore takes place from the extrapallial fluid – which has a pH of 7.5 at normal conditions and 7.35 at 2700 pCO₂ ([Heinemann et al., 2012](#)) – and not from the surrounding sea water. So when the micro-environment is different from seawater, for example when the pH of the EPF is different than that of the surrounding water, the amount of metals, such as e.g. uranium precipitated into the shell will also differ. This is one way that vital effects of a mussel shell affect element incorporation. When metal to calcium ratios are to be determined, then the organic matrix must be removed. The periostracum for example (outermost organic layer) can have boron or magnesium concentrations magnitudes higher than the CaCO_3 ([Heinemann et al., 2012](#)). Even though the organic layer is a small part, it may significantly influence measurements. This is even more important when using laser ablation instead of wet chemistry to introduce sample into the plasma for analysis, since only a small shallow area is ablated. Besides the periostracum, organics are also found at growth bands caused by slowed growth in the winter months. In fact, biominerals are always a composite association of organics and mineral, down to the smallest level, as biological mineral growth is typically initiated by an organic matrix or template and “organically” controlled. These organics also increased concentrations for some elements; figure 17 shows this for the similar species *Mytilus californianus* ([McCoy et al., 2011](#)).

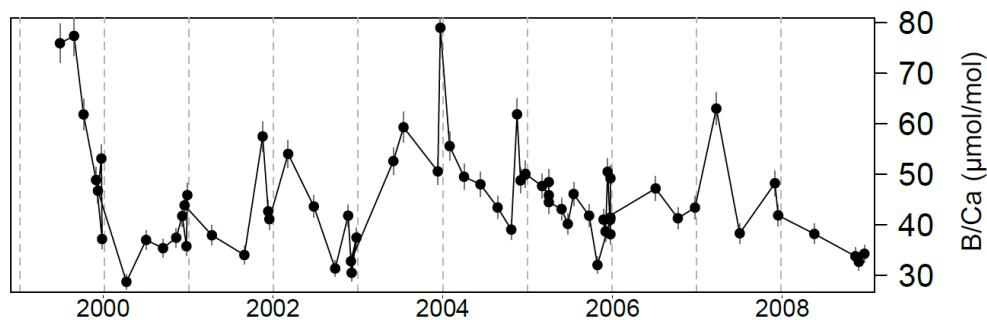


Figure 17 – B/Ca of *Mytilus californianus* ratios near growth bands are usually higher than in between them, this is most likely caused by a higher amount of organics. The dotted grey lines represent the winter (image modified from [McCoy et al. \(2011\)](#)).

The organic matrix is mostly on the edge of crystal structures and not completely enclosed by CaCO_3 , it is intercrystalline. Since growth of crystal structures is strongly influenced by organics, it is fair to assume that organics are present at a very small scale, at nanometer level ([Gordillo et al., 2014](#)). Bulk organics of the periostracum for example can be removed by bleaching with NaOCl (which will be discussed later). By crushing the shell, part of the organics from growth bands can be removed. However, it will be impossible to remove all organics, since the powder is simply too coarse. Although this may seem like a problem, the amount of organic matrix besides the periostracum might be negligible. This is one of the issues that will be tested in this research. By measuring the effect on Me/Ca ratios of bleaching a whole shell or as a powder, the influence of organics in growth bands can be determined.

To remove organics, several chemicals can be used however NaOCl is mostly used on valves and bivalves. [Krause-Nehring et al. \(2011\)](#) tested several techniques on the bivalve *Arctica islandica* (figure 18). They tested acetone, NaOH, H₂O₂, NaOCl and combinations of these chemicals. None of the techniques was without side-effects. However NaOCl seemed to be most favorable. The issue here was that during drying of the sample, NaCl was precipitated. But because it is highly soluble in water, it could be washed away relatively easy. Then, different studies used varying cleaning durations and strengths of bleach such as: 10 % for 24 hours ([Sanyal et al., 2001](#)) and 1% for 48 hours ([Heinemann et al., 2012](#)). Therefore, an experiment was done to see the effects of cleaning with NaOCl on elemental ratios.



Figure 18 – A specimen of *Arctica islandica*

1.6 Analytical techniques

At the Alfred Wegener Institute, three ICP-MS' were used: Spectro MS, Nu Attom and Nu Plasma II. The Spectro MS is a double-focusing sector field ICP-MS based on a Mattauch-Herzog geometry. It focusses both the ion angles and ion energies. The Spectro MS was equipped with a desolvating nebulizer system (Apex Q, ESI), which increases sensitivity by about 8-10x and lowers oxide interferences. The Mattauch-Herzog geometry allows the use of a Direct Charge Detector (DCD) so it can measure the entire mass spectrum from lithium to uranium simultaneously.

The Nu attom is a double-focussing HR-ICP-MS with a Nier-Johnson geometry. It can measure elements in both high and low concentration by making use of Faraday cups or electron multipliers respectively. The resolution can be set high or low depending on what is needed. For this research however, only boron, uranium and calcium were measured. For these elements, a low detection limit is required and not a very high resolution, 300 was enough.

The Nu Plasma II MS is magnetic sector double focusing instrument with a Nier-Johnson geometry. It has 16 Faraday detectors and 6 ion-counting electron multipliers, spread out over the mass range. The high resolution and stability of the instrument allows for the precise measurements of isotopic ratios. The Nier-Johnson geometry allows for simultaneous detection of multiple ion beams.

2 – Effect of bleaching on organic matrix of a *Mytilus edulis* shell

2.1 Introduction

In this experiment the effect of NaOCl on the organic matrix and Me/Ca ratios was investigated. This was necessary because other experiments used varying combinations of bleaching times and concentrations. For example, bleaching times ranged from 2 hours in an oven (Krause-Nehring *et al.*, 2011) to two days at room temperature (Heineman *et al.*, 2012). To determine the effects, two series of experiments were done. The first method involved crushing an untreated sample and subsequently submerging it in bleach for 1, 2, 3, 4 and 5 hours. The second method involved the same steps, except that prior to crushing the shell was subjected to two days of bleaching. All samples were then dissolved in 1 N HCl and analyzed on the Spectro MS ICP-MS.

2.2 Materials and methods

The materials needed for this experiment where:

- 1.5 ml Safe-lock tubes
- 50 ml sample tube
- Two valves of a mussel shell
- Drying oven
- Centrifuge
- Pestle and Mortar
- Spectro MS ICP-MS
- NaOCl (Acros Organics; 10 – 15 %; CAS#: 7681-52-9)
- HCl (1N; CAS#: 7647-01-0)
- HNO₃ (2 %; CAS#: 7697-37-2)
- Ultrasonic bath
- Milli-Q water
- Nu Attom ICP-MS
- Calibration and tuning standards

A single valve from a shell grown at 1120 μatm pCO₂ was crushed to a powder using a pestle and mortar. Approximately 6.5 mg of this crushed powder was added to six (pre-weighed) 1.5 ml Eppendorf Safe-lock tubes. Subsequently 1 000 μl of NaOCl was added to each of these tubes except for the control sample (control 1). Vials were occasionally rapped on the table to remove any gas buildup resulting from the dissolution of organics, and to bring the sample into suspension. After corresponding bleaching times of 1, 2, 3, 4 and 5 hours, tubes were removed one by one. These six samples were then washed three times by using an ultrasonic bath and a centrifuge.

All powdered samples where then washed at the same time another five times with 1 ml extra boron filtered MQ. During washing, each sample put in an ultrasonic bath for 2 minutes to bring everything into suspension. After that, they were centrifuged for 2 minutes at 10000 rpm so the water could be pipetted out. After washing, samples were dried above a 100 °C hotplate for 4 hours.

The other valve was weighed as a whole and was put in a 50 ml sample tube. Approximately 10 ml of bleach was added so that the complete valve was submerged. After 24 hours the tube was put in an ultrasonic bath for 10 minutes and the NaOCl was then refreshed. The sample was then bleached for another 24 hours followed by another 10 minutes of sonication. After sonication, the valve was rinsed five times with plenty MQ and placed in an oven at 50 °C for 2 hours. After drying the shell was crushed and approximately 6.5 mg of powder was divided over six (pre-weighed) 1.5 ml sample tubes. These samples were then bleached with 1 000 μl NaOCl for 1, 2, 3, 4 and 5 hours with again one control (control 2). When a sample was done, it was also washed three times and another 5 times as described above.

2 – Effect of bleaching on organic matrix of a *Mytilus edulis* shell

After drying, the powders were dissolved in approximately 300 µl of 1 N HCl. Aliquots of approximately 5 µl were taken and diluted in 1 ml of 2 % HNO₃ to get a Ca concentration of around 20 ppm. The samples were measured on the Spectro MS with the experimental conditions listed in table 4. Tuning of the machine was done by optimizing the nebulizer flow, torch position and plasma power while measuring a tuning solution. The tuning solution contained several elements of high and low mass. The goal of the tuning was to get experimental conditions which resulted in symmetrical peak shapes for elements of high and low mass.

Table 4 – Experimental conditions and instrument settings.

Parameter	Setting
Plasma Torch	Quartz
Nebulizer	PFA Micro-flow
Spray chamber	Quartz cyclonic spray chamber
Cones	Platinum
Power	1 545 W
Coolant gas	12 l/min
Auxiliary gas	2.70 l/min
Nebulizer gas	0.64 l/min
Cycles	3
Integration time	10 (for Ca measurements) / 20 s

When the exact calcium concentrations in the sample were known, the original samples were diluted again to a more precise calcium concentration of about 100 ppm. Then, the same experimental conditions were used to simultaneously measure 33 elements including: ⁷Li, ²³Na, ²⁴Mg, ²⁵Mg, ²⁷Al, ⁴³Ca, ⁴⁵Sc, ⁴⁸Ca, ⁵⁵Mn, ⁶⁴Zn, ⁸⁷Sr, ⁸⁸Sr, ⁸⁹Y, ¹¹⁴Cd, ¹³⁷Ba, ¹³⁹La, ¹⁴⁰Ce, ¹⁴¹Pr, ¹⁴²Nd, ¹⁴⁴Nd, ¹⁴⁶Nd, ¹⁴⁷Sm, ¹⁴⁹Sm, ¹⁵³Eu, ¹⁵⁷Gd, ¹⁵⁹Tb, ¹⁶³Dy, ¹⁶⁵Ho, ¹⁶⁶Er, ¹⁶⁹Tm, ¹⁷²Yb, ¹⁷⁵Lu and ²³⁸U. But, not all elements had a concentration above the detection limit (DL).

To determine the calcium concentration, four standards were used of 0, 33, 66 and 100 ppm Ca. Five mixed calibration standards were used for the other elements which had a calcium concentration of 0, 25, 50, 75 and 100 ppm. Exact concentrations can be found in appendix 1. The standards were made by diluting from a 100 ppm Ca stock solution according to table 5. The volume of the standards for the blank and 75 ppm Ca are higher because before and after every three samples a bracketing standard and a control blank was measured. With the bracketing standard, all the samples were corrected for drift.

Table 5 – Dilution table to get the necessary concentrations of the calibration standards.

Aimed Ca concentration (ppm)	Total volume (µl)	Volume 100 ppm stock (µl)	Volume 2 % HNO ₃ (µl)
0	4 000	0	4 000
25	1 000	250	750
50	1 000	500	500
75	4 000	3 000	1 000
100	1 000	1 000	0

After determination of the exact calcium concentration in the undiluted samples, they were diluted to a 100 ppm Ca solution. It turned out that uranium, a potential proxy-element was below the detection limit of the spectro MS. This element was therefore measured again on the Nu Attom along with boron (¹¹B) and calcium (⁴³Ca). Boron cannot be measured on the Spectro MS because of the ESI APEX Q nebulizer,

2 – Effect of bleaching on organic matrix of a *Mytilus edulis* shell

which retains some of the very ‘sticky’ boron. On the Nu Attom the instrument settings shown in table 6 were used. The Nu Attom is much more sensitive and samples were diluted to a 15 ppm Ca concentration. These measurements were also corrected for drift by measuring all 5 calibration solutions before the samples, after the sixth sample and after the last sample.

Table 6 – Experimental conditions and instrument settings for Nu Attom.

Parameter	Setting
Plasma Torch	Quartz
Nebulizer	PFA (80 µl)
Spray chamber	Plasma II Cyclon Quartz
Cones	Platinum
Power	1 375 W
Coolant gas	13 l/min
Auxiliary gas	1.55 l/min
Nebulizer gas	45.9 PSI
Cycles	5
Resolution	300

2.3 Results

One valve was crushed and approximately 6.5 mg of powder was added to six 1.5 ml tubes. These samples were then bleached for different times, washed and dissolved. Results for weight loss after bleaching are shown table 7 and marked with an “a” in the sample name. The other valve was first bleached for two days in one piece which resulted in a weight loss of $100.4 - 91.6 = 8.8$ mg or 8.8 %. This valve was then crushed and bleached for different times; these results are also in table 7 but marked with a “b”.

Table 7 – Results for weight loss after bleaching once with five different times are have sample id with A. samples with B were two days as a whole before crushing and bleaching again.

Sample	Bleaching time (h)	Sample (mg)	Sample after bleaching (mg)	Weight loss (%)
c1 (control 1)	0	6.1	N.A.	N.A.
1a	1	6.7	6.3	6.0
2a	2	6.5	6.2	4.6
3a	3	6.4	5.8	9.4
4a	4	6.3	5.7	9.5
5a	5	6.4	6.1	4.7
c2 (control 2)	48	6.3	N.A.	N.A.
1b	48 + 1	6.3	6.0	4.8
2b	48 + 2	6.5	5.5	15
3b	48 + 3	6.1	5.7	6.6
4b	48 + 4	6.2	6.1	1.6
5b	48 + 5	6.6	6.3	4.5

After the bleaching, rinsing and drying, the samples were dissolved in 1 N HCl. All samples produced CO₂ because of the reaction of calcium carbonate with acid. The first control sample also produced brown solid matter. This is most likely the organic matter of the periostracum. Other samples did not show this. After dissolving the samples were shortly centrifuged to get the suspended particles down. Then aliquots of approximately 5 µl were taken and diluted in 1 ml 2 % HNO₃. After measurement on the Spectro ICP-MS, the concentration in the diluted vials was known, and the calcium concentration of the undiluted samples could be calculated according to:

$$C_{undiluted} = \frac{m_{(sample\ and\ HNO_3)}}{m_{(sample)}} \cdot C_{measured}$$

Where m represents the mass of the sample and HNO₃ together and the sample separately. C is the concentration of calcium in the diluted (C_{measured}) and undiluted vial. The results for these dilutions and calculations are shown in table 8.

2 – Effect of bleaching on organic matrix of a *Mytilus edulis* shell

Table 8 – Dilutions and results from the calcium measurements.

Sample	Aliquot (mg)	Total (g)	Dilution factor	Ca in diluted vial (ppm)	Ca in undiluted vial (ppm)
c1 (control 1)	5.4	1.0155	188.06	46.04	8 658
1a	5.3	1.0156	191.62	41.62	7 975
2a	5.4	1.0173	188.39	39.98	7 532
3a	5.5	1.0167	184.85	37.02	6 843
4a	5.5	1.0163	184.78	34.24	6 326
5a	5.5	1.0163	184.78	34.27	6 331
c2 (control 2)	5.2	1.0135	194.90	42.12	8 210
1b	5.3	1.0150	191.51	28.77	5 510
2b	5.4	1.0157	188.09	26.98	5 075
3b	5.3	1.0153	191.57	39.32	7 532
4b	5.4	1.0154	188.04	34.42	6 471
5b	5.4	1.0142	187.81	38.82	7 291

Using the numbers in the last column of table 8, dilutions for a 100 ppm calcium solution were calculated with (15 ppm for ^{11}B , ^{238}U and ^{43}Ca measurements on Nu Atom):

$$V_{\text{aliquot}} = \frac{V_{\text{total}}}{\left(\frac{C_{\text{undiluted}}}{C_{\text{aimed}}}\right)}$$

Where V_{aliquot} is the volume of aliquot to be taken from the undiluted sample and to be diluted in a volume of V_{total} 2 % HNO_3 . Samples were diluted in 2 ml of 2 % HNO_3 so the formula for c1 would be:

$$V_{\text{aliquot}} = \frac{2000}{\left(\frac{8658.0}{100}\right)} = 23.1 \mu\text{l}$$

The experimental conditions for all other metals were identical to those for the calcium measurements. The concentrations of the rare earth elements as well as scandium, yttrium, cadmium and uranium were all below the detection limit of the Spectro MS. Detection limits for these elements were on average at 1.5 parts per trillion. Aluminium, an element used to check for contamination, was generally below 1.5 ppb which is acceptable. Values for manganese (measured on mass 55) and zinc (measured on mass 64) varied quite a lot between samples, this is most likely due to spectral interferences for the two elements. Such as $^{40}\text{Ar}^{14}\text{N}^+\text{H}^+$, $^{37}\text{Cl}^{18}\text{O}^+$ and $^{38}\text{Ar}^{17}\text{O}^+$ for ^{55}Mn and $^{48}\text{Ca}^{16}\text{O}^+$, $^{32}\text{S}^{16}\text{O}_2^+$ and $^{36}\text{Ar}^{14}\text{N}_2^+$ for ^{64}Zn . The concentration of sodium was generally above 700 ppm (4.4 mmol/mol), far beyond the calibration line (between 100 to 420 ppm (2.3 mmol/mol), table 33). Even so, calcium ratios could still be calculated by extrapolation of the calibration lines, however these values should be taken with caution.

2 – Effect of bleaching on organic matrix of a *Mytilus edulis* shell

Calcium ratios for ^{23}Na and the remaining elements: ^7Li , ^{24}Mg , ^{87}Sr and ^{137}Ba (^{25}Mg , ^{48}Ca and ^{88}Sr are left out since they are redundant for now, because they show the exact same trend as their lighter counterpart) were calculated by:

$$\text{Me/Ca} = \frac{\left(\frac{C_{\text{Me}}}{C_{\text{Ca}}}\right)}{M_{\text{Me}}} \cdot M_{\text{Ca}}$$

Where C_{Me} is the concentration of the metal in ppb and M_{Me} the molar mass of the specific metal. This gives a metal/calcium ratio in mol/mol. The Me/Ca ratios are shown in table 9 along with their 95 % confidence interval. These intervals have been calculated using:

$$\bar{x} \pm \frac{T_{(\alpha: 0.05; v: 2)} \cdot s}{\sqrt{n}}$$

Where $T_{(\alpha: 0.05; v: 2)} = 4.30$, is the standard deviation of the Me/Ca ratios for the three cycles and $n = 3$. The value for Ba/Ca for sample 1a is much higher compared to the other samples. Using a Dixons Q test, it can be shown that this is an outlier:

$$Q_{\text{calc}} = \frac{\text{Gap}}{\text{Range}} = \frac{30.5 - 55.7}{25.0 - 55.7} = 0.821 \quad Q_{(\alpha: 0.05; n: 12)} = 0.426$$

$Q_{\text{calc}} > Q_{(\alpha: 0.05; n: 12)}$ so the Ba/Ca for sample 2a is an outlier.

B/Ca ratios were also calculated this way. However, for their 95 % confidence interval 4 degrees of freedom were used because each measurement had 5 cycles. The concentrations for ^{238}U were also too low to be accurately measured on the Nu Attom (ca. 50 ppq at 15 ppm Calcium). All data is shown in table 9.

2 – Effect of bleaching on organic matrix of a *Mytilus edulis* shell

Table 9 – Me/Ca ratios for ^7Li , ^{23}Na , ^{24}Mg , ^{87}Sr , ^{137}Ba and ^{11}B (Nu Attom data) along with their 95 % confidence intervals. Results show the effect of different bleaching times on the Me/Ca ratios.

Sample	Bleach time (h)	$^7\text{Li}/^{43}\text{Ca}$ ($\mu\text{mol/mol}$)	$^{23}\text{Na}/^{43}\text{Ca}$ (mmol/mol)	$^{24}\text{Mg}/^{43}\text{Ca}$ (mmol/mol)	$^{87}\text{Sr}/^{43}\text{Ca}$ (mmol/mol)	$^{137}\text{Ba}/^{43}\text{Ca}$ ($\mu\text{mol/mol}$)	$^{11}\text{B}/^{43}\text{Ca}$ ($\mu\text{mol/mol}$)
Control 1	0	7.8	13.44	4.736	1.082	2.274	99.1
95 % C.I.		0.6	0.12	0.035	0.010	0.14	1.2
1a	1	6.3	13.92	4.416	1.112	4.746	79.8
95 % C.I.		6.2	14.27	4.278	1.078	2.596	2.0
2a	2	5.8	14.14	4.395	1.059	2.253	45.6
95 % C.I.		1.6	0.16	0.015	0.019	0.09	1.3
3a	3	5.8	14.14	4.395	1.059	2.25	55.6
95 % C.I.		0.9	0.13	0.028	0.010	0.06	1.5
4a	4	6.3	14.46	4.56	1.082	2.240	41.1
95 % C.I.		1.6	0.27	0.05	0.013	0.024	0.8
5a	5	6.0	15.33	4.247	1.070	2.196	55.0
95 % C.I.		0.6	0.17	0.036	0.007	0.020	1.9
Control 2	48	6.3	13.85	4.48	1.050	2.277	60.9
95 % C.I.		0.7	0.19	0.05	0.013	0.05	2.0
1b	48 + 1	6.2	14.57	4.117	1.081	2.356	54.9
95 % C.I.		1.5	0.20	0.028	0.012	0.08	1.9
2b	48 + 2	6.2	15.13	4.058	1.039	2.127	51.7
95 % C.I.		1.3	0.17	0.025	0.009	0.035	0.8
3b	48 + 3	5.9	15.15	4.197	1.0494	2.229	76.3
95 % C.I.		1.6	0.21	0.037	0.0027	0.06	2.0
4b	48 + 4	5.3	14.28	4.33	1.039	2.269	50.6
95 % C.I.		0.7	0.23	0.04	0.010	0.110	1.3
5b	48 + 5	5.7	15.19	4.20	1.040	2.208	57.1
95 % C.I.		0.6	0.23	0.05	0.007	0.05	1.1

2.4 Discussion

Samples were weighed before and after cleaning with bleach. Weight losses were variable and covered a wide range from 1.6 to 15.0 %. [Klunder et al. \(2008\)](#) reported an organic content for mussel shells of approximately 1 to 5 %. These relatively larger losses most likely happened during the washing steps. When removing the water after centrifuging some carbonate may be lost as well. Hence, weight loss is not a good indicator of the organic content removed during the bleaching process.

Lithium (figure 19), does not show a clear pattern after bleaching for 1 hour. The large deviations are probably caused by the low concentrations of lithium in the sample (90 to 120 ppt, DL is 20 ppt).

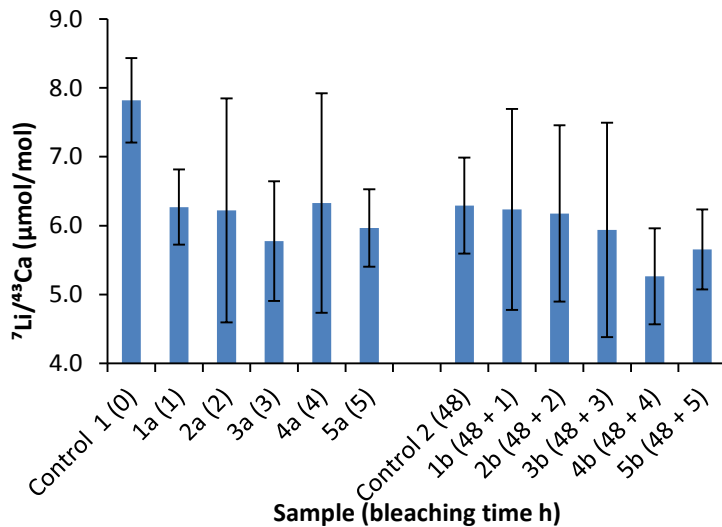


Figure 19 – The Li/Ca ratio for each sample. Sample names are shown with their bleaching time in brackets. Deviations are the 95 % confidence intervals.

2 – Effect of bleaching on organic matrix of a *Mytilus edulis* shell

Na/Ca shows a positive correlation with bleaching time for both treatments (Figure 20). Interestingly, bleaching once as a whole valve (control 2) does not significantly increase the Na/Ca compared to sample 1a. However when control 2 is compared with sample 2a, 2a has a significantly higher Na/Ca concentration, suggesting that Na from the bleach (NaOCl) adheres to the particles. Control 2 had a significant higher Na/Ca ratio than the first control and all other samples in turn had a significantly higher Na/Ca ratio when compared with control 2.

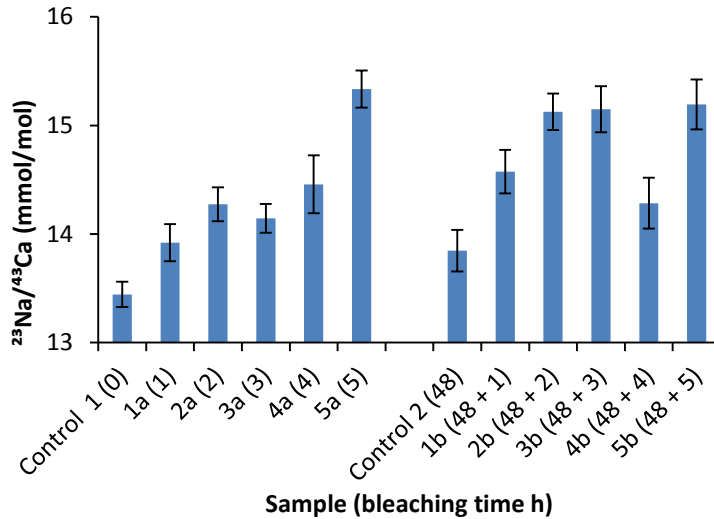


Figure 20 – The Na/Ca ratio for each sample. Sample names are shown with their bleaching time in brackets. Deviations are the 95 % confidence intervals.

The following procedure was applied to determine whether samples were significantly different. Firstly, it was verified if the standard deviations could be combined using an F-test:

$$F_{calc} = \frac{s_a^2}{s_b^2}$$

Where the higher standard deviation of the samples (s) is the numerator, while the lower acts as denominator, so that $s_a^2 > s_b^2$. This was then checked against $F_{(\alpha: 0.05; v: 2, 2)} = 39.00$. F_{calc} was lower than $F_{(\alpha: 0.05; v: 2, 2)}$ for all tests. Hence, all standard deviations were allowed to be combined using the following equation:

$$s_{comb} = \sqrt{\frac{v_a \cdot s_a^2 + v_b \cdot s_b^2}{v_a + v_b}}$$

Where the degrees of freedom (v) were 2 and s_a and s_b the respective standard deviations of the tested samples. This combined standard deviation was then used to calculate a t-value to be tested against $t_{(\alpha: 0.05; v: 4)} = 2.78$:

$$t_{calc} = \frac{|\bar{x}_a - \bar{x}_b|}{s_{comb} \cdot \sqrt{\frac{1}{n_a} + \frac{1}{n_b}}}$$

If $t_{calc} > t_{(\alpha: 0.05; v: 4)}$, then the values differed significantly and vice versa.

2 – Effect of bleaching on organic matrix of a *Mytilus edulis* shell

Mg is known to be enriched in the organics of the bivalve *Arctica islandica* (Schone et al., 2010), corals and foraminifera (Barker et al., 2003; Watanabe et al., 2001). So it could be a good indicator for the removal of organics. Mg/Ca shows for both series an initial drop in concentration after the control sample (figure 21). After that the concentration increases until the sample, 4a and 4b, after which it is lower again. This pattern could suggest the dissolution of Mg and subsequent adsorption back onto the sample. However this could also be attributed to some inhomogeneity's in the crushed powder due to a difference in particle size. Particles of larger size have a smaller surface area, so less organics can be removed. Alternatively, it may stem from inhomogeneity of the valve itself.

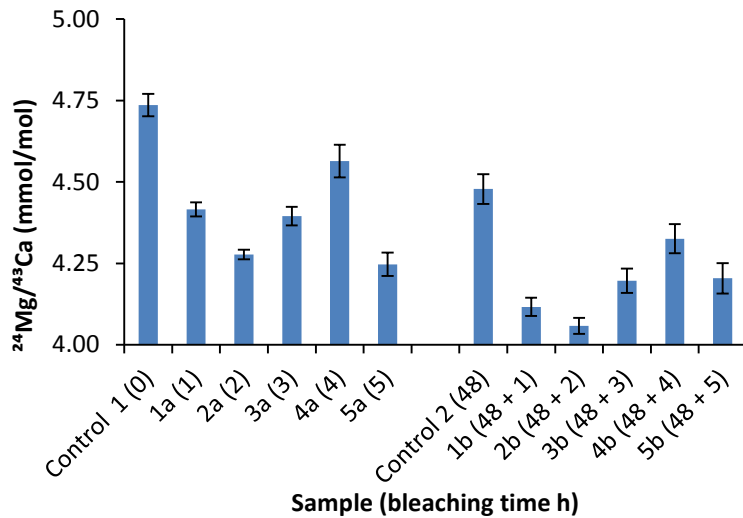


Figure 21 – The Mg/Ca ratio for each sample. Sample names are shown with their bleaching time in brackets. Deviations are the 95 % confidence intervals.

For strontium and barium (figure 22 and figure 23), the pattern is less obvious. Overall the Sr/Ca ratio seems to be stable for the both treatments. However, when both series are compared, 5 of the 6 six samples from the second series are significantly lower than control 1 (using the same approach explained before). Barium is quite stable except for sample 2a and 2b which differ significantly from control 1. The other samples do not show any significant response to different bleaching times.

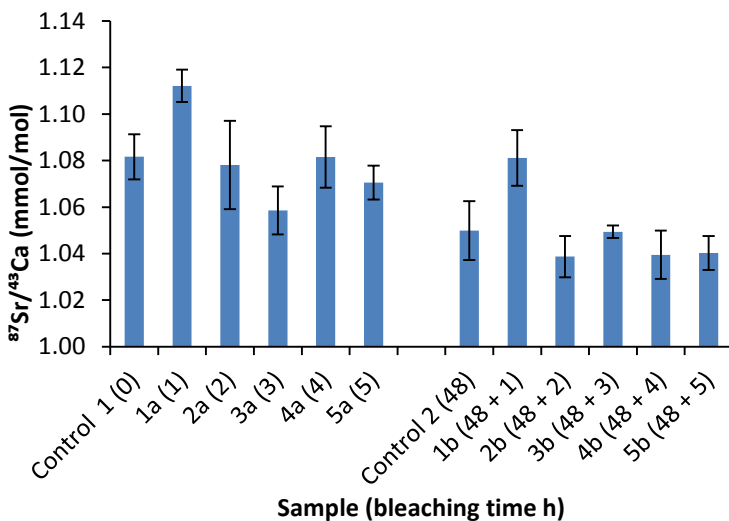


Figure 22 – The Sr/Ca ratio for each sample. Sample names are shown with their bleaching time in brackets. Deviations are the 95 % confidence intervals.

2 – Effect of bleaching on organic matrix of a *Mytilus edulis* shell

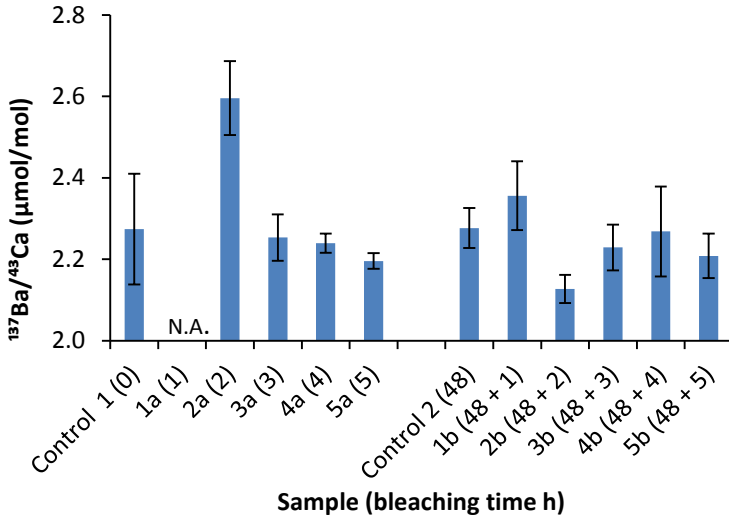


Figure 23 – The Ba/Ca ratio for each sample except 1a which has been shown to be an outlier. Sample names are shown with their bleaching time in brackets. Deviations are the 95 % confidence intervals.

The first series of samples show a decrease in B/Ca during the first 2 hours of bleaching. After that it seems to stabilize, because the values show no clear pattern anymore. The same is true for all values of the second series. The two treatments show very similar results, suggesting that the organic boron is mainly in the periostracum. Also, when this organic boron is removed, the B/Ca ratios vary but neither decrease nor increase significantly.

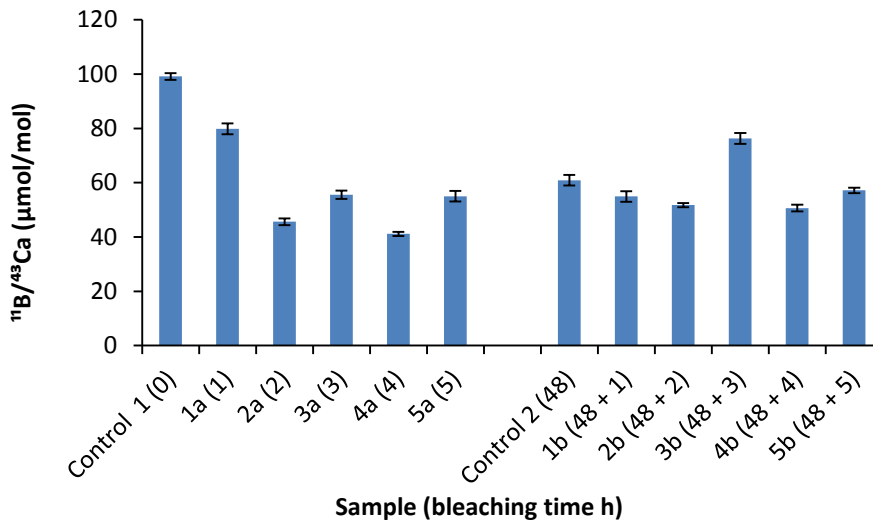


Figure 24 – The B/Ca ratio for each sample. Sample names are shown with their bleaching time in brackets. Deviations are the 95 % confidence intervals.

2.5 Conclusion

Lithium, strontium and barium did not show clear significant differences that could be attributed to the difference in bleaching times, or to the different bleaching methods used e.g. crushed and directly bleached or bleached, crushed and bleached again.

Sodium showed a clear increase of Na/Ca with increased bleaching times. This indicates that sodium from the bleach was adhering to the carbonate or stuck to the vial. Mg/Ca showed the expected negative correlation with longer cleaning times (i.e. removal with the organics) but concentrations increased after cleaning two hours, indicating that a shorter cleaning time for Mg/Ca could be beneficial. However, these variations may also be influenced by inhomogeneities in the sample caused by different particle sizes in the samples. Larger particles have a larger surface area, so they interact differently with the bleach. Boron is only affected within the first 2 hours of cleaning. When the periostracum has been removed, the B/Ca ratios stay more or less the constant.

Some elements gave inconclusive results. Hence, the next experiment was to examine the impact of size fraction on the cleaning procedure.

3 – Effects of bleaching times on a single size fraction

3.1 Introduction

In this experiment, again, the effect of NaOCl on the organic matrix and Me/Ca ratios was investigated. However this time, the shell powder was sieved over two sieves of 100 and 63 μm . This resulted in three size fractions: >100 μm (large), <100 and >63 μm (middle) and <63 μm (small). The goal of this experiment was to investigate if the variability of the Me/Ca ratios from the previous experiment were caused by inhomogeneous powders. The same bleaching method as in the previous experiment was used.

3.2 Materials and methods

The materials needed for this experiment where:

- 1.5 ml Safe-lock tubes
- 50 ml sample tube
- Two valves of a mussel shell
- Drying oven
- Centrifuge
- Pestle and Mortar
- Spectro MS ICP-MS
- NaOCl (Acros Organics; 10 – 15 %; CAS#: 7681-52-9)
- HCl (1N; CAS#: 7647-01-0)
- HNO₃ (2 %; CAS#: 7697-37-2)
- Ultrasonic bath
- Milli-Q water
- Two sieves (100 and 63 μm)
- Calibration and tuning standards

A single valve from a shell grown at 390 μatm pCO₂ was crushed into a powder using a pestle and mortar. This powder was subsequently sieved over sieves of 100 and 63 μm to get a total of three size fractions. The middle fraction (<100 and >63 μm) was divided over six pre-weighed 1.5 ml Eppendorf vials. Then 1000 μl NaOCl was added to each vial, except for the control (control 3). To remove any gas buildup and to mix the sample, samples were occasionally rapped on the table. Then every hour, the bleach from a sample was removed by centrifuging and pipetting it out. When the bleach was removed the sample was washed 3 times with MQ water.

The other valve from the same shell was put in a 50 ml tube again with approximately 10 ml NaOCl. After 24 hours, the sample was sonicated and the bleach was replaced by a new 10 ml of bleach. After another 25 hours in bleach the valve was sonicated for 10 minutes and rinsed thoroughly with plenty of water. Then it was dried for 2 hours in an oven at 50 °C, crushed, sieved and divided over six 1.5 ml vials like the other valve (<100 and >63 μm). These were then bleached for respectively 0 (control 4), 1, 2, 3, 4 and 5 hours. When the bleach was removed the sample was washed 3 times with MQ water. A blank without any sample was also taken, it was filled with bleach for 5 hours and underwent the same treatment as the samples.

All 12 samples were washed 10 times with 1 ml boron free filtered MQ (10 times to try to reduce the remaining sodium). After washing, the samples were dried over the weekend at room temperature in a flow-bench. They were weighed and dissolved in 150 μl 1 N HCl. This time no calcium measurements were carried out, but concentrations in HCl were estimated from the sample weight in the vial. Table 10 shows which aliquots were taken and how dilutions were made

3 – Effects of bleaching times on a single size fraction

Table 10 – Samples where dissolved in 150 µl 1 N HCl what resulted in the listed Ca concentrations. An aliquot of listed volume was taken and diluted in 2 ml 2 % HNO₃ to obtain a solution with a 100 ppm Ca concentration.

Sample	Bleaching time (h)	Sample (mg)	Ca concentration (ppm)	Aliquot for 100 ppm Ca in 2 ml 2 % HNO ₃ (µl)
Control 3	0	5.5	14 187	14.1
1d	1	4.3	11 183	17.9
2d	2	4.1	10 754	18.6
3d	3	4.1	10 678	18.7
4d	4	4.5	11 587	17.3
5d	5	5.5	14 063	14.2
Control 4	48	5.6	14 286	14.0
1e	48 + 1	5.3	13 540	14.8
2e	48 + 2	4.2	11 007	18.2
3e	48 + 3	5.2	13 515	14.8
4e	48 + 4	5.4	13 914	14.4
5e	48 + 5	4.9	12 741	15.7
Blank	5	NA	NA	15.0

The formula below shows how the calcium concentrations were calculated, exemplified for sample 1d:

$$C_{undiluted} = \frac{\left(\frac{m_{sample} \cdot M_{Ca}}{M_{CaCO_3}}\right)}{V_{HCl} + V_{sample}} \rightarrow \frac{\left(\frac{4.31 \cdot 40.078}{100.087}\right)}{150 + 4.31} = 11183 \text{ ppm Ca}$$

The formula to calculate the volume of the aliquot is the same as for the previous experiment:

$$V_{aliquot} = \frac{V_{total}}{\left(\frac{C_{undiluted}}{C_{aimed}}\right)}$$

Where $V_{aliquot}$ is the volume of aliquot to be taken from the undiluted sample for dilution into 2 ml (V_{total}) 2 % HNO₃.

When the samples were ready, the nebulizer flow, torch position and plasma power were optimized (experimental settings in table 11. Another five calibration standards were made using the dilution table (table 5). Exact concentrations of the standards are listed in table 34.

3 – Effects of bleaching times on a single size fraction

Table 11 – Experimental conditions and instrument settings.

Parameter	Setting
Plasma Torch	Quartz
Nebulizer	PFA Micro-flow
Spray chamber	Quartz cyclonic spray chamber
Cones	Platinum
Power	1 550 W
Coolant gas	12 l/min
Auxiliary gas	2.70 l/min
Nebulizer gas	0.71 l/min
Cycles	3
Integration time	20 s

3.3 Results

Sieving may not have been completely successful because the powder is a bit sticky and readily forms agglomerates. Even so, three size fractions were obtained with visibly different particle sizes, such that the size fractions were clearly better constrained than in the previous experiment. Samples were diluted by taking the aliquots from table 10 and diluting them into 2 ml 2 % HNO₃. Me/Ca ratios and 95 % C.I. are provided in table 12. Concentrations of the solution blank expressed in ppb can be found in table 13. Most elements were below the detection limit. Although, the blank measurement for Ba relatively high with 20.4 % of the average values. Sodium was also quite high which may be due to the proximity of the lab to the sea.

Even though, [Na] was outside of the calibration range again, with an average value of 961 ppb, the Na/Ca ratios have been calculated again by extrapolation.

3 – Effects of bleaching times on a single size fraction

Table 12 – Me/Ca ratios for ^7Li , ^{23}Na , ^{24}Mg , ^{87}Sr and ^{137}Ba along with their 95 % confidence intervals as a function of bleaching time.

Sample	Bleach time (h)	$^7\text{Li}/^{43}\text{Ca}$ ($\mu\text{mol}/\text{mol}$)	$^{23}\text{Na}/^{43}\text{Ca}$ (mmol/mol)	$^{24}\text{Mg}/^{43}\text{Ca}$ (mmol/mol)	$^{87}\text{Sr}/^{43}\text{Ca}$ (mmol/mol)	$^{137}\text{Ba}/^{43}\text{Ca}$ ($\mu\text{mol}/\text{mol}$)
Control 3	0	6.58	16.38	4.098	1.275	1.954
95 % C.I.		0.25	0.23	0.022	0.014	0.038
1d	1	5.4	17.10	3.61	1.258	1.88
95 % C.I.		1.0	0.30	0.05	0.019	0.07
2d	2	4.93	17.1	3.58	1.244	2.06
95 % C.I.		0.28	0.5	0.09	0.008	0.09
3d	3	5.0	17.2	3.67	1.241	1.83
95 % C.I.		0.7	0.5	0.08	0.019	0.10
4d	4	4.87	17.31	3.58	1.245	1.92
95 % C.I.		0.25	0.35	0.07	0.016	0.08
5d	5	5.03	17.13	3.60	1.224	1.91
95 % C.I.		0.38	0.31	0.05	0.024	0.09
Control 4	48	4.7	16.9	3.43	1.218	1.729
95 % C.I.		0.6	0.5	0.10	0.016	0.027
1e	48 + 1	4.9	16.98	3.493	1.203	1.75
95 % C.I.		0.8	0.26	0.038	0.011	0.07
2e	48 + 2	4.5	17.3	3.48	1.190	1.69
95 % C.I.		0.8	0.4	0.07	0.013	0.12
3e	48 + 3	4.2	16.36	3.41	1.197	1.780
95 % C.I.		0.5	0.37	0.05	0.028	0.030
4e	48 + 4	4.60	16.62	3.565	1.195	1.78
95 % C.I.		0.32	0.16	0.029	0.022	0.04
5e	48 + 5	4.78	16.93	3.50	1.206	1.78
95 % C.I.		0.28	0.23	0.04	0.024	0.09

Table 13 – Average values of the blank measurements for the 12 samples in ppb. The partitioning of the blank to the signals given as well as the percentage of the average signal.

	^7Li (ppb)	^{23}Na (ppb)	^{24}Mg (ppb)	^{25}Mg (ppb)	^{43}Ca (ppb)	^{48}Ca (ppb)	^{87}Sr (ppb)	^{88}Sr (ppb)	^{137}Ba (ppb)
Blank	D.L.	39	1.1	D.L.	172	176	0.35	0.67	0.13
Average	0.084	961	214.8	203	98 939	101 745	264.78	255.74	0.62
% of average	NA	4.02	0.50	NA	0.17	0.17	0.13	0.26	20.4

3.4 Discussion

Li/Ca ratios showed an initial decrease after 1 hour of bleaching and remained more or less constant after that. Additional bleaching after 48 hours of initial bleaching did not lead to significant different results. In addition, the concentrations were not significantly different from the treatment without 48 hours of pre-bleaching (cf. 1d to 5d with control 4). To determine whether samples differed significantly a T-test with $T_{(\alpha: 0.05; v: 4)} = 2.78$ was applied. Using four degrees of freedom was allowed because the standard deviations could be combined (table 14).

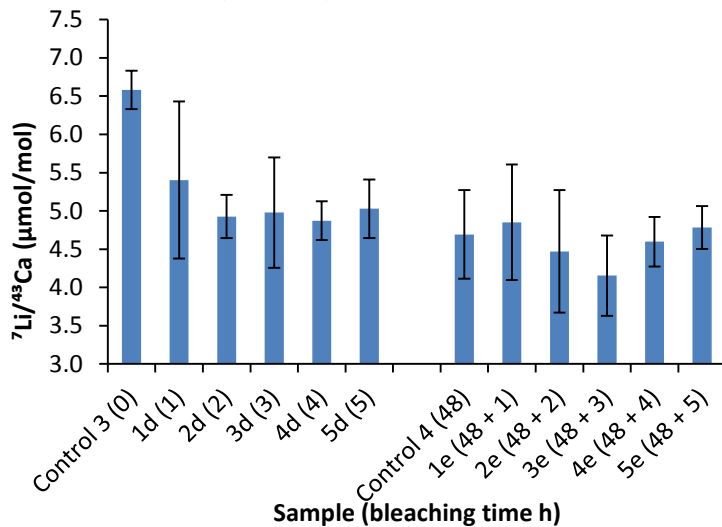


Figure 25 – The Li/Ca ratio for each sample. Sample names are shown with their bleaching time in brackets. Deviations are the 95 % confidence intervals.

Again Na/Ca was higher for all samples that had been in contact with the bleach. The control sample already has almost 1 mmol/mol more sodium than previous experiment. Although it looked as if the second series had lower ratios, none of the tests (table 14) were significantly different. Consequently, bleaching increases the sodium concentration in the sample, independent of the cleaning method used, and the data cannot be used. All values are beyond the calibration line which goes up to 2.3 mmol/mol Na/Ca.

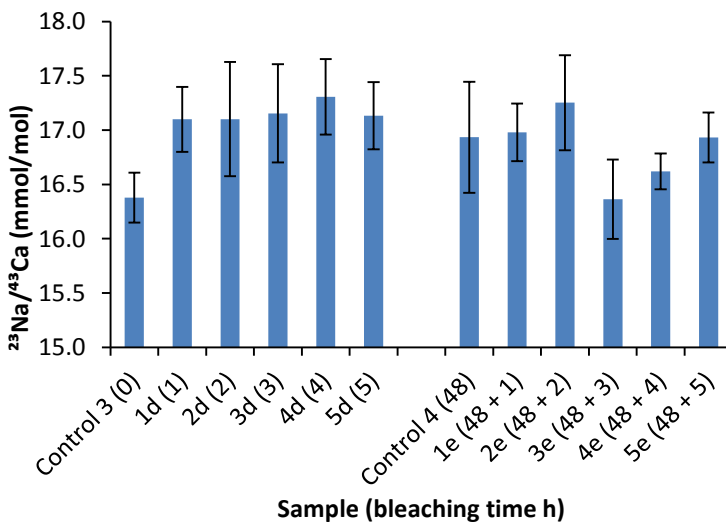


Figure 26 – The Na/Ca ratio for each sample. Sample names are shown with their bleaching time in brackets. Deviations are the 95 % confidence intervals.

3 – Effects of bleaching times on a single size fraction

Mg/Ca demonstrates a clear impact of pre-bleaching. Without the additional pre-bleaching for 48 hours, the ratio for all samples (1d to 5d) was significantly lower than the control (control 1) and not significantly different from each other. Apparently, one hour of bleaching is sufficient for Mg. The other series (control 2 to 5e) did not change significantly between samples. However when compared to the first series, a significant difference could be found. This would indicate that only removal of the periostracum is needed for Mg/Ca.

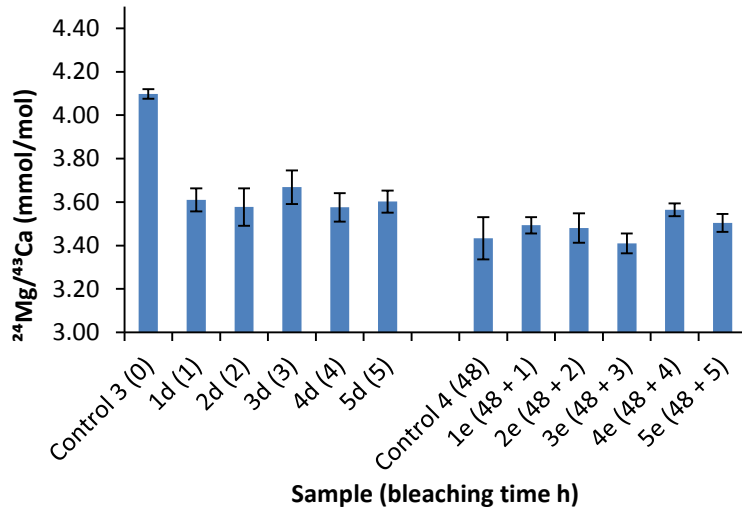


Figure 27 – The Mg/Ca ratio for each sample. Sample names are shown with their bleaching time in brackets. Deviations are the 95 % confidence intervals.

Strontium shows a steady decrease with increasing bleaching time at first. For the second series it is more or less stable and without significant differences between the samples. This shows that most of the organic strontium is not located within the shell, but in the periostracum. This conclusion is substantiated by the fact that after removal of the periostracum (control 4), no significant changes are observed when the sample is bleached again as a powder.

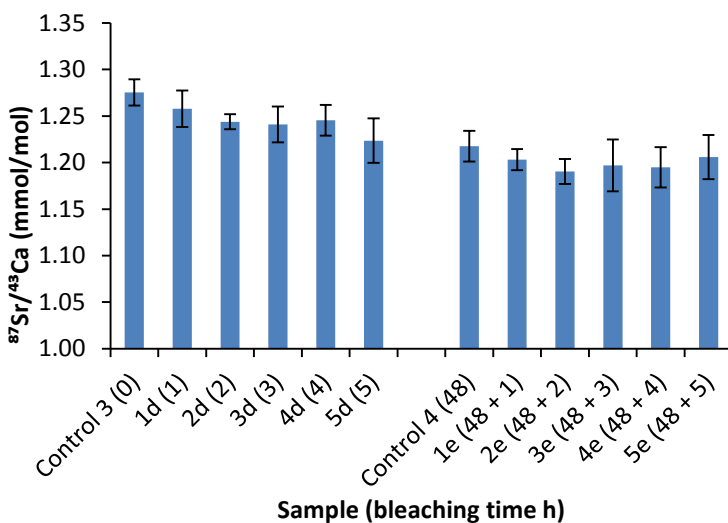


Figure 28 – The Sr/Ca ratio for each sample. Sample names are shown with their bleaching time in brackets. Deviations are the 95 % confidence intervals.

3 – Effects of bleaching times on a single size fraction

There is not a significant change of the Ba/Ca ratio over either the first or second series. In between the series, a small significant difference can be found. However all Ba/Ca ratios are sensitive to the relatively high background signal found in the blank. Even so, figure 29 suggests, again, that most of the organic barium is contained in the periostracum. Table 14 shows the results of the T-tests. The asterisk indicates that the F-test showed that standard deviations of the two samples differed significantly. Thus they were not allowed to be combined so another set of equations was used to do a T-Test:

$$F_{calc} > F_{(\alpha: 0.05; v=2,2)} \rightarrow t_{calc} = \frac{|\bar{x}_a - \bar{x}_b|}{\sqrt{\frac{s_a^2}{n_a} + \frac{s_b^2}{n_b}}}$$

For the T_{test} value, the degrees of freedom had to be calculated by:

$$v = \frac{\left(\frac{s_a^2}{n_a} + \frac{s_b^2}{n_b}\right)^2}{\frac{(s_a^2/n_a)^2}{n_a + 1} + \frac{(s_b^2/n_b)^2}{n_b + 1}} - 2 = 2$$

Where v is the degrees of freedom for the T_{test} value, s the standard deviations for the cycles and n the amount of measurements/cycles. From these equations it follows that $T_{(\alpha: 0.05; v: 2)} = 4.30$. T_{calc} was 0.94 so samples control 4 and 5e did not differ significantly.

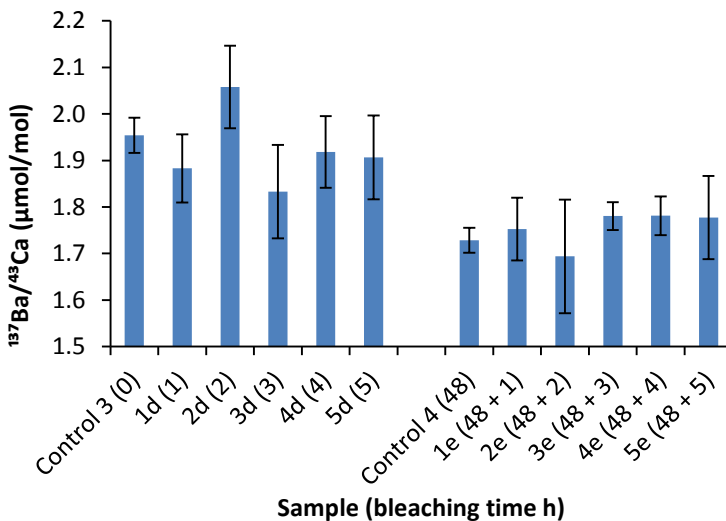


Figure 29 – The Ba/Ca ratio for each sample. Sample names are shown with their bleaching time in brackets. Deviations are the 95 % confidence intervals.

3 – Effects of bleaching times on a single size fraction

Table 14 – Overview of which samples differed significantly (95 %) for the five elements. The asterisk denotes that standard deviations could not be combined, so a different formula was used for the T-test. ‘Sign. Diff.’ means significant difference and ‘Same’ means there was no significant difference found between the two tested samples.

Tested	⁷ Li	²³ Na	²⁴ Mg	⁸⁷ Sr	¹³⁷ Ba
Control 3 - 1d	Sign. Diff.	Sign. Diff.	Sign. Diff.	Sign. Diff.	Sign. Diff.
1d - 5 d	Same	Same	Same	Sign. Diff.	Same
5d - control 4	Same	Same	Sign. Diff.	Same	Sign. Diff.
Control 4 - 5e	Same	Same	Same	Same	Same*

Taking one size fraction helped to reduce deviations between the samples. The effects of different bleaching times and methods became more pronounced than during the previous experiment. This is probably because all samples are more homogeneous now. However how good the samples were fractionated is not sure since the powder readily formed conglomerates that did not break apart easily.

3.5 Conclusion

Using a restricted size fraction helped to reduce the variability between samples and produced a more distinct patterns. Lithium, magnesium and strontium showed a similar pattern: an initial drop in Me to calcium ratio and no further change when bleaching time increased. No further change after the periostracum has been removed suggests that most metals within the organics are located in the periostracum. No significant amounts of metals are incorporated in the organics enclosed within the composite shell, i.e. are associated with the growth bands of the shell. Interestingly, barium showed a more pronounced reaction to a different bleaching method this time. This could mean that barium perhaps needs more time to be removed from the periostracum or that leaching within the calcite/aragonite occurred. Still, these values should be taken with caution because the blank values were relatively high. The amount of sodium again increased, as in the previous experiment, to values far outside the calibration range. Cleaning the sample an additional five times did not prevent sodium from increasing. These high values also increased the deviations, so it is difficult to draw more conclusions about this.

Another way of investigating how particle size affects bleaching is, is to use one method of bleaching for different size fractions. This was done in the next experiment.

4 – Effects of size fractionation on a single bleaching method

4.1 Introduction

Here, three different size fractions were taken and bleached using a fixed bleaching time for all samples. These were then analyzed to see the effect of size fractionation.

4.2 Materials and methods

The materials needed for this experiment where:

- 1.5 ml Safe-lock tubes
- 50 ml sample tube
- Two valves of a mussel shell
- Drying oven
- Centrifuge
- Pestle and Mortar
- Spectro MS ICP-MS
- NaOCl (Acros Organics; 10 – 15 %; CAS#: 7681-52-9)
- HCl (1N; CAS#: 7647-01-0)
- HNO₃ (2 %; CAS#: 7697-37-2)
- Ultrasonic bath
- Milli-Q water
- Two sieves (100 and 63 μm)
- Calibration and tuning standards

A single bivalve grown at a pCO₂ of 390 μatm was put into 10 ml bleach for 24 hours, sonicated for 10 minutes after which the bleach was replaced with a new 10 ml of bleach. After another 24 hours, the shell was sonicated 10 minutes and rinsed five times with plenty of MQ. The two valves were then dried in an oven at 50 °C, crushed and sieved over 2 sieves of 100 and 63 μm. 6 mg of each of the three fractions were then put in three 1.5 ml vials each (for triplicates). These nine samples and a blank were then all bleached for five hours. After bleaching the samples were washed 5 times with boron free MQ. After drying overnight on a 60 °C hotplate, the samples were weighed and dissolved in 500 μl 1 N HCl. Aliquots were taken according to table 15 and diluted into 2 ml 2 % HNO₃.

Table 15 – Samples where dissolved in 500 μl 1 N HCl what resulted in the listed Ca concentrations. An aliquot of listed volume was taken and diluted in 2 ml 2 % HNO₃ to obtain a solution with a 100 ppm Ca concentration.

Sample	Sample (mg)	Ca concentration (ppm)	Aliquot for 100 ppm Ca in 2 ml 2 % HNO ₃ (μl)
Large 1	5.4	4 281	46.7
Large 2	3.9	3 100	64.5
Large 3	4.5	3 547	56.4
Medium 1	4.7	3 713	53.9
Medium 2	2.9	2 319	86.2
Medium 3	2.4	1 892	105.7
Small 1	2.4	1 906	104.9
Small 2	4.4	3 480	57.5
Small 3	5.2	4 156	48.1
Blank	0	NA	70.0

For analysis, the Spectro MS was optimized (settings in table 16). Concentrations of the calibration standards can be found in table 35.

4 – Effects of size fractionation on a single bleaching method

Table 16 – Experimental conditions and instrument settings

Parameter	Setting
Plasma Torch	Quartz
Nebulizer	PFA Micro-flow
Spray chamber	Quartz cyclonic spray chamber
Cones	Platinum
Power	1 570 W
Coolant gas	12 l/min
Auxiliary gas	2.70 l/min
Nebulizer gas	0.66 l/min
Cycles	3
Integration time	20 s

4.3 Results

The powder formed conglomerates again so the middle size fraction (<100 μm and >63 μm) could still have particles <63 μm . Me/Ca ratios are given in table 17 with a 95 % C.I. and values for the blank in table 18. 95 % confidence intervals were this time calculated with $n=9$ and $v=8$, as each size fraction was analyzed in triplicate and was measured with 3 cycles on the ICP-MS.

Table 17 – Me/Ca ratios for ${}^7\text{Li}$, ${}^{23}\text{Na}$, ${}^{24}\text{Mg}$, ${}^{87}\text{Sr}$ and ${}^{137}\text{Ba}$ along with their 95 % confidence intervals.

Sample	${}^7\text{Li}/{}^{43}\text{Ca}$ ($\mu\text{mol/mol}$)	${}^{23}\text{Na}/{}^{43}\text{Ca}$ (mmol/mol)	${}^{24}\text{Mg}/{}^{43}\text{Ca}$ (mmol/mol)	${}^{87}\text{Sr}/{}^{43}\text{Ca}$ (mmol/mol)	${}^{137}\text{Ba}/{}^{43}\text{Ca}$ ($\mu\text{mol/mol}$)
Small	240	5.099	1.595	6.53	29.97
	9	0.020	0.005	0.05	0.31
Medium	243	5.10	1.586	6.52	28.4
	22	0.06	0.030	0.05	0.6
Large	265	4.07	2.100	6.11	26.02
	5	0.05	0.029	0.18	0.35

Table 18 – Results of method blank measurements in ppb. The average values for the 12 samples are also given as well as the fraction of the blank from the average.

	${}^7\text{Li}$ (ppb)	${}^{23}\text{Na}$ (ppb)	${}^{24}\text{Mg}$ (ppb)	${}^{25}\text{Mg}$ (ppb)	${}^{43}\text{Ca}$ (ppb)	${}^{48}\text{Ca}$ (ppb)	${}^{87}\text{Sr}$ (ppb)	${}^{88}\text{Sr}$ (ppb)	${}^{137}\text{Ba}$ (ppb)
Blank	D.L.	3.2	0.42	D.L.	1011	D.L.	D.L.	1.8	D.L.
Average	0.14	809	293	283	99 062	102 369	288	290	0.8
% of average	NA	0.40	0.14	NA	1.02	NA	NA	0.61	NA

4 – Effects of size fractionation on a single bleaching method

Figure 30 shows the data from Table 17 normalized against values of the largest size fraction. This clearly shows how the different elements respond to bleaching of a powder of different particle size. Table 19 shows which samples are significantly different from each other. Values with an asterisk did not pass the F-test, indicating that standard deviations were not combined. They have been tested with the equations below (same as in the previous experiment) where $n = 9$, s the standard deviations and the degrees of freedom were calculated for T_{test} using the equation on the right side.

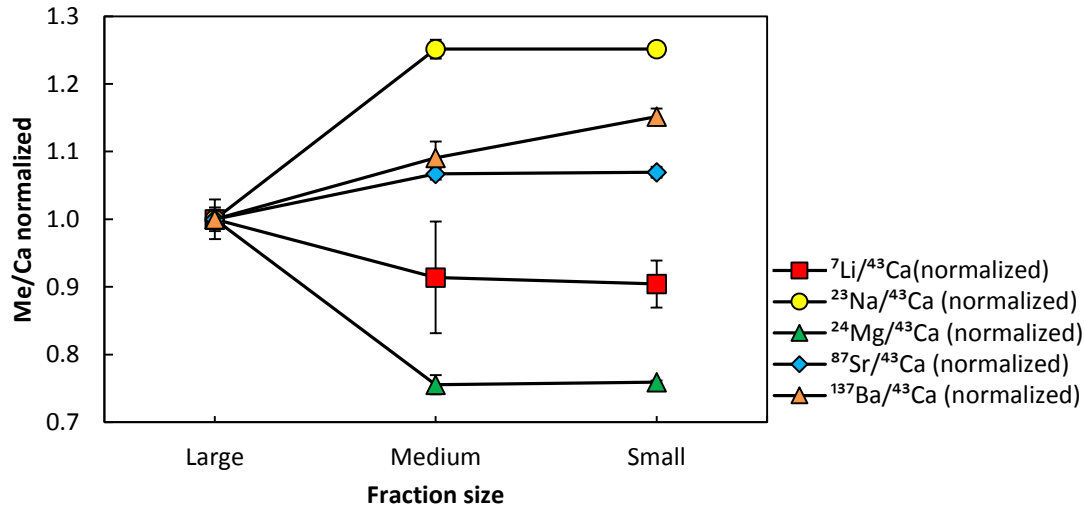


Figure 30 – Me/Ca ratios from table 17 normalized against the largest size fraction. Large: >100 μm ; Medium: <100 – >63 μm ; Small: <63 μm .

Table 19 – Overview of which samples differed significantly (95 %) for the five elements. The asterisk denotes that standard deviations could not be combined, so a different formula was used for the T-test. ‘Sign. Diff.’ means significant difference and ‘Same’ means there was no significant difference found between the two tested samples.

Tested	${}^7\text{Li}$	${}^{23}\text{Na}$	${}^{24}\text{Mg}$	${}^{87}\text{Sr}$	${}^{137}\text{Ba}$
Large to medium	Sign. Diff.*	Sign. Diff.	Sign. Diff.	Sign. Diff.*	Sign. Diff.
Medium to small	Same*	same*	Same*	Same	Sign. Diff.
Large to small	Sign. Diff.	Sign. Diff.*	Sign. Diff.*	Sign. Diff.*	Sign. Diff.

$$t_{calc} = \frac{|\bar{x}_a - \bar{x}_b|}{\sqrt{\frac{s_a^2}{n_a} + \frac{s_b^2}{n_b}}} \quad \& \quad v = \frac{\left(\frac{s_a^2}{n_a} + \frac{s_b^2}{n_b}\right)^2}{\frac{(s_a^2/n_a)^2}{n_a + 1} + \frac{(s_b^2/n_b)^2}{n_b + 1}} - 2$$

4.4 Discussion

Figure 30 clearly shows how the element concentration depend on the size fraction analyzed. Most elements do not show a significant difference between the medium and small size fraction. This can probably be attributed to the fact that sieving of the powder was not completely successful. Although ^{137}Ba does show a difference, this may partly be caused by a higher background signal that was discussed in chapter 3. The different behavior for the elements can't arise from the removal of the periostracum, since it was removed for all fractions. It can therefore be attributed to three other reasons. First, there is the effect of removing organic material within the calcite and aragonite that is either depleted or enriched in a certain element (depending on whether it increases or decreases). Second, because the particles are increasingly smaller, surface area increases, thus more elements could be leached from the calcium carbonate. And finally, the powder will also have more surface area that can be contaminated by the bleach. It is very difficult to distinguish between these causes and it's most likely a combination of the three. Therefore, for final cleaning procedure to be used, the choice was made to only remove the periostracum by putting a whole valve in bleach for 48 hours. This minimizes the possible effects of contamination, leaching or removal of organically complexed elements that are difficult to quantify.

4.5 Conclusion

Size fractionation was not successful, as the middle fraction exhibited the same behavior as the smallest one. However, a difference that was visible between the large and middle/small fraction which is likely caused by a combination of: contamination by NaOCl, leaching of elements within the calcite and aragonite and removal of organically complexed elements. Since these individual processes are difficult to quantify, the choice was made to only remove the periostracum for following cleaning procedures.

5 – Stability of dissolved samples and inter-/intra-variability between valves and bivalves

5.1 Introduction

Samples from the first experiment (chapter 2) were kept dissolved in 1 N HCl and stored. After 99 days they were analyzed again to see if and how much Me/Ca ratios change over time. Simultaneously, another experiment was carried out on 4 bivalves (8 single valves). The valves were measured separately to see if ratios differ between the left and right valve, and to quantify differences between individual bivalves from the same experimental treatment.

5.2 Materials and methods

- 1.5 ml Safe-lock tubes
- 50 ml sample tube
- Two valves of a mussel shell
- Drying oven
- Centrifuge
- Pestle and Mortar
- Spectro MS ICP-MS
- NaOCl (Acros Organics; 10 – 15 %; CAS#: 7681-52-9)
- HCl (MERK; 1N; CAS#: 7647-01-0)
- HNO₃ (MERK; 1N; CAS#: 7697-37-2)
- Ultrasonic bath
- Milli-Q water
- Calibration and tuning standards

The same dilution method as described in chapter 2 was used to test the stability of dissolved samples over time. Experimental conditions are shown in table 20.

Four bivalves were split from pCO₂ 390 µatm, bleached for 48 hours and crushed. Approximately 10 mg from each of the 8 samples were divided over three 1.5 ml vials (triplicates). These 24 samples were washed 5 times and dissolved in 400 µl 1 N HCl and diluted following the same protocol of the other experiments. Results for dilutions are shown in table 21. For sample names: 1Lb, stands for the second subsample “b” from the first “1” left “L” bivalve and so on. Experimental settings are shown in table 22. Concentrations for calibrations are shown in table 36 and table 37.

Table 20 – Experimental conditions and instrument settings.

Parameter	Setting
Plasma Torch	Quartz
Nebulizer	PFA Micro-flow
Spray chamber	Quartz cyclonic spray chamber
Cones	Platinum
Power	1 560 W
Coolant gas	12 l/min
Auxiliary gas	2.70 l/min
Nebulizer gas	0.66 l/min
Cycles	3
Integration time	20 s

5 – Stability of dissolved samples and inter-/intra-variability between valves and bivalves

Table 21 – Samples where dissolved in 400 µl 1 N HCl what resulted in the listed Ca concentrations. An aliquot of listed volume was taken and diluted in 2 ml 2 % HNO₃ to obtain a solution with a 100 ppm Ca concentration.

Sample	Sample (mg)	Ca concentration (ppm)	Aliquot for 100 ppm Ca in 2 ml 2 % HNO ₃ (µl)
1La	10.0	4 943	40.5
1Lb	10.0	4 943	40.5
1Lc	9.8	4 846	41.3
1Ra	9.9	4 894	40.9
1Rb	9.8	4 846	41.3
1Rc	10.2	5 041	39.7
2La	10.0	4 943	40.5
2Lb	10.8	5 333	37.5
2Lc	9.9	4 894	40.9
2Ra	10.2	5 041	39.7
2Rb	10.1	4 992	40.1
2Rc	10.3	5 090	39.3
3La	9.6	4 748	42.1
3Lb	10.1	4 992	40.1
3Lc	10.6	5 236	38.2
3Ra	9.5	4 699	42.6
3Rb	10.6	5 236	38.2
3Rc	10.9	5 382	37.2
4La	9.6	9 384	21.3
4Lb	10.2	9 956	20.1
4Lc	10.5	10 242	19.5
4Ra	9.9	9 671	20.7
4Rb	10.4	10 147	19.7
4Rc	9.9	9 671	20.7

Table 22 – Experimental conditions and instrument settings.

Parameter	Setting
Plasma Torch	Quartz
Nebulizer	PFA Micro-flow
Spray chamber	Quartz cyclonic spray chamber
Cones	Platinum
Power	1 570 W
Coolant gas	12 l/min
Auxiliary gas	2.70 l/min
Nebulizer gas	0.66 l/min
Cycles	3
Integration time	20 s

5.3 Results

Data of all single measurements are shown in table 23. Individual analyses can be found in appendix 2. Figure 25 and table 24 show the average for 7 elements of the 12 samples along with their 95% confidence intervals (the averaged data from appendix 2). Measured blank values for both experiments were mostly below DL or less than 1 % of the average concentration. ^{7}Na was again outside the calibration range and was linearly extrapolated.

Table 23 – Me/Ca ratios for ^{23}Na , ^{24}Mg , ^{25}Mg , ^{48}Ca , ^{87}Sr , ^{88}Sr and ^{137}Ba along with their 95 % confidence intervals.

Name	$^{23}\text{Na}/^{43}\text{Ca}$ (mmol/mol)	$^{24}\text{Mg}/^{43}\text{Ca}$ (mmol/mol)	$^{25}\text{Mg}/^{43}\text{Ca}$ (mmol/mol)	$^{48}\text{Ca}/^{43}\text{Ca}$ (mol/mol)	$^{87}\text{Sr}/^{43}\text{Ca}$ (mmol/mol)	$^{88}\text{Sr}/^{43}\text{Ca}$ (mmol/mol)	$^{137}\text{Ba}/^{43}\text{Ca}$ ($\mu\text{mol/mol}$)
Control 1	13.03	4.59	4.03	1.0123	0.818	1.04347	2.18
95 % C.I.	0.26	0.06	0.13	0.0014	0.007	0.00027	0.32
1a	13.17	4.282	3.81	1.016	0.821	1.072	2.19
95 % C.I.	0.25	0.035	0.20	0.004	0.006	0.014	0.20
2a	13.47	4.141	3.70	1.013	0.816	1.056	2.28
95 % C.I.	0.20	0.008	0.09	0.006	0.014	0.020	0.16
3a	13.62	4.30	3.79	1.0117	0.801	1.031	2.08
95 % C.I.	0.23	0.05	0.14	0.0024	0.009	0.007	0.16
4a	13.71	4.422	3.90	1.012	0.817	1.051	2.029
95 % C.I.	0.23	0.037	0.13	0.005	0.010	0.010	0.011
5a	14.50	4.17	3.67	1.0114	0.880	1.088	2.072
95 % C.I.	0.37	0.04	0.16	0.0025	0.016	0.018	0.030
Control 2	13.01	4.348	3.830	1.027	0.872	1.036	2.18
95 % C.I.	0.20	0.032	0.013	0.005	0.006	0.013	0.36
1b	13.75	3.98	3.506	1.0121	0.841	1.063	2.23
95 % C.I.	0.30	0.06	0.029	0.0023	0.012	0.009	0.21
2b	14.07	3.913	3.38	1.017	0.808	1.014	2.01
95 % C.I.	0.28	0.035	0.18	0.005	0.005	0.020	0.19
3b	14.08	4.045	3.50	1.0198	0.827	1.020	2.14
95 % C.I.	0.17	0.027	0.15	0.0024	0.009	0.010	0.13
4b	13.55	4.193	3.69	1.0254	0.8431	1.029	2.13
95 % C.I.	0.21	0.028	0.08	0.0016	0.0016	0.007	0.21
5b ⁺	14.18	4.09	3.596	1.0317	0.845	1.018	2.12
95 % C.I.	0.16	0.04	0.036	0.0034	0.013	0.018	0.27

Table 24 – Average change in Me/Ca ratios after storage for 99 days in a closed 1.5 ml vial, dissolved in 1 N HCl.

	$^{23}\text{Na}/^{43}\text{Ca}$ (mmol/mol)	$^{24}\text{Mg}/^{43}\text{Ca}$ (mmol/mol)	$^{25}\text{Mg}/^{43}\text{Ca}$ (mmol/mol)	$^{48}\text{Ca}/^{43}\text{Ca}$ (mol/mol)	$^{87}\text{Sr}/^{43}\text{Ca}$ (mmol/mol)	$^{88}\text{Sr}/^{43}\text{Ca}$ (mmol/mol)	$^{137}\text{Ba}/^{43}\text{Ca}$ ($\mu\text{mol/mol}$)
Average	-5.5	-3.0	-9.3	3.2	-21.8	-4.6	-6.3
95 % C.I.	0.75	0.34	0.51	0.49	1.95	0.83	1.63

5 – Stability of dissolved samples and inter-/intra-variability between valves and bivalves

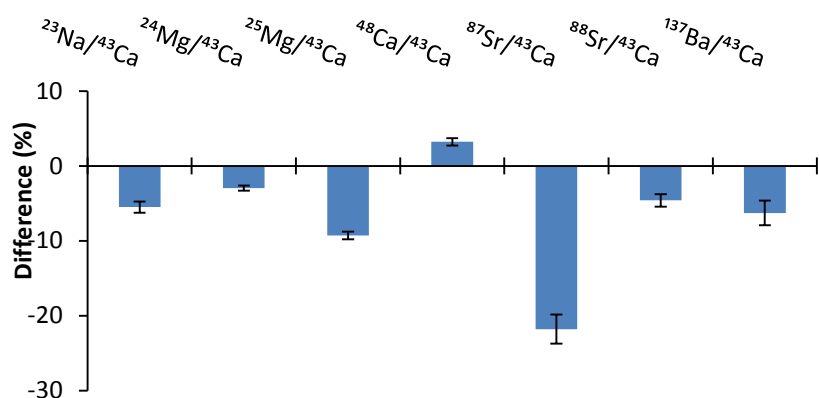


Figure 31 – Average change in Me/Ca ratios after storage for 99 days in a closed 1.5 ml vial, dissolved in 1 N HCl.

All values in table 24 changed significantly compared to the Me/Ca ratios at the start.

Results from the inter-/intra-variability tests are shown in table 25 and in figure 32. An overview of the significance is listed in table 26.

Table 25 – Me/Ca ratios for ^7Li , ^{23}Na , ^{24}Mg , ^{87}Sr and ^{137}Ba along with their 95 % confidence intervals.

Sample	$^7\text{Li}/^{43}\text{Ca}$ ($\mu\text{mol}/\text{mol}$)	$^{23}\text{Na}/^{43}\text{Ca}$ (mmol/mol)	^{24}Mg (mmol/mol)	$^{87}\text{Sr}/^{43}\text{Ca}$ (mmol/mol)	$^{137}\text{Ba}/^{43}\text{Ca}$ ($\mu\text{mol}/\text{mol}$)
Right 1	6.0	13.3	4.84	0.885	1.76
95 % C.I.	0.5	0.4	0.13	0.008	0.14
Left 1	6.1	13.67	4.83	0.853	1.73
95 % C.I.	0.9	0.32	0.12	0.011	0.06
Right 2	6.27	13.40	4.03	0.9331	1.732
95 % C.I.	0.20	0.18	0.04	0.0031	0.034
Left 2	6.33	13.22	4.04	0.9402	1.727
95 % C.I.	0.37	0.11	0.05	0.0038	0.023
Right 3	5.70	13.17	3.89	1.0019	1.890
95 % C.I.	0.32	0.14	0.04	0.0036	0.035
Left 3	5.53	13.03	3.965	0.998	1.959
95 % C.I.	0.25	0.12	0.033	0.004	0.029
Right 4	7.28	13.04	4.331	1.062	2.014
95 % C.I.	0.25	0.13	0.029	0.004	0.029
Left 4	7.39	13.08	4.390	1.029	2.052
95 % C.I.	0.31	0.11	0.024	0.006	0.023

5 – Stability of dissolved samples and inter-/intra-variability between valves and bivalves

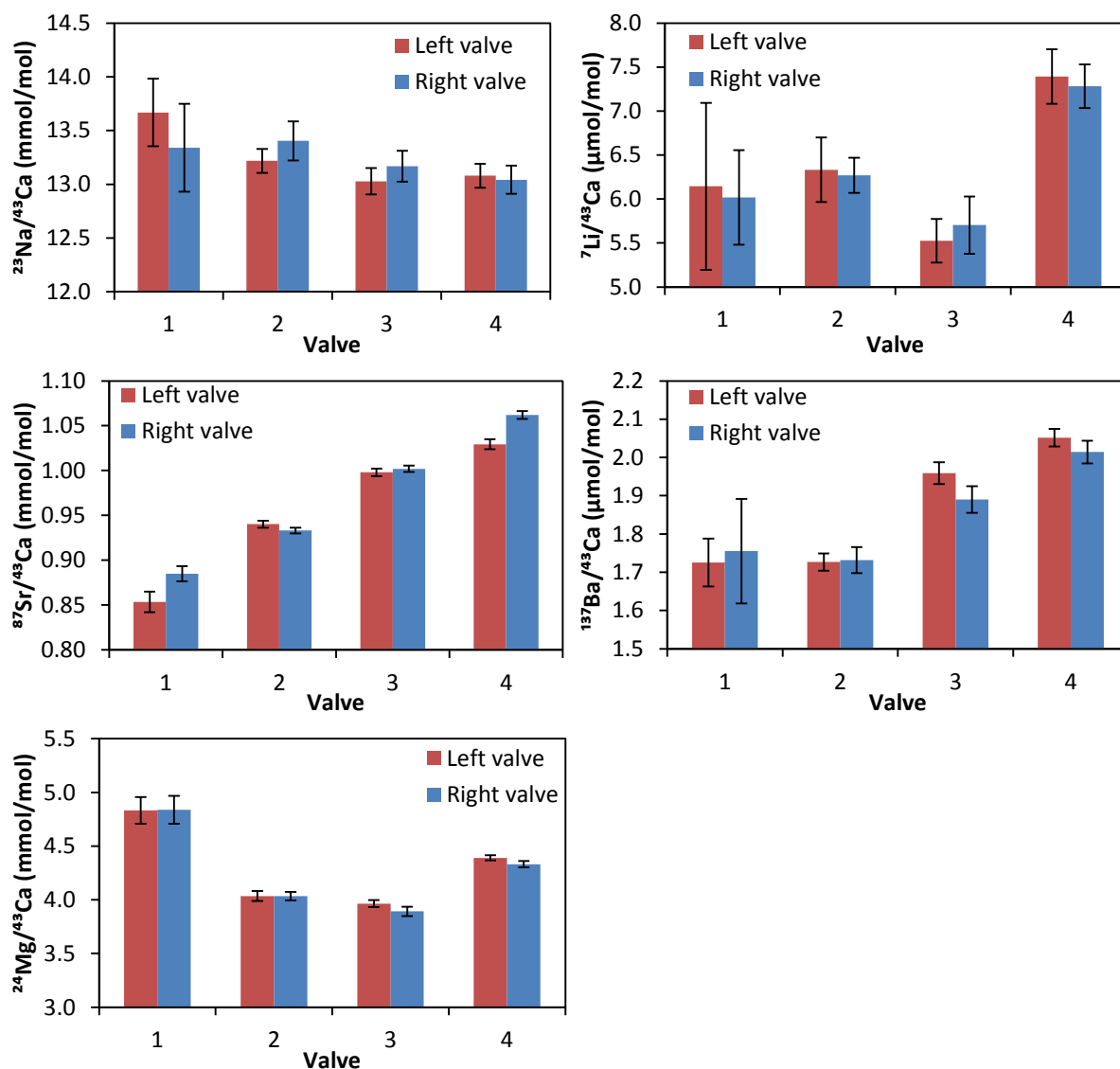


Figure 32 – Variability of Me/Ca ratios between valves of four different bivalves from the same experimental treatment.

Table 26 – Overview of which elements differed significantly (95 %) between valves of a single bivalve. The asterisk denotes that standard deviations could not be combined, so a different formula was used for the T-test. ‘Sign. Diff.’ means significant difference and ‘Same’ means there was no significant difference found between the two tested samples.

Tested	^7Li	^{23}Na	^{24}Mg	^{87}Sr	^{137}Ba
Left 1 – Right 1	Same	Sign. Diff.	Same	Sign. Diff.	Same*
Left 2 – Right 2	Same	Same	Same	Sign. Diff.	Same
Left 3 – Right 3	Same	Same	Sign. Diff.	Same	Sign. Diff.
Left 4 – Right 4	Same	Same	Sign. Diff.	Sign. Diff.	Sign. Diff.

To evaluate if the Me/Ca ratios differed between bivalves, the 4 right valves were compared to each other. The relative standard deviations for these 4 values were calculated to be: Li: 0.11, Na: 0.012, Mg: 0.09, Sr: 0.08, Ba: 0.07.

5.4 Discussion

All measured elements, except for ^{48}Ca show a decrease in Me/Ca ratio. Part of these changes can be attributed to loss of ^{43}Ca which is used to calculate ratios. Remaining losses are due to the element specific volatility. Evaporation of only the solute (HNO_3) should not produce any changes, since elemental ratios would not change. The heavier isotopes of Ca and Mg do not change as much as their lighter sister isotopes, indicating that because of their difference in vibrational energy, the elements are less prone to evaporation or adsorption onto the vial. Magnesium does not exhibit this trend, thus ^{25}Mg is possibly stronger adsorbed onto the vial. All elements show an overall decrease (except ^{48}Ca), since Ca is the most stable of the measured elements. However, the magnitude of change for ^{87}Sr compared to other elements is remarkable and not understood. This shows that stability of elements is complex and is likely affected by a variety of factors such as: stability (with regard to melting point), adsorption onto vial walls, concentration effects and, possibly, the place of storage. Another factor that is important for all element ratios is the sensitivity of the instrument. After tuning, responses for certain elements may be slightly different giving rise to concentrations a few percentage higher or lower.

Figure 32 shows that variability within valves of a single bivalve differ only slightly. Although table 26 shows that 8 out of 20 tests differed significantly. It can be seen in table 25 that these differences are still very small, the largest difference is for bivalve 3 for lithium. The Li/Ca ratio is 3.2 % lower than the right valve (also lithium is very close to the DL, it may be affected by noise more than the other elements). Thus differences can be found between valves but they are almost negligible for most purposes.

The differences between bivalves, however, are more evident, and up to 11 % for Li. These differences were to be expected since species have different genetics, different physiologies and probably slightly different ambient environmental conditions in their microenvironment. Since these factors will be more pronounced in a natural environment, it is crucial to combine multiple bivalves for analyses.

5.5 Conclusion

After 99 days, Me/Ca ratios changed significantly while being stored in 1 N HCl in a closed 1.5 ml vial. Although this cannot tell much about the “expiration date”, it is clear that dissolved samples should be analyzed as soon as possible to avoid uncontrolled alteration of Me/Ca ratios.

Differences between valves of a single bivalve were very small, largest difference was 3.2 % for lithium. Which is still small and within range of the general precision of an ICP-MS (5 %). Hence, valves grow and incorporate elements in the same way. Variations between species ranged from 1.2 % for Na to 11 % for Li. Differences between valves were expected and are confirmed with this experiment. Hence it is necessary to pool samples together for proxy measurements.

6 – Analysis of valves cultured at four different pCO₂ atmospheres

6.1 Introduction

From each of the four replicates per pCO₂ treatment, 5 bivalves were taken, amounting up to 80 shells (20 per pCO₂ treatment). These valves were split into right and left valves along the hinge; left valves were analyzed for REY and right valves for ⁷Li, ¹¹B, ²⁴Mg, ⁴³Ca, ⁸⁷Sr and ¹³⁷Ba. Boron isotopes were measured on 1 of 3 subsamples from the right valves.

6.2 Materials and methods

The materials needed for this experiment where:

- 1.5 ml Safe-lock tubes
- Pestle and Mortar
- 50 ml sample tube
- 20 bivalves of a mussel shell grown at 390, 1 120, 2 400 and 4 000 μatm
- Drying oven
- Centrifuge
- Spectro MS ICP-MS
- NaOCl (Acros Organics; 10 – 15 %; CAS#: 7681-52-9)
- HCl (1N; CAS#: 7647-01-0)
- HNO₃ (2 %; CAS#: 7697-37-2)
- Ultrasonic bath
- Calibration and tuning standards
- Nu Attom ICP-MS

From each of the four treatments, 20 valves were completely submerged in bleach for 48 hours. The cleaning method was the same as already mentioned in previous chapters. The samples were washed 5 times, dissolved in 1 N HCl and diluted in 2 % HNO₃. From each pooled sample three subsamples were taken for triplicate measurements. Weights and aliquots for dilution are shown in table 27. Concentrations of the calibration solutions are shown in table 38. The sample names show the experimental treatment and the subsample number. For instance, “1120 2” is the second subsample of cultured at a pCO₂ of 1120 μatm.

6 – Analysis of valves cultured at four different pCO₂ atmospheres

Table 27 – Samples where dissolved in 400 µl 1 N HCl what resulted in the given Ca concentration. An aliquot of given volume was taken and diluted in 2 ml 2 % HNO₃ to get a solution with a 100 ppm Ca concentration.

Sample	Sample (mg)	Ca concentration (ppm)	Aliquot for 100 ppm Ca in 2 ml 2 % HNO ₃ (µl)
390 1	6.5	12 603	15.9
390 2	6.6	12 791	15.6
390 3	5.8	11 284	17.7
1120 1	6.2	12 039	16.6
1120 2	4.7	9 193	21.8
1120 3	5.4	10 526	19.0
2400 1	5.8	11 284	17.7
2400 2	6.0	11 662	17.1
2400 3	6.6	12 791	15.6
4000 1	6.5	12 603	15.9
4000 2	5.8	11 284	17.7
4000 2	5.9	11 473	17.4
blanc	0.0	NA	20

Experimental conditions for the Spectro MS and Nu Attom are shown in table 28.

Table 28 – Experimental settings and conditions for the Spectro MS and Nu Attom.

Parameter	Settings Spectro MS	Settings Nu Attom
Plasma Torch	Quartz	Quartz
Nebulizer	PFA Micro-flow	PFA (80 µl)
Spray chamber	Quartz cyclonic spray chamber	Plasma II Cyclon Quartz
Cones	Platinum	Platinum
Power	1 580 W	1 400 W
Coolant gas	12 l/min	13 l/min
Auxiliary gas	2.70 l/min	1.55 l/min
Nebulizer gas	0.67 l/min	45.6 PSI
Cycles	3	5
Integration time	20 s	20 s
Resolution	NA	300

The REY elements were analyzed in the laboratory of Prof. Dr. M. Bau at the Jacobs University, Bremen. Details of the method can be found in [Ponnurangam et al. \(2015\)](#). In short: four samples of 20 left valves each were pooled and measured. The samples were bleached, crushed and digested for 2h at 90 °C in 30 ml Suprapur® HNO₃. Samples were dried and re-dissolved. This solution was diluted, acidified and passed through C¹⁸ cartridges to retain the REY. The use of cartridges removes all elements with relatively low mass. After elution the samples were analyzed on an ICP-MS (Perkin-Elmer/Sciex ELAN DRC-e). Tm was added as an internal standard and therefore not reported. It is common use to report the data normalized against the Post-Archean Australian Shale (PAAS, ([McLennan, 1989](#))).

Hence, for Boron isotope analysis, the first subsample of every pooled sample was analyzed in triplicate. Every measurement was bracketed by measurements of the standard, SRM NIST 951 boric acid. Analyses were carried out by Dr. M. Raitzsch at the Alfred Wegener Institute, Bremerhaven.

6.3 Results

Data from the measurements from the Spectro MS and Nu Attom are reported below in table 29 along with their 95 % C.I. (n=9). Blanks were generally below the DL or less than <2 % of the average values and are therefore insignificant.

Table 29 – Me/Ca ratios for ⁷Li, ²³Na, ²⁴Mg, ⁸⁷Sr, ¹³⁷Ba and ¹¹B along with their 95 % confidence intervals.

Sample	⁷ Li/ ⁴³ Ca (μmol/mol)	²³ Na/ ⁴³ Ca (mmol/mol)	²⁴ Mg (mmol/mol)	⁸⁷ Sr/ ⁴³ Ca (mmol/mol)	¹³⁷ Ba/ ⁴³ Ca (μmol/mol)	¹¹ B/ ⁴³ Ca (μmol/mol)
390 μatm	5.25	15.89	3.764	1.1676	2.168	66.7
95 % C.I.	0.19	0.07	0.013	0.0036	0.033	0.8
1120 μatm	4.41	13.32	4.324	1.099	2.07	52.9
95 % C.I.	0.29	0.07	0.027	0.010	0.05	0.8
2400 μatm	3.98	14.875	4.511	1.170	2.01	47.93
95 % C.I.	0.32	0.039	0.018	0.016	0.05	0.35
4000 μatm	3.75	13.08	4.767	1.113	2.056	42.47
95 % C.I.	0.35	0.08	0.019	0.015	0.038	0.38

Lithium was plotted against the saturation state, since it is expected that both are correlated (figure 33). Strontium ratios (possible proxy for temperature) seemed fairly constant, even though all values were significantly different, variations were only small (on the order of 5 %). However, because the temperature, although varying over the experimental period, were similar for all treatments, the data are not plotted as a function of temperature.

The goal of the experiments is to find a possible proxy for [CO₃²⁻] ions in sea water. However, a proxy for any of the other parameters of the carbonate system would be equally valuable. All Me/Ca ratios were also plotted against pCO₂ (derived from “CO2sys”), pH_{NBS}, DIC, [HCO₃⁻], [CO₃²⁻], [B(OH)₃], [B(OH)₄⁻] and [B(OH)₄⁻]/[HCO₃⁻]. Plotting Me/Ca concentrations against [HCO₃⁻], [CO₃²⁻], [B(OH)₃], [B(OH)₄⁻] and [B(OH)₄⁻]/[HCO₃⁻] results in almost the exact same correlation coefficients (<Δ1 %). This is because all variables are related/connected, such that when one increases, the other increases/decreases and vice versa. This is especially pronounced in carbonate chemistry programs such as CO2sys, which assume equilibrium and do not account for biological fractionation. Therefore, graphs for these variables are omitted except for [CO₃²⁻]. Samples with corresponding variables are show below in table 30.

Below are the graphs which had a correlation coefficient >0.8. These and other graphs, that did not show a good correlation, are reported in appendix 3. Results for ⁷Li are shown in figure 34, for ²⁴Mg in figure 35, ¹³⁷Ba in figure 36 and ¹¹B in figure 37.

6 – Analysis of valves cultured at four different pCO₂ atmospheres

Table 30 – Recap of some parameters of the experimental conditions. *calculated from DIC and pH_{NBS} measurements using CO2SYS. Carbonate ion concentration was calculated later, however since no raw data was available, no SD was calculated.

Treatment	pH _{NBS}	DIC (μmol/kgSW)	pCO ₂ * (μatm)	[CO ₃ ²⁻]* (μmol/kgSW)	Ω calcite*
380 μatm (N=53)	8.03	1 894.1	612	57.15	1.47
SD	± 0.06	± 84.6	± 87		0.28
1 120 μatm (N=53)	7.73	1 953.6	1 254	29.35	0.76
SD	± 0.05	± 93.9	± 146		0.18
2 400 μatm (N=53)	7.46	2 025.0	2 360	16.05	0.42
SD	± 0.07	± 101.7	± 343		0.11
4 000 μatm (N=53)	7.21	2 112.5	4 237	9.11	0.24
SD	± 0.06	± 109.8	± 461		0.07

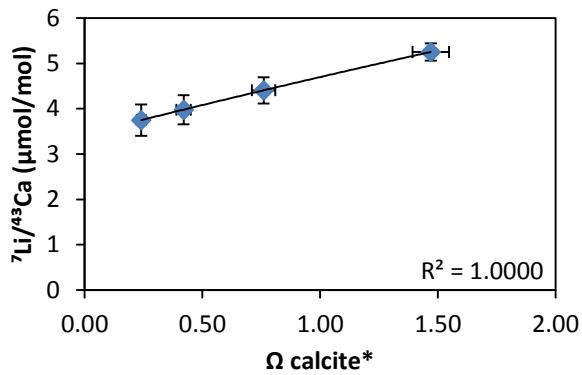


Figure 33 – Li/Ca ratios as a function of calcite saturation state. Vertical (n: 3) and horizontal (n: 53) error bars are given as the 95 % confidence interval.

6 – Analysis of valves cultured at four different pCO₂ atmospheres

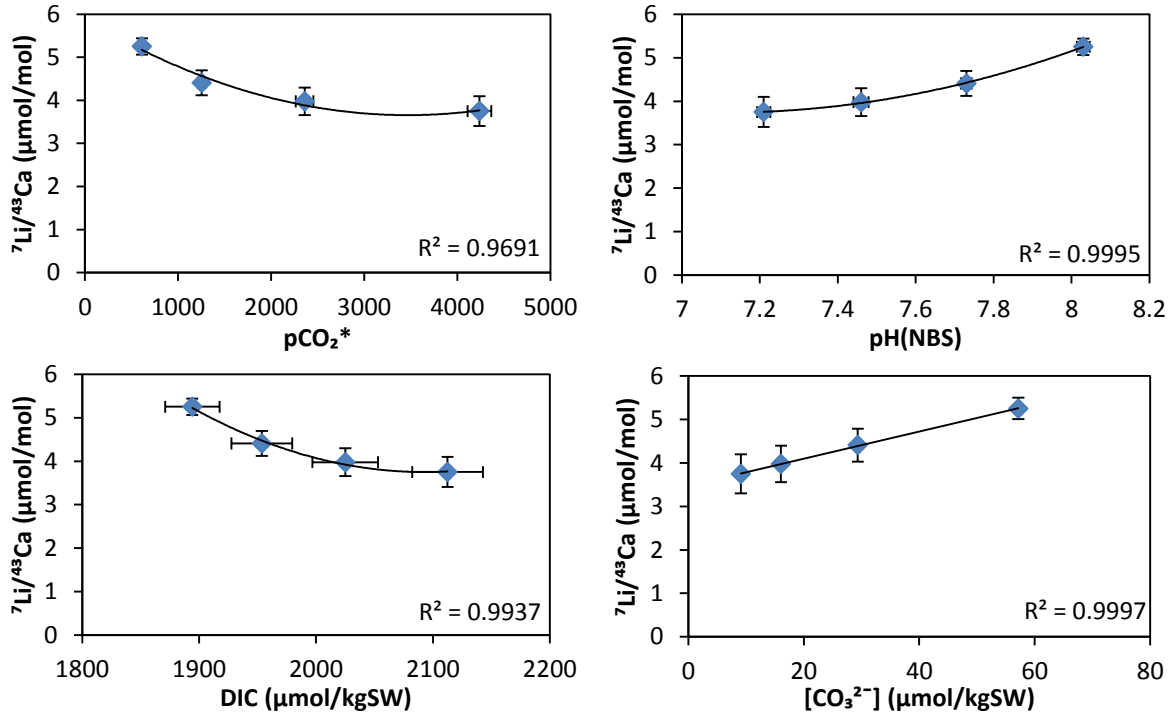


Figure 34 – Li/Ca ratios as a function of pCO₂, pH_{NBS}, DIC (C_T) and [CO₃²⁻]. Vertical (n: 3) and horizontal (n: 53) error bars are given as the 95 % confidence interval except for [CO₃²⁻], which was not available.

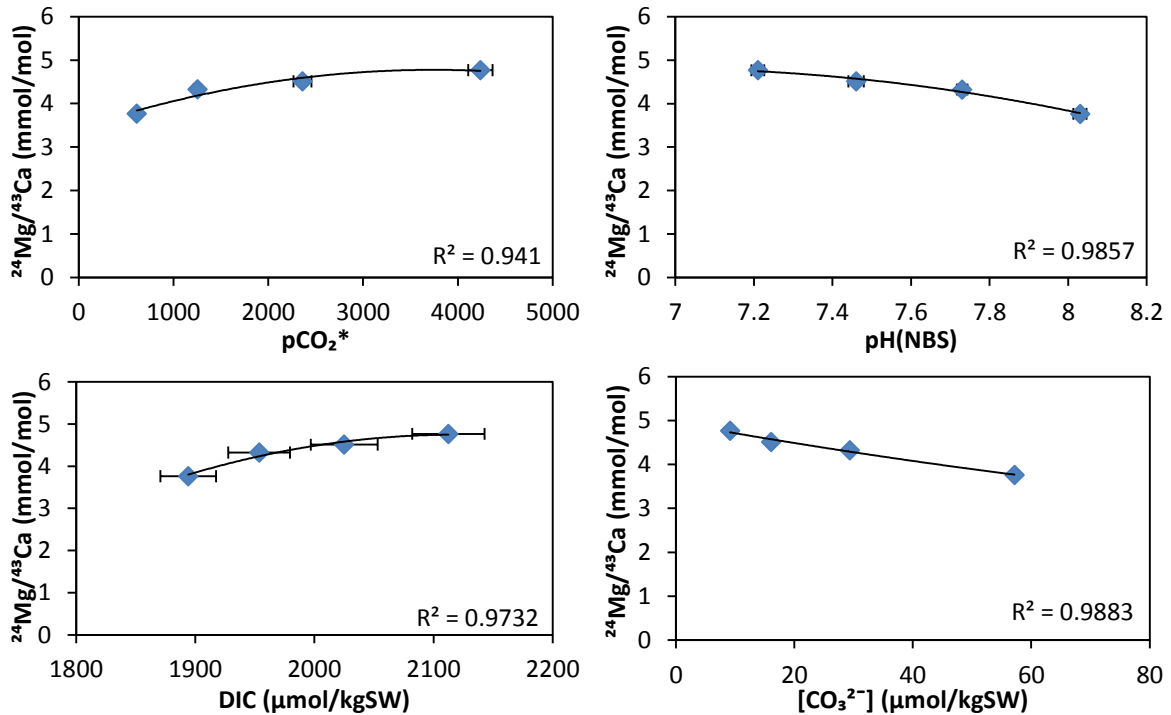


Figure 35 – Mg/Ca ratios as a function of pCO₂, pH_{NBS}, DIC (C_T) and [CO₃²⁻]. Vertical (n: 3) and horizontal (n: 53) error bars are given as the 95 % confidence interval except for [CO₃²⁻], which was not available.

6 – Analysis of valves cultured at four different pCO₂ atmospheres

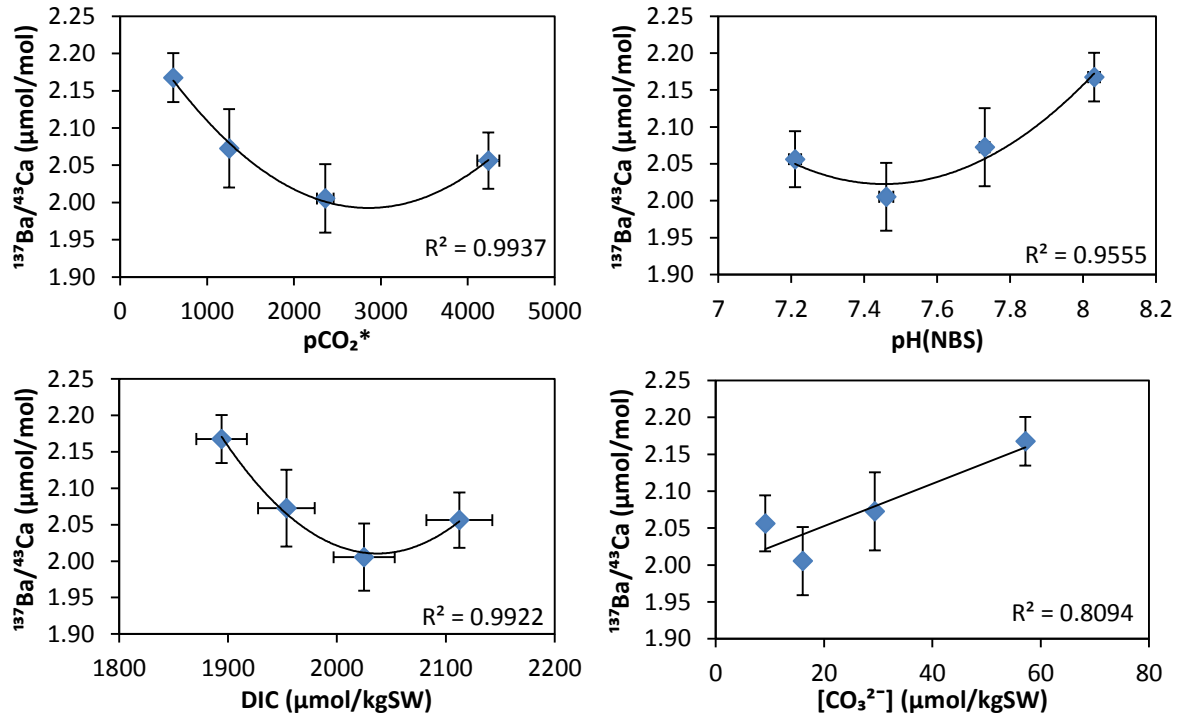


Figure 36 – Ba/Ca ratios as a function of pCO₂, pH_{NBS}, DIC (C_T) and [CO₃²⁻]. Vertical (n: 3) and horizontal (n: 53) error bars are given as the 95 % confidence interval except for [CO₃²⁻], which was not available.

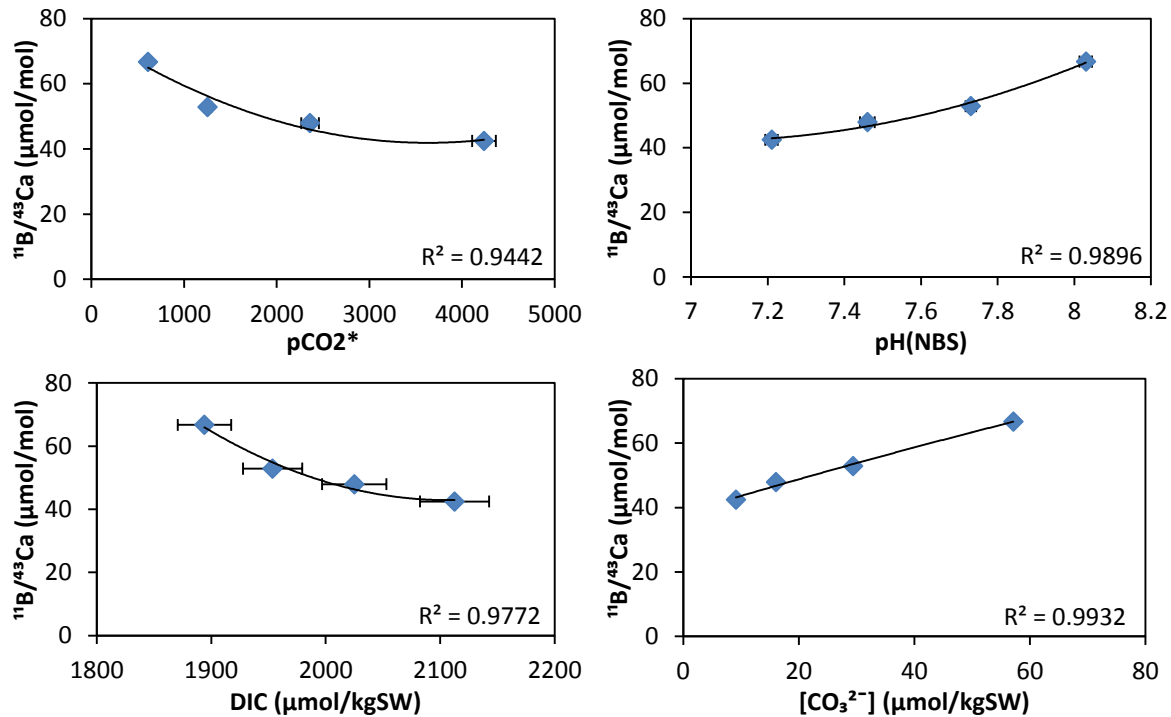


Figure 37 – B/Ca ratios as a function of pCO₂, pH_{NBS}, DIC (C_T) and [CO₃²⁻]. Vertical (n: 3) and horizontal (n: 53) error bars are given as the 95 % confidence interval except for [CO₃²⁻], which was not available.

6 – Analysis of valves cultured at four different pCO₂ atmospheres

Table 31 shows that almost all successive calcium ratios are significantly different from each other. Statistical tests were done again using an F-test and student-t test for n: 9 at 95 %.

Table 31 – Statistical analysis of Me/Ca ratios in the pooled samples.

Tested	⁷ Li	²³ Na	²⁴ Mg	⁸⁷ Sr	¹³⁷ Ba	¹¹ B
390 – 1 120	Sign. Diff.	Sign. Diff.	Sign. Diff.	Sign. Diff.	Sign. Diff.	Sign. Diff.
1 120 – 2 400	Sign. Diff.	Sign. Diff.	Sign. Diff.	Sign. Diff.	Sign. Diff.	Sign. Diff.
2 400 – 4 000	Same	Sign. Diff.	Sign. Diff.	Sign. Diff.	Same	Sign. Diff.

The results for REY analysis are shown in figure 38 and table 32 as PAAS normalized ratios. Data was in good agreement with [Ponnurangam et al. \(2015\)](#). They modelled the REY concentrations and predicted that Y, La, and Gd would have small anomalies. These anomalies are visible in figure 38: It was expected that concentrations would increase and decrease over the mass range of REY, however Ce, Y and Gd do not completely follow this trend. These anomalies are in accordance with [\(Ponnurangam et al., 2015\)](#)

All elements other than REY, Sr and Ba were below the DL, indicating a successful separation using the C¹⁸ cartridges. Yields were between 95 % and 105 %.

Table 32 – PAAS normalized REY concentrations of the four pooled samples.

Element	390 µatm	1 120 µatm	2 400 µatm	4 000 µatm
La	0.52	0.66	0.72	1.38
Ce	0.08	0.17	0.12	0.77
Pr	0.29	0.42	0.42	1.43
Nd	0.31	0.45	0.42	1.51
Sm	0.38	0.55	0.44	2.17
Eu	0.45	0.67	0.52	2.73
Gd	0.66	0.85	0.73	3.02
Tb	0.48	0.68	0.57	2.64
Dy	0.44	0.66	0.56	2.53
Y	1.07	1.44	1.39	3.25
Ho	0.41	0.64	0.59	2.41
Er	0.41	0.60	0.55	2.50
Yb	0.22	0.41	0.32	1.95
Lu	0.20	0.37	0.30	1.90

6 – Analysis of valves cultured at four different pCO₂ atmospheres

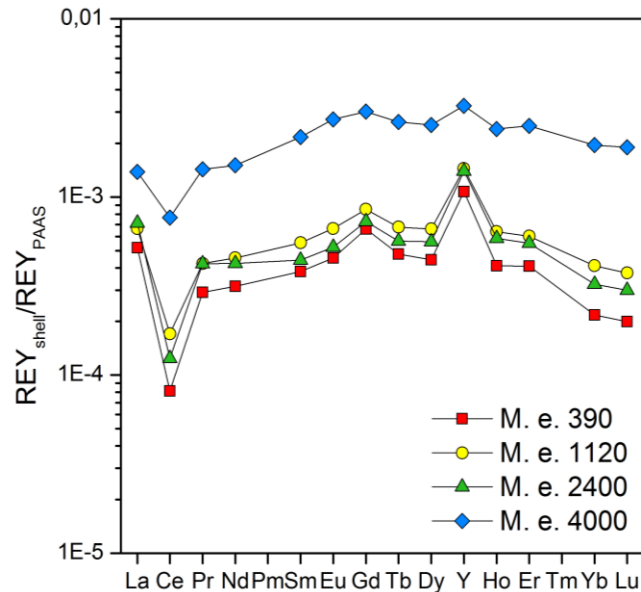


Figure 38 – Results for REY analysis for the four pooled samples with 20 single valves each.

The boron isotope data plotted versus $[\text{CO}_3^{2-}]$ and pH is shown in figure 39. The analysis went well, blanks were low and all deviations were within an acceptable range. Also, concentration-effects on the isotopic ratios were absent. To see whether measurements were significantly different, successive samples were tested again at 95 % confidence interval. It turned out that “390 – 1120” and “2400 – 4000” were not significantly different. “1120 – 4000” however, was significantly different. Even though not all measurements differed significantly, a trend is still clearly visible in the graphs.

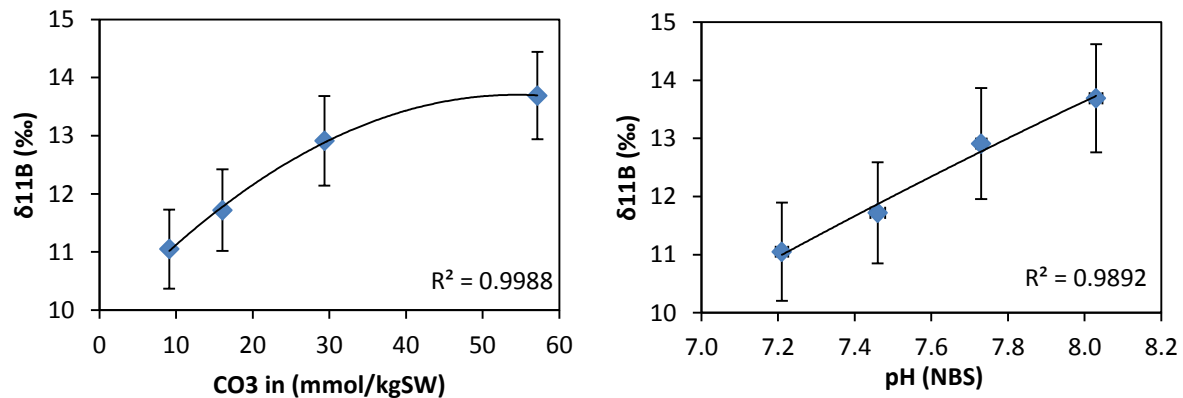


Figure 39 – $\delta^{11}\text{B}$ versus $[\text{CO}_3^{2-}]$ modelled with CO₂sys. Error bars are expressed as 95 % confidence intervals, n: 3 for DB and n: 53 for pH_{NBS}.

6.4 Discussion

Not all measurements of lithium were significantly different, the spread of individual measurements was quite large. This is most likely due to the fact that concentrations were close to the detection limit of the Spectro MS. Nonetheless, a trend was still clearly visible. The data showed an excellent correlation between saturation state and Li/Ca ratio, confirming expectations ([Bryan and Marchitto, 2008](#); [Hall and Chan, 2004](#)). Since all carbonate system parameters are related, a good correlation for Li/Ca versus pCO₂*, pH, DIC and [CO₃²⁻] was also found. To detect the controlling variable, deconvolution experiments are needed, where the different parameters are experimentally decoupled. This was not the focus of the current experiments.

Na/Ca remained fairly constant but a slight decrease in ratios was observed. It is expected to correlate with salinity which varied in a similar way between the different treatments over the course of the experiment. The slight decrease could indicate that Na/Ca ratios are not solely dependent on salinity. Besides a possible co-variation, a contamination from bleach (NaOCl) cannot be excluded. In addition, sodium concentrations were relatively high and outside of the calibration range without bleaching. Hence, these concentrations should be interpreted with caution.

Mg/Ca, a proxy for temperature, showed good correlation also with the carbonate system parameters. So clearly it is not solely dependent on temperature. Since salinity and temperature variations were for the four treatments kept constant, a co-variation with one or more carbonate system parameters is likely.

Sr/Ca ratios did not show any correlation to the carbonate system. On top of that, measurements were mostly within 5 % of each other. These values, when compared to Mg/Ca – also a temperature proxy – look to be more stable. Indicating that strontium could be a more robust proxy for temperature in *Mytilus edulis*. This is remarkable because in other studies with corals ([Cole et al., 2016](#)) and foraminifers ([Keul et al., 2015](#)), Sr/Ca ratios were clearly affected by the carbonate chemistry. For now, it is not possible to determine the cause of this contradiction.

Ba/Ca, used as a proxy for the nutrient silica, also showed correlations with the carbonate system. Interestingly, at high pCO₂/DIC and low DIC/[CO₃²⁻], Ba/Ca ratios seemed to increase again. While values did not deviate that much from each other, an unknown complex process is controlling barium availability for incorporation. It cannot be explained by a simple increase or decrease of a parameter from the carbonate system.

Correlations for boron to the carbonate system are clearly evident. Some papers suggest it can be used as a pH proxy. However, when looking at the correlation coefficient, a relation between B/Ca and [CO₃²⁻] (thus also [B(OH)₄⁻]/[HCO₃⁻]) is more likely. Thus confirming the hypothesis of [Kaczmarek et al. \(2015b\)](#) and [Howes et al. \(2016\)](#).

REY results correspond to data from [Ponnurangam et al. \(2015\)](#), where they proposed that REY elements are mainly incorporated as the free Ln³⁺ ion. The succeeding increase, decrease and increase again in ratios again suggest the presence of a complex process possibly including vital effects. Incorporation is especially higher when the pH shifts from 7.46 (2 400 µatm) to 7.21 (4 000 µatm). This large jump cannot be explained by the carbonate system because neither concentrations of DIC or saturation state exhibit a large jump between these samples. Perhaps a crucial change related to the biological control on growth is the cause however this remains to be investigated. It is worth noting that at pCO₂ of 452 µatm the pH of extrapallial fluid is 7.52 and at 2724 µatm pH is 7.34. The intersection of ambient seawater pH with the extrapallial fluid could be of importance.

Lastly, the boron isotopes show the expected and very good correlation with pH. Confirming boron isotopes as proxy for pH also holds up for *Mytilus edulis*. Isotopic ratios versus CO₂ concentrations are,

however, slightly better. This could mean there is a minor relation to the carbonate system. Despite not all measurements being significantly different, a good correlation between pH and isotopic ratios cannot be denied.

6.5 Conclusion

Li/Ca clearly shows a correlation to saturation state, which could be used as an aid to reconstruct the carbonate system. Sodium could be used as a proxy for salinity but more work needs to be done with a different cleaning technique. Magnesium and strontium, both temperature proxies, remain fairly constant with strontium being more robust and less influenced by the carbonate system. If Mg/Ca ratios can somehow be corrected for temperature, it could provide useful information for the carbonate system. Ba/Ca ratios seem to be too complex to be used as a proxy for a carbonate system parameter. Possible proxy information will most likely be overprinted by the biological control on nutrients in seawater.

B/Ca as well as $\delta^{11}\text{B}$ show a very good correlation to the carbonate system. $\delta^{11}\text{B}$ was confirmed as a pH proxy in *Mytilus edulis* with possible minor co-variation from the carbonate system. B/Ca shows good promise as a proxy for $[\text{B}(\text{OH})_4^-]/[\text{HCO}_3^-]$. However experiments with natural conditions will show how it holds up in a complex environment.

REY data also shows promise for use as a proxy especially at low pH, where changes in calcium ratio are very sensitive to changes in carbonate system. For now more research should be done on the precise mechanism for incorporation to see if it is indeed viable as a proxy for, for example carbonate ions.

It should be noted, once again, for all measurements that this was a culturing experiment. Correlating parameters are naturally less perfect in an uncontrolled natural environment. How these results hold up in a natural environment remains to be seen. A proxy has not been found, but a start has been made to find a proxy in *Mytilus edulis* for carbonate ions in seawater. More work should be done with decoupled carbonate chemistry. To understand how single components of DIC and the pH interact with specific trace element incorporation into biogenic precipitated calcite.

7 – Acknowledgements

I am very grateful for the support I got from many people. Without them, this thesis could not have been completed. First of all I would like to thank my supervisor Prof. Dr. Jelle Bijma, for all his support and help throughout my project. Also for the many things he taught me and the opportunities he has given me, for which I cannot express enough gratitude.

I would like to thank Dr. Markus Raitzsch for taking time and effort to show me how to prepare, analyze and interpret data from the samples on the ICP-MS. For the help with the Nu Attom I want to thank Ir. Klaus-Uwe Richter and Dr. Dorothee Wilhelms-Dick. I also want to thank Dr. Albert Benthien for allowing me to assist him in trying to get the femto-second laser up and running. I'm also thankful for the help I got from many other people for their general assistance in the day to day work: Beate Müller, Ulrike Richter, Dr. Grit Steinhöfel, Dr. Gernot Nehrke and Dr. Karina Kaczmarek. I very much enjoyed working with everyone.

Finally, I would like to thank Prof. Dr. F. Melzner from GEOMAR, Kiel and Dr. S. Hahn from Ruhr-Universität, Bochum, for providing me the samples and data. And Prof. Dr. M. Bau from the Jacobs University, Bremen, for analyzing the REY in the samples.

7 – Acknowledgements

8 – References

- Allen, K.A. and Hönisch, B.** (2012) The planktic foraminiferal B/Ca proxy for seawater carbonate chemistry: A critical evaluation. *Earth and Planetary Science Letters*, **345-348**, 203-211.
- Bacastow, R.B., Keeling, C.D. and Whorf, T.P.** (1985) Seasonal Amplitude Increase in Atmospheric CO₂ Concentration at Mauna Loa, Hawaii, 1959-1982. *Journal of Geophysical Research-Atmospheres*, **90**, 10529-10540.
- Barker, S., Greaves, M. and Elderfield, H.** (2003) A study of cleaning procedures used for foraminiferal Mg/Ca paleothermometry. *Geochemistry, Geophysics, Geosystems*, **4**.
- Bergman, N.M., Lenton, T.M. and Watson, A.J.** (2004) COPSE: A new model of biogeochemical cycling over Phanerozoic time. *American Journal of Science*, **304**, 397-437.
- Berner, R.A. and Kothavala, Z.** (2001) GEOCARB III: A revised model of atmospheric CO₂ over phanerozoic time. *American Journal of Science*, **301**, 182-204.
- Bijma, J., Portner, H.O., Yesson, C. and Rogers, A.D.** (2013) Climate change and the oceans--what does the future hold? *Marine Pollution Bulletin*, **74**, 495-505.
- Bijma, J., Spero, H.J. and Lea, D.W.** (1999) Reassessing foraminiferal stable isotope geochemistry: Impact of the oceanic carbonate system (experimental results). In: *Use of Proxies in Paleoceanography: Examples from the South Atlantic* (Eds G. Fischer and G. Wefer), pp. 489-512. Springer-Verlag, New York.
- Birch, H.S., Coxall, H.K., Pearson, P.N., Kroon, D. and Schmidt, D.N.** (2016) Partial collapse of the marine carbon pump after the Cretaceous-Paleogene boundary. *Geology*, **44**, 287-290.
- Broecker, W.S.** (1963) A preliminary evaluation of Uranium Series Inequilibrium as a Tool for Absolute Age Measurement on Marine Carbonates. *Journal of Geophysical Research*, **68**, 2817-2834.
- Broecker, W.S.** (1982) Ocean Chemistry during Glacial Time. *Geochimica Et Cosmochimica Acta*, **46**, 1689-1705.
- Brown, R.E., Anderson, L.D., Thomas, E. and Zachos, J.C.** (2011) A core-top calibration of B/Ca in the benthic foraminifers *Nuttallides umbonifera* and *Oridorsalis umbonatus*: A proxy for Cenozoic bottom water carbonate saturation. *Earth and Planetary Science Letters*, **310**, 360-368.
- Bryan, S.P. and Marchitto, T.M.** (2008) Mg/Ca–temperature proxy in benthic foraminifera: New calibrations from the Florida Straits and a hypothesis regarding Mg/Li. *Paleoceanography*, **23**, n/a-n/a.
- Byrne, R.H.** (2002) Inorganic speciation of dissolved elements in seawater: the influence of pH on concentration ratios. *Geochemical Transactions*, **2**, 11.
- Byrne, R.H., Yao, W., Klochko, K., Tossell, J.A. and Kaufman, A.J.** (2006) Experimental evaluation of the isotopic exchange equilibrium $^{10}\text{B}(\text{OH})_3 + ^{11}\text{B}(\text{OH})_4^- = ^{11}\text{B}(\text{OH})_3 + ^{10}\text{B}(\text{OH})_4^-$ in aqueous solution. *Deep Sea Research Part I: Oceanographic Research Papers*, **53**, 684-688.

- Cantrell, K.J. and Byrne, R.H.** (1987) Rare earth element complexation by carbonate and oxalate ions. *Geochimica et Cosmochimica Acta*, **51**, 597-605.
- Cole, C., Finch, A., Hintz, C., Hintz, K. and Allison, N.** (2016) Understanding cold bias: Variable response of skeletal Sr/Ca to seawater pCO₂ in acclimated massive Porites corals. *Sci Rep*, **6**, 26888.
- de Villiers, S., Shen, G.T. and Nelson, B.K.** (1994) The SrCa-temperature relationship in coralline aragonite: Influence of variability in (SrCa)seawater and skeletal growth parameters. *Geochimica et Cosmochimica Acta*, **58**, 197-208.
- Etheridge, D.M., Steele, L.P., Langenfelds, R.L., Francey, R.J., Barnola, J.M. and Morgan, V.I.** (1996) Natural and anthropogenic changes in atmospheric CO₂ over the last 1000 years from air in Antarctic ice and firn. *Journal of Geophysical Research*, **101**, 4115-4128.
- Felis, T., Suzuki, A., Kuhnert, H., Dima, M., Lohmann, G. and Kawahata, H.** (2009) Subtropical coral reveals abrupt early-twentieth-century freshening in the western North Pacific Ocean. *Geology*, **37**, 527-530.
- Fischer, H., Schmitt, J., Schneider, R., Eggleston, S.S., Joos, F., Bauska, T.K., Marcott, S.A., Brook, E.J., Köhler, P. and Chappellaz, J.** (2015) Latest Insights into Past Carbon Cycle Changes from CO₂ and δ¹³C_{atm}. *Nova Acta Leopoldina*, **121**, 59-63.
- Foster, G.L.** (2008) Seawater pH, pCO₂ and [CO₃²⁻] variations in the Caribbean Sea over the last 130 kyr: A boron isotope and B/Ca study of planktic foraminifera. *Earth and Planetary Science Letters*, **271**, 254-266.
- Foster, G.L., Pogge von Strandmann, P.A.E. and Rae, J.W.B.** (2010) Boron and magnesium isotopic composition of seawater. *Geochemistry, Geophysics, Geosystems*, **11**.
- Furst, M., Lowenstam, H.A. and Burnett, D.S.** (1976) Radiographic Study of Distribution of Boron in Recent Mollusk Shells. *Geochimica Et Cosmochimica Acta*, **40**, 1381-1386.
- Gehlen, M., Gruber, N., Gangstø, R., Bopp, L. and Oschlies, A.** (2011) Biogeochemical consequences of ocean acidification and feedbacks to the earth system. In: *Ocean acidification* (Eds J.-P. Gattuso and L. Hansson), pp. 230-248. Oxford University Press, Oxford; New York.
- Gordillo, S., Bayer, M.S., Boretto, G. and Charó, M.** (2014) Mollusk shells as bio-geo-archives : evaluating environmental changes during the Quaternary. In: *Springer briefs in earth system sciences South America and the Southern Hemisphere*. Springer,, Cham Switzerland ; New York.
- Groeneveld, J., Nurnberg, D., Tiedemann, R., Reichart, G.J., Steph, S., Reuning, L., Crudeli, D. and Mason, P.** (2008) Foraminiferal Mg/Ca increase in the Caribbean during the pliocene: Western Atlantic Warm Pool formation, salinity influence, or diagenetic overprint? *Geochemistry, Geophysics, Geosystems*, **9**.
- Gussone, N., Zonneveld, K. and Kuhnert, H.** (2010) Minor element and Ca isotope composition of calcareous dinoflagellate cysts of cultured *Thoracosphaera heimii*. *Earth and Planetary Science Letters*, **289**, 180-188.

- Hahn, S., Griesshaber, E., Schmahl, W.W., Neuser, R.D., Ritter, A.-C., Hoffmann, R., Buhl, D., Niedermayr, A., Geske, A., Immenhauser, A. and Pufahl, P. (2014) Exploring aberrant bivalve shell ultrastructure and geochemistry as proxies for past sea water acidification. *Sedimentology*, **61**, 1625-1658.
- Hall, J.M. and Chan, L.H. (2004) Li/Ca in multiple species of benthic and planktonic foraminifera: thermocline, latitudinal, and glacial-interglacial variation 1. *Geochimica et Cosmochimica Acta*, **68**, 529-545.
- Hartmann, D.L., Tank, A.M.G.K., Rusticucci, M., Alexander, L.V., Brönnimann, S., Charabi, Y., Dentener, F.J., Dlugokencky, E.J., Easterling, D.R., Kaplan, A., Soden, B.J., Thorne, P.W., Wild, M. and Zhai, P.M. (2013) Observations: Atmosphere and Surface. In: *Climate change 2013 : the physical science basis : Working Group I contribution to the Fifth assessment report of the Intergovernmental Panel on Climate Change* (Eds T.F. Stocker, D. Qin, G.-K. Plattner, M. Tignor, S.K. Allen, J. Boschung, A. Nauels, Y. Xia, V. Bex and P.M. Midgley), pp. 159-254. Cambridge University Press, New York.
- Heinemann, A., Fietzke, J., Melzner, F., Böhm, F., Thomsen, J., Garbe-Schönberg, D. and Eisenhauer, A. (2012) Conditions of *Mytilus edulis* extracellular body fluids and shell composition in a pH-treatment experiment: Acid-base status, trace elements and $\delta^{11}\text{B}$. *Geochemistry, Geophysics, Geosystems*, **13**.
- Hemming, N.G. and Hanson, G.N. (1992) Boron Isotopic Composition and Concentration in Modern Marine Carbonates. *Geochimica Et Cosmochimica Acta*, **56**, 537-543.
- Henehan, M.J., Foster, G.L., Rae, J.W.B., Prentice, K.C., Erez, J., Bostock, H.C., Marshall, B.J. and Wilson, P.A. (2015) Evaluating the utility of B/Ca ratios in planktic foraminifera as a proxy for the carbonate system: A case study of *Globigerinoides ruber*. *Geochemistry, Geophysics, Geosystems*, **16**, 1052-1069.
- Hesemann, M. (2016a) *Amphistegina lessonii* d'Orbigny, 1843. In: *Hesemann, M. 2016 Foraminifera.eu Project Database*.
- Hesemann, M. (2016b) *Orbulina universa* d'Orbigny, 1839. In: *Foraminifera.eu Project Database*.
- Hönisch, B., Bickert, T. and Hemming, N.G. (2008) Modern and Pleistocene boron isotope composition of the benthic foraminifer *Cibicides wuellerstorfi*. *Earth and Planetary Science Letters*, **272**, 309-318.
- Howes, E.L., Kaczmarek, K., Raitzsch, M., Mewes, A., Bijma, N., Horn, I., Misra, S., Gattuso, J.P. and Bijma, J. (2016) Decoupled carbonate chemistry controls on the incorporation of boron into *Orbulina universa*. *Biogeosciences Discussions*, 1-26.
- Kaczmarek, K., Horn, I., Nehrke, G. and Bijma, J. (2015a) Simultaneous determination of $\delta^{11}\text{B}$ and B/Ca ratio in marine biogenic carbonates at nanogram level. *Chemical Geology*, **392**, 32-42.
- Kaczmarek, K., Langer, G., Nehrke, G., Horn, I., Misra, S., Janse, M. and Bijma, J. (2015b) Boron incorporation in the foraminifer *Amphistegina lessonii* under a decoupled carbonate chemistry. *Biogeosciences*, **12**, 1753-1763.
- Kakihana, H. and Kotaka, M. (1977) Equilibrium constants for boron isotope-exchange reactions. *Bulletin of the Research Laboratory for Nuclear Reactors (Tokyo Institute of Technology)*, 1-12.

- Kaufmann, A., Broecker, W.S., Ku, T.L. and Thurber, D.L.** (1971) The status of U-series methods of mollusk dating. *Geochimica et Cosmochimica Acta*, **35**, 1155-1183.
- Kennett, J.P. and Stott, L.D.** (1991) Abrupt Deep-Sea Warming, Palaeoceanographic Changes and Benthic Extinctions at the End of the Paleocene. *Nature*, **353**, 225-229.
- Keul, N., Langer, G., de Nooijer, L.J., Nehrke, G., Reichart, G.-J. and Bijma, J.** (2013) Incorporation of uranium in benthic foraminiferal calcite reflects seawater carbonate ion concentration. *Geochemistry, Geophysics, Geosystems*, **14**, 102-111.
- Keul, N., Langer, G., Nooijer, L.d., Nehrke, G., Reichart, G.-J., Bijma, J. and Schneider, R.** (2015) New Carbonate System Proxies: Foram Culturing and Pteropod Potentials. *Nova Acta Leopoldina*, **121**, 305-309.
- Key, R.M., Kozyr, A., Sabine, C.L., Lee, K., Wanninkhof, R., Bullister, J.L., Feely, R.A., Millero, F.J., Mordy, C. and Peng, T.H.** (2004) A global ocean carbon climatology: Results from Global Data Analysis Project (GLODAP). *Global Biogeochemical Cycles*, **18**.
- Klochko, K., Cody, G.D., Tossell, J.A., Dera, P. and Kaufman, A.J.** (2009) Re-evaluating boron speciation in biogenic calcite and aragonite using ^{11}B MAS NMR. *Geochimica et Cosmochimica Acta*, **73**, 1890-1900.
- Klunder, M.H., Hippler, D., Witbaard, R. and Frei, D.** (2008) Laser ablation analysis of bivalve shells - archives of environmental information. *Geological Survey of Denmark and Greenland Bulletin*, 89-92.
- Krause-Nehring, J., Klügel, A., Nehrke, G., Brellocks, B. and Brey, T.** (2011) Impact of sample pretreatment on the measured element concentrations in the bivalve *Arctica islandica*. *Geochemistry, Geophysics, Geosystems*, **12**.
- LaVigne, M., Hill, T.M., Spero, H.J. and Guilderson, T.P.** (2011) Bamboo coral Ba/Ca: Calibration of a new deep ocean refractory nutrient proxy. *Earth and Planetary Science Letters*, **312**, 506-515.
- Lee, K., Kim, T.-W., Byrne, R.H., Millero, F.J., Feely, R.A. and Liu, Y.-M.** (2010) The universal ratio of boron to chlorinity for the North Pacific and North Atlantic oceans. *Geochimica et Cosmochimica Acta*, **74**, 1801-1811.
- Levin, L., Hönisch, B. and Frieder, C.** (2015) Geochemical Proxies for Estimating Faunal Exposure to Ocean Acidification. *Oceanography*, **25**, 62-73.
- Liu, Y. and Tossell, J.A.** (2005) Ab initio molecular orbital calculations for boron isotope fractionations on boric acids and borates. *Geochimica et Cosmochimica Acta*, **69**, 3995-4006.
- Locarnini, R.A., Mishonov, A.V., Antonov, J.I., Boyer, T.P., Garcia, H.E., Baranova, O.K., Zweng, M.M. and Johnson, D.R.** (Eds)(2010) *World Ocean Atlas 2009 Volume 1: Temperature* U.S. Government Printing Office, Washington, D.C., 184 pp.
- Marriott, C.S., Henderson, G.M., Crompton, R., Staubwasser, M. and Shaw, S.** (2004) Effect of mineralogy, salinity, and temperature on Li/Ca and Li isotope composition of calcium carbonate. *Chemical Geology*, **212**, 5-15.

- McCoy, S.J., Robinson, L.F., Pfister, C.A., Wootton, J.T. and Shimizu, N.** (2011) Exploring B/Ca as a pH proxy in bivalves: relationships between *Mytilus californianus* B/Ca and environmental data from the northeast Pacific. *Biogeosciences*, **8**, 2567-2579.
- McLennan, S.M.** (1989) Rare Earth elements in sedimentary rocks; influence of provenance and sedimentary processes. *Rev. Min. Geochem.*, **21**, 169-200.
- Millero, F.J.** (2010) Carbonate constants for estuarine waters. *Marine and Freshwater Research*, **61**, 139-142.
- Mora, C., Wei, C.L., Rollo, A., Amaro, T., Baco, A.R., Billett, D., Bopp, L., Chen, Q., Collier, M., Danovaro, R., Gooday, A.J., Grupe, B.M., Halloran, P.R., Ingels, J., Jones, D.O., Levin, L.A., Nakano, H., Norling, K., Ramirez-Llodra, E., Rex, M., Ruhl, H.A., Smith, C.R., Sweetman, A.K., Thurber, A.R., Tjiputra, J.F., Usseglio, P., Watling, L., Wu, T. and Yasuhara, M.** (2013) Biotic and human vulnerability to projected changes in ocean biogeochemistry over the 21st century. *PLoS Biol*, **11**, 1-14.
- Noireaux, J., Mavromatis, V., Gaillardet, J., Schott, J., Montouillout, V., Louvat, P., Rollion-Bard, C. and Neuville, D.R.** (2015) Crystallographic control on the boron isotope paleo-pH proxy. *Earth and Planetary Science Letters*, **430**, 398-407.
- Orr, J.C., Fabry, V.J., Aumont, O., Bopp, L., Doney, S.C., Feely, R.A., Gnanadesikan, A., Gruber, N., Ishida, A., Joos, F., Key, R.M., Lindsay, K., Maier-Reimer, E., Matear, R., Monfray, P., Mouchet, A., Najjar, R.G., Plattner, G.K., Rodgers, K.B., Sabine, C.L., Sarmiento, J.L., Schlitzer, R., Slater, R.D., Totterdell, I.J., Weirig, M.F., Yamanaka, Y. and Yool, A.** (2005) Anthropogenic ocean acidification over the twenty-first century and its impact on calcifying organisms. *Nature*, **437**, 681-686.
- Ponnurangam, A., Bau, M., Brenner, M. and Koschinsky, A.** (2015) Mussel shells of *Mytilus edulis* as bioarchives of the rare earth elements and yttrium distribution in seawater and the potential impact of pH and temperature on the partitioning behaviour. *Biogeosciences Discussions*, **12**, 14911-14939.
- Rae, J.W.B., Foster, G.L., Schmidt, D.N. and Elliott, T.** (2011) Boron isotopes and B/Ca in benthic foraminifera: Proxies for the deep ocean carbonate system. *Earth and Planetary Science Letters*, **302**, 403-413.
- Raitzsch, M., Hathorne, E.C., Kuhnert, H., Groeneveld, J. and Bickert, T.** (2011a) Modern and late Pleistocene B/Ca ratios of the benthic foraminifer *Planulina wuellerstorfi* determined with laser ablation ICP-MS. *Geology*, **39**, 1039-1042.
- Raitzsch, M. and Honisch, B.** (2013) Cenozoic boron isotope variations in benthic foraminifers. *Geology*, **41**, 591-594.
- Raitzsch, M., Kuhnert, H., Hathorne, E.C., Groeneveld, J. and Bickert, T.** (2011b) U/Ca in benthic foraminifers: A proxy for the deep-sea carbonate saturation. *Geochemistry, Geophysics, Geosystems*, **12**.
- Rampino, M.R. and Caldeira, K.** (2005) Major perturbation of ocean chemistry and a 'Strangelove Ocean' after the end-Permian mass extinction. *Terra Nova*, **17**, 554-559.
- Ridgwell, A. and Zeebe, R.** (2005) The role of the global carbonate cycle in the regulation and evolution of the Earth system. *Earth and Planetary Science Letters*, **234**, 299-315.

- Ries, J.B., Cohen, A.L. and McCorkle, D.C.** (2009) Marine calcifiers exhibit mixed responses to CO₂-induced ocean acidification. *Geology*, **37**, 1131-1134.
- Rothman, D.H.** (2002) Atmospheric carbon dioxide levels for the last 500 million years. *Proceedings of the National Academy of Sciences of the United States of America*, **99**, 4167-4171.
- Russell, A.D., Hönisch, B., Spero, H.J. and Lea, D.W.** (2004) Effects of seawater carbonate ion concentration and temperature on shell U, Mg, and Sr in cultured planktonic foraminifera. *Geochimica et Cosmochimica Acta*, **68**, 4347-4361.
- Sanyal, A., Bijma, J., Spero, H. and Lea, D.W.** (2001) Empirical relationship between pH and the boron isotopic composition of *Globigerinoides sacculifer*: Implications for the boron isotope paleo-pH proxy. *Paleoceanography*, **16**, 515-519.
- Schone, B.R., Zhang, Z., Jacob, D., Gillikin, D.P., Tutken, T., Garbe-Schonberg, D., McConnaughey, T. and Soldati, A.** (2010) Effect of organic matrices on the determination of the trace element chemistry (Mg, Sr, Mg/Ca, Sr/Ca) of aragonitic bivalve shells (*Arctica islandica*)-Comparison of ICP-OES and LA-ICP-MS data. *Geochemical Journal*, **44**, 23-37.
- Sigman, D.M. and Boyle, E.A.** (2000) Glacial/interglacial variations in atmospheric carbon dioxide. *Nature*, **407**, 859-869.
- Solomon, S., Intergovernmental Panel on Climate Change. and Intergovernmental Panel on Climate Change. Working Group I.** (2007) *Climate change 2007 : the physical science basis : contribution of Working Group I to the Fourth Assessment Report of the Intergovernmental Panel on Climate Change*. Cambridge University Press, Cambridge ; New York, viii, 996 p. pp.
- Spero, H.J., Bijma, J., Lea, D.W. and Bemis, B.E.** (1997) Effect of seawater carbonate concentration on foraminiferal carbon and oxygen isotopes. *Nature*, **390**, 497-500.
- Team, E.W.** (2005) ESRL Global Monitoring Division-Global Greenhouse Gas Reference Network.
- Thurman, H.V. and Trujillo, A.P.** (2004) *Introductory oceanography*. Pearson Prentice Hall, Upper Saddle River, N.J., xvi, 608 p. pp.
- Watanabe, T., Minagawa, M., Oba, T. and Winter, A.** (2001) Pretreatment of coral aragonite for Mg and Sr analysis: Implications for coral thermometers. *Geochemical Journal*, **35**, 265-269.
- Weber, J.N.** (1973) Incorporation of strontium into reef coral skeletal carbonate. *Geochimica et Cosmochimica Acta*, **37**, 2173-2190.
- Wiebe, R. and Gaddy, V.L.** (1940) The Solubility of Carbon Dioxide in Water at Various Temperatures from 12 to 40 C and at Pressures to 500 Atmospheres. *Journal of the American Chemical Society*, **62**, 815-817.
- Wolf-Gladrow, D.A., Zeebe, R.E., Klaas, C., Kortzinger, A. and Dickson, A.G.** (2007) Total alkalinity: The explicit conservative expression and its application to biogeochemical processes. *Marine Chemistry*, **106**, 287-300.

- Yu, J. and Elderfield, H.** (2007) Benthic foraminiferal B/Ca ratios reflect deep water carbonate saturation state. *Earth and Planetary Science Letters*, **258**, 73-86.
- Yu, J., Elderfield, H., Jin, Z. and Booth, L.** (2008) A strong temperature effect on U/Ca in planktonic foraminiferal carbonates. *Geochimica et Cosmochimica Acta*, **72**, 4988-5000.
- Zachos, J.C., Rohl, U., Schellenberg, S.A., Sluijs, A., Hodell, D.A., Kelly, D.C., Thomas, E., Nicolo, M., I, R., Lourens, L.J., McCarren, H. and Kroon, D.** (2005) Rapid acidification of the ocean during the Paleocene-Eocene thermal maximum. *Science*, **308**, 1611-1615.
- Zeebe, R.E.** (2005) Stable boron isotope fractionation between dissolved $B(OH)_3$ and $B(OH)^{-4}$. *Geochimica et Cosmochimica Acta*, **69**, 2753-2766.
- Zeebe, R.E.** (2012) History of Seawater Carbonate Chemistry, Atmospheric CO_2 , and Ocean Acidification. *Annual Review of Earth and Planetary Sciences*, **40**, 141-165.
- Zeebe, R.E., Bijma, J., Honisch, B., Sanyal, A., Spero, H.J. and Wolf-Gladrow, D.A.** (2008) Vital effects and beyond: a modelling perspective on developing palaeoceanographical proxy relationships in foraminifera. *Geological Society, London, Special Publications*, **303**, 45-58.
- Zeebe, R.E., Sanyal, A., Ortiz, J.D. and Wolf-Gladrow, D.A.** (2001) A theoretical study of the kinetics of the boric acid-borate equilibrium in seawater. *Marine Chemistry*, **73**, 113-124.
- Zeebe, R.E. and Westbroek, P.** (2003) A simple model for the $CaCO_3$ saturation state of the ocean: The “Strangelove,” the “Neritan,” and the “Cretan” Ocean. *Geochemistry, Geophysics, Geosystems*, **4**.
- Zeebe, R.E., Zachos, J.C. and Dickens, G.R.** (2009) Carbon dioxide forcing alone insufficient to explain Palaeocene-Eocene Thermal Maximum warming. *Nature Geoscience*, **2**, 576-580.

8 – References

Appendix 1: exact concentrations of standards used for all experiments

Table 33 – Concentrations of calibration standards used for the first bleaching experiment. All concentrations are in ppb.

Element	Ca 100 ppm	Ca 75 ppm	Ca 50 ppm	Ca 25 ppm	Blank
Ca	103 438.52	76 543.85	51 747.24	25 897.91	0
Mg	409.95	303.36	205.09	102.64	0
Sr	397.96	294.48	199.09	99.64	0
Na	419.95	310.76	210.09	105.14	0
REE (excl. Nd)	2.1998	1.6278	1.1005	0.5508	0
U	0.0315	0.0233	0.0158	0.0079	0
Fe	0.0309	0.0228	0.0154	0.0077	0
V	0.0315	0.0233	0.0158	0.0079	0
Nd	2.2514	1.6660	1.1263	0.5637	0
Cu	0.0513	0.0380	0.0257	0.0128	0
Cd	0.0730	0.0540	0.0365	0.0183	0
Li	1.0596	0.7841	0.5301	0.2653	0
Al	3.1824	2.3549	1.5921	0.7968	0
Ba	4.2240	3.1258	2.1132	1.0576	0
B	8.3025	6.1438	4.1535	2.0787	0
Zn	15.5588	11.5134	7.7836	3.8955	0
Mn	26.3612	19.5071	13.1877	6.6000	0

Table 34 – Concentrations of the calibration standards used for the second bleaching experiment where only one size fraction was taken. Particle sizes were between 63 and 100 µm. All concentrations are in ppb.

Element	Ca 100 ppm	Ca 75 ppm	Ca 50 ppm	Ca 25 ppm	Blank
Ca	103 438.52	77 053.16	51 000.38	253 33.09	0
Mg	409.95	305.38	202.13	100.40	0
Sr	397.96	296.44	196.21	97.46	0
Na	419.95	312.83	207.06	102.85	0
REE (excl. Nd)	2.1998	1.6386	1.0846	0.5387	0
U	0.0315	0.0235	0.0155	0.0077	0
Fe	0.0309	0.0230	0.0152	0.0076	0
V	0.0315	0.0235	0.0155	0.0077	0
Nd	2.2514	1.6771	1.1100	0.5514	0
Cu	0.0513	0.0382	0.0253	0.0126	0
Cd	0.0730	0.0544	0.0360	0.0179	0
Li	1.0596	0.7893	0.5224	0.2595	0
Al	3.1824	2.3706	1.5691	0.7794	0
Ba	4.2240	3.1465	2.0827	1.0345	0
B	8.3025	6.1847	4.0935	2.0334	0
Zn	15.5588	11.5900	7.6713	3.8105	0
Mn	26.3612	19.6369	12.9974	6.4561	0

Appendix 1: exact concentrations of standards used for all experiments

Table 35 – Concentrations of the calibration standards used for the experiment to see how different size fractions, affect the bleaching process. All concentrations are in ppb.

Elements	Ca 100 ppm	Ca 75 ppm	Ca 50 ppm	Ca 25 ppm	Blank
Ca	103 438.52	78 534.13	51 816.29	25 928.73	0
Mg	409.95	308.08	206.24	102.94	0
Sr	397.96	299.06	200.20	99.93	0
Na	419.95	315.59	211.27	105.45	0
REE (excl. Nd)	2.1998	1.6531	1.1066	0.5524	0
U	0.0315	0.0237	0.0158	0.0079	0
Fe	0.0309	0.0232	0.0155	0.0078	0
V	0.0315	0.0237	0.0158	0.0079	0
Nd	2.2514	1.6919	1.1326	0.5653	0
Cu	0.0513	0.0385	0.0258	0.0129	0
Cd	0.0730	0.0549	0.0367	0.0183	0
Li	1.0596	0.7963	0.5330	0.2661	0
Al	3.1824	2.3915	1.6010	0.7991	0
Ba	4.2240	3.1743	2.1250	1.0607	0
B	8.3025	6.2392	4.1767	2.0848	0
Zn	15.5588	11.6923	7.8271	3.9070	0
Mn	26.3612	19.8102	13.2615	6.6195	0

Table 36 – Concentrations of calibration standards used for the experiment where the stability of 12 samples were tested over 99 days. All concentrations are in ppb.

Element	Ca 100 ppm	Ca 75 ppm	Ca 50 ppm	Ca 25 ppm	Blank
Ca	103 438.5	77 628.2	51 770.2	25 974.6	0
Mg	409.95	307.66	205.18	102.94	0
Sr	397.96	298.66	199.17	99.93	0
Na	420.0	315.2	210.2	105.5	0
REE (excl. Nd)	2.1998	1.6509	1.1010	0.5524	0
U	0.0315	0.0236	0.0158	0.0079	0
Fe	0.0309	0.0232	0.0155	0.0078	0
V	0.0315	0.0236	0.0158	0.0079	0
Nd	2.2514	1.6896	1.1268	0.5653	0
Cu	0.0513	0.0385	0.0257	0.0129	0
Cd	0.0730	0.0548	0.0366	0.0183	0
Li	1.0596	0.7952	0.5303	0.2661	0
Al	3.1824	2.3883	1.5928	0.7991	0
Ba	4.2240	3.1700	2.1141	1.0607	0
B	8.3025	6.2308	4.1553	2.0849	0
Zn	15.5588	11.6765	7.7871	3.9070	0
Mn	26.3612	19.7834	13.1936	6.6196	0

Appendix 1: exact concentrations of standards used for all experiments

Table 37 – Concentrations of the calibration standards used to measure inter-/intravariability between valves and bivalves.

Element	Ca 100 ppm	Ca 70 ppm	Ca 40 ppm	Ca 10 ppm	Blank
Ca	100 004.40	69 903.33	39 898.36	10 262.29	0
Mg	410.45	286.91	163.76	42.12	0
Sr	411.25	287.47	164.08	42.20	0
Na	466.83	326.32	186.25	47.91	0
REE (excl. Nd)	2.1942	1.5338	0.8754	0.2252	0
U	0.0310	0.0217	0.0124	0.0032	0
Fe	0.0304	0.0213	0.0121	0.0031	0
V	0.0310	0.0217	0.0124	0.0032	0
Nd	2.2450	1.5693	0.8957	0.2304	0
Cu	0.0505	0.0353	0.0202	0.0052	0
Cd	0.0719	0.0503	0.0287	0.0074	0
Li	1.0436	0.7295	0.4164	0.1071	0
Al	3.1345	2.1910	1.2505	0.3217	0
Ba	4.1604	2.9081	1.6599	0.4269	0
B	8.1775	5.7161	3.2625	0.8392	0
Zn	15.3245	10.7119	6.1140	1.5726	0
Mn	25.9643	18.1491	10.3589	2.6644	0

Table 38 – Concentrations of the calibration standards used to measure the four pooled samples grown at different pCO₂ atmospheres. All concentrations are in ppb.

Elements	Ca 100 ppm	Ca 75 ppm	Ca 50 ppm	Ca 25 ppm	Blank
Ca	103 438.52	77 622.29	51 831.67	25 948.92	0
Mg	409.95	307.64	205.42	102.84	0
Sr	397.96	298.63	199.41	99.83	0
Na	419.95	315.14	210.43	105.35	0
REE (excl. Nd)	2.1998	1.6507	1.1023	0.5518	0
U	0.0315	0.0236	0.0158	0.0079	0
Fe	0.0309	0.0232	0.0155	0.0077	0
V	0.0315	0.0236	0.0158	0.0079	0
Nd	2.2514	1.6895	1.1281	0.5648	0
Cu	0.0513	0.0385	0.0257	0.0129	0
Cd	0.0730	0.0548	0.0366	0.0183	0
Li	1.0596	0.7951	0.5309	0.2658	0
Al	3.1824	2.3881	1.5946	0.7983	0
Ba	4.2240	3.1698	2.1166	1.0597	0
B	8.3025	6.2303	4.1603	2.0828	0
Zn	15.5588	11.6756	7.7963	3.9031	0
Mn	26.3612	19.7819	13.2092	6.6130	0

Appendix 1: exact concentrations of standards used for all experiments

Appendix 2: individual graphs showing change of Me/Ca ratios after 99 days of storage

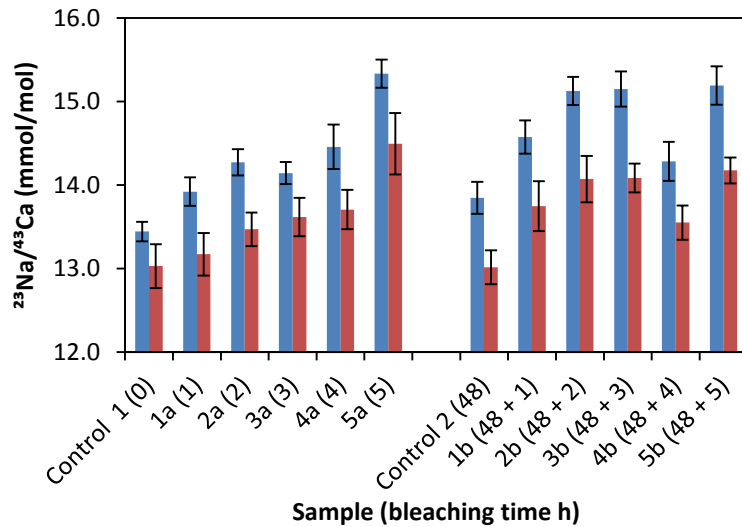


Figure 40 – Change in $^{23}\text{Na}/^{43}\text{Ca}$ ratio of a dissolved sample that has been remeasured after being stored in a closed vial for 99 days. Blue bars represent the old values from chapter 2, red bars are the newly measured values from chapter 5.

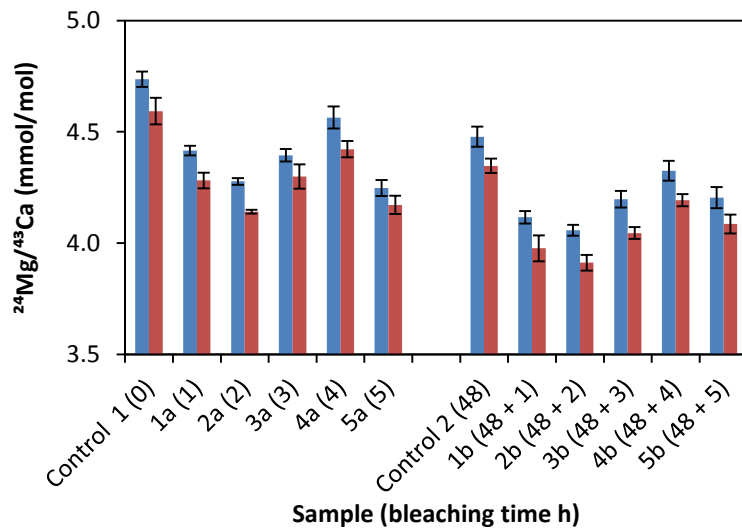


Figure 41 – Change in $^{24}\text{Mg}/^{43}\text{Ca}$ ratio of a dissolved sample that has been remeasured after being stored in a closed vial for 99 days. Blue bars represent the old values from chapter 2, red bars are the newly measured values from chapter 5.

Appendix 2: individual graphs showing change of Me/Ca ratios after 99 days of storage

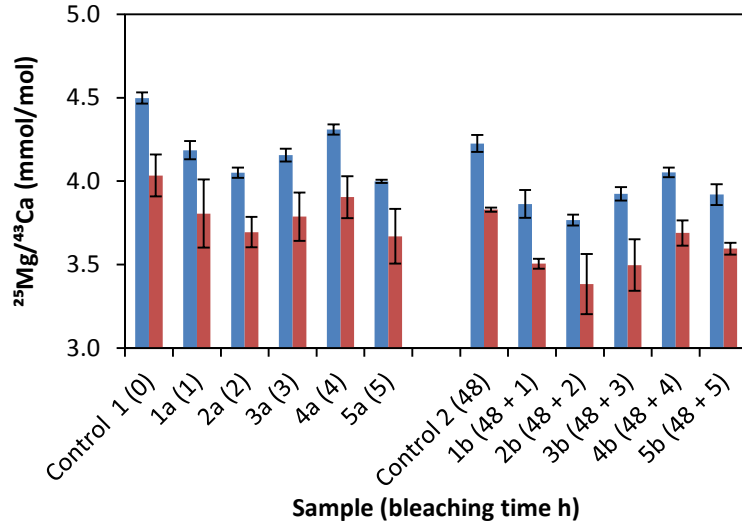


Figure 42 – Change in $^{25}\text{Mg}/^{43}\text{Ca}$ ratio of a dissolved sample that has been remeasured after being stored in a closed vial for 99 days. Blue bars represent the old values from chapter 2, red bars are the newly measured values from chapter 5.

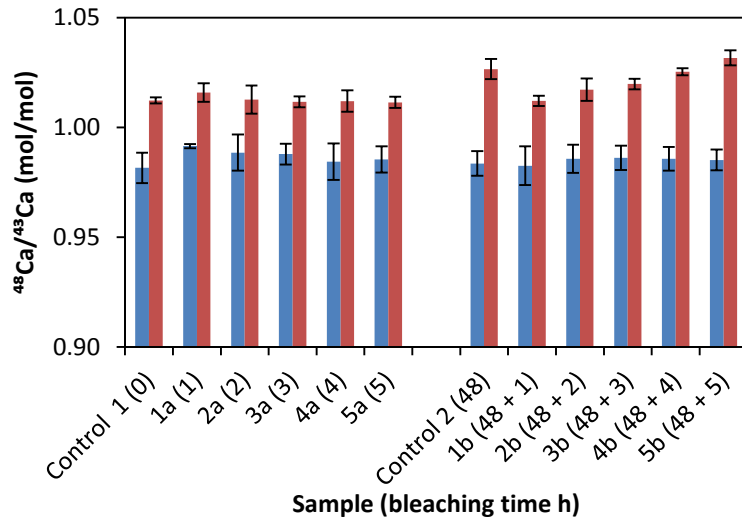


Figure 43 – Change in $^{48}\text{Ca}/^{43}\text{Ca}$ ratio of a dissolved sample that has been remeasured after being stored in a closed vial for 99 days. Blue bars represent the old values from chapter 2, red bars are the newly measured values from chapter 5.

Appendix 2: individual graphs showing change of Me/Ca ratios after 99 days of storage

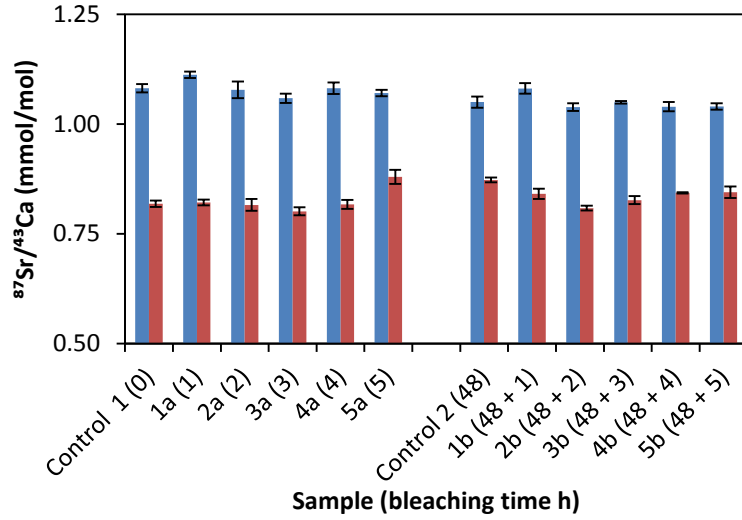


Figure 44 – Change in $^{87}\text{Sr}/^{43}\text{Ca}$ ratio of a dissolved sample that has been remeasured after being stored in a closed vial for 99 days. Blue bars represent the old values from chapter 2, red bars are the newly measured values from chapter 5.

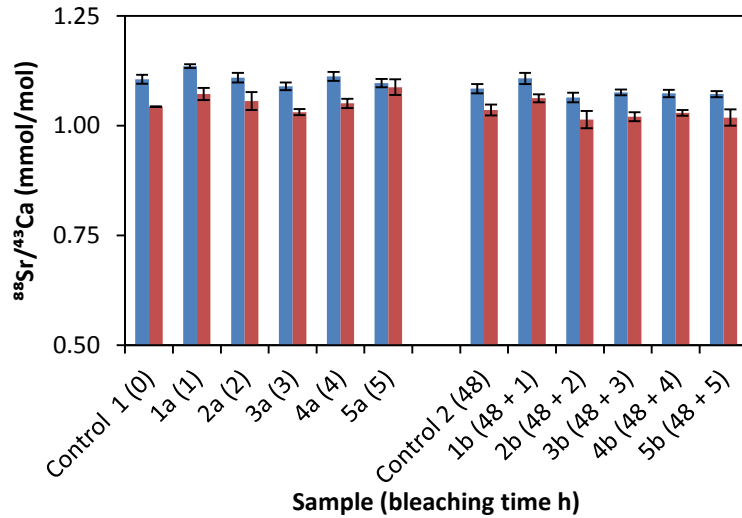


Figure 45 – Change in $^{88}\text{Sr}/^{43}\text{Ca}$ ratio of a dissolved sample that has been remeasured after being stored in a closed vial for 99 days. Blue bars represent the old values from chapter 2, red bars are the newly measured values from chapter 5.

Appendix 2: individual graphs showing change of Me/Ca ratios after 99 days of storage

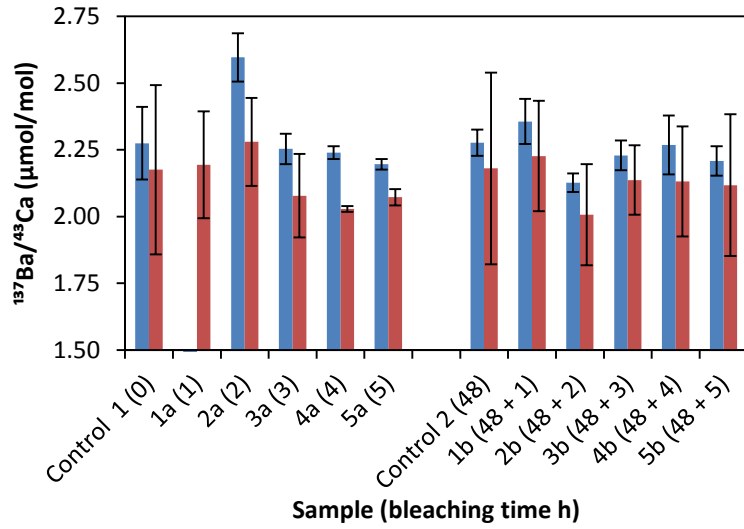


Figure 46 – Change in $^{137}\text{Ba}/^{43}\text{Ca}$ ratio of a dissolved sample that has been remeasured after being stored in a closed vial for 99 days. Blue bars represent the old values from chapter 2, red bars are the newly measured values from chapter 5.

Appendix 3: graphs for Me/Ca versus parameters of the carbonate system

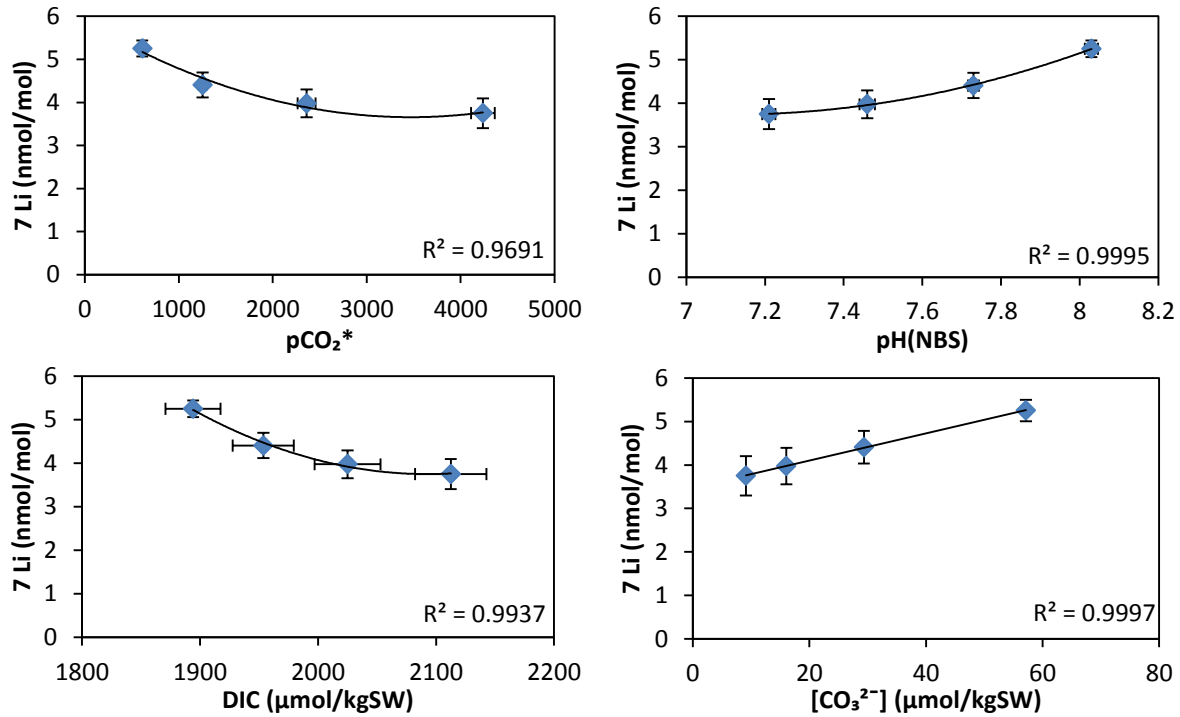


Figure 47 – Li/Ca ratios as a function of pCO_2 , pH_{NBS} , $\text{DIC } (C_T)$ and $[\text{CO}_3^{2-}]$. Vertical (n: 3) and horizontal (n: 53) error bars are given as the 95 % confidence interval except for $[\text{CO}_3^{2-}]$, which was not available.

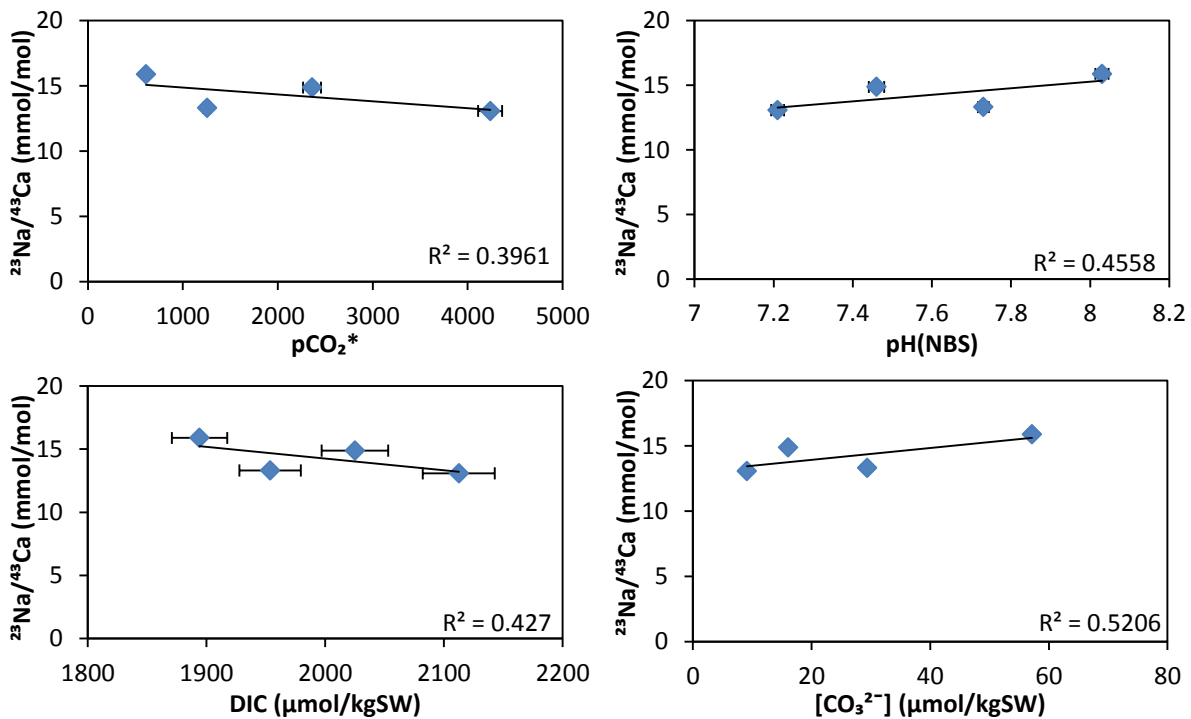


Figure 48 – Na/Ca ratios as a function of pCO_2 , pH_{NBS} , $\text{DIC } (C_T)$ and $[\text{CO}_3^{2-}]$. Vertical (n: 3) and horizontal (n: 53) error bars are given as the 95 % confidence interval except for $[\text{CO}_3^{2-}]$, which was not available.

Appendix 3: graphs for Me/Ca versus parameters of the carbonate system

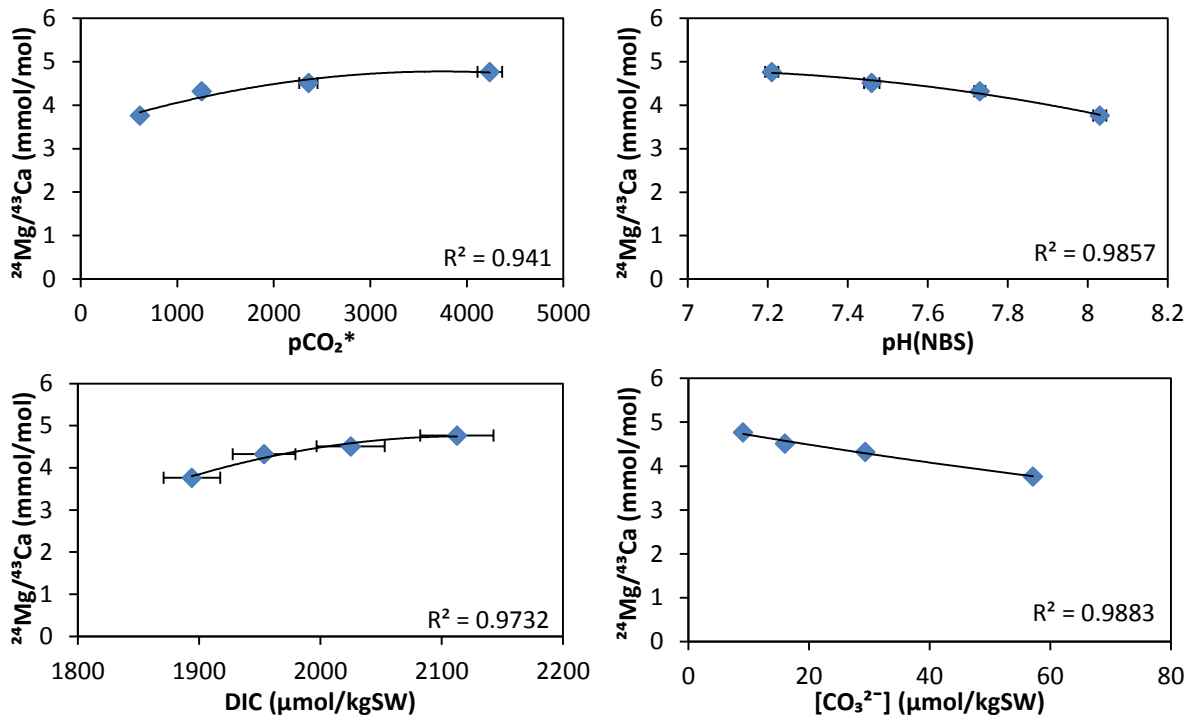


Figure 49 – Mg/Ca ratios as a function of pCO_2 , pH_{NBS} , DIC (C_T) and $[\text{CO}_3^{2-}]$. Vertical (n: 3) and horizontal (n: 53) error bars are given as the 95 % confidence interval except for $[\text{CO}_3^{2-}]$, which was not available.

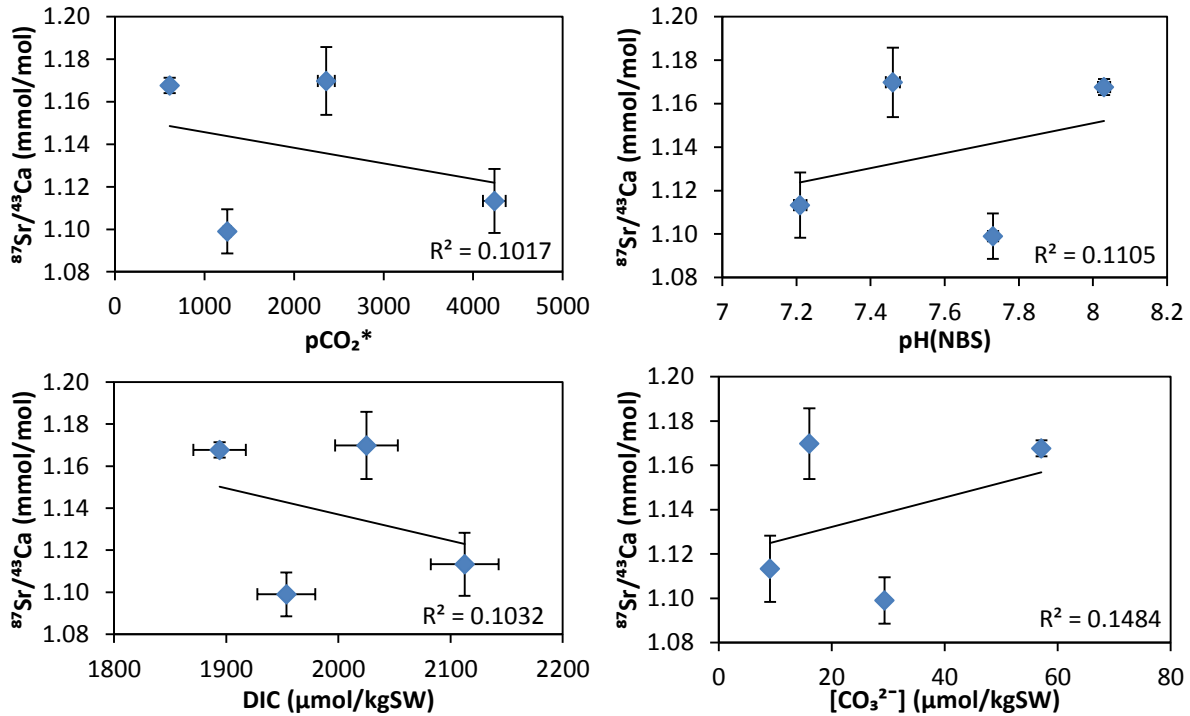


Figure 50 – Sr/Ca ratios as a function of pCO_2 , pH_{NBS} , DIC (C_T) and $[\text{CO}_3^{2-}]$. Vertical (n: 3) and horizontal (n: 53) error bars are given as the 95 % confidence interval except for $[\text{CO}_3^{2-}]$, which was not available.

Appendix 3: graphs for Me/Ca versus parameters of the carbonate system

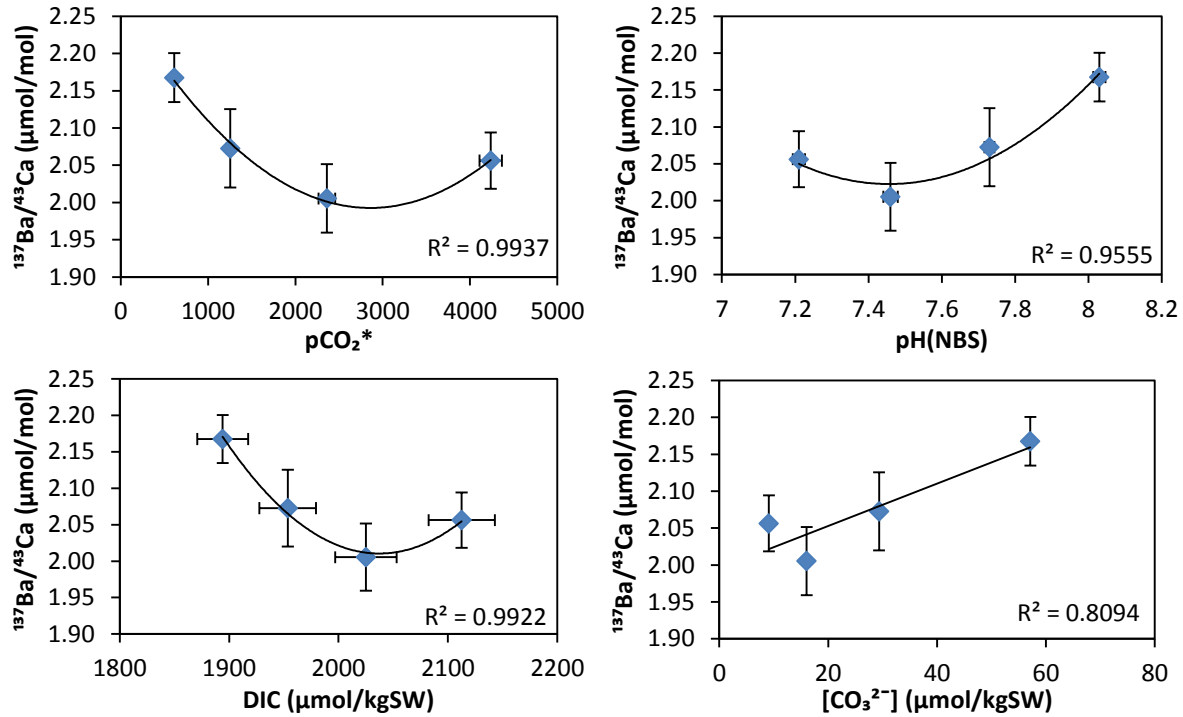


Figure 51 – Ba/Ca ratios as a function of pCO_2 , pH_{NBS} , DIC (C_T) and $[\text{CO}_3^{2-}]$. Vertical (n: 3) and horizontal (n: 53) error bars are given as the 95 % confidence interval except for $[\text{CO}_3^{2-}]$, which was not available.

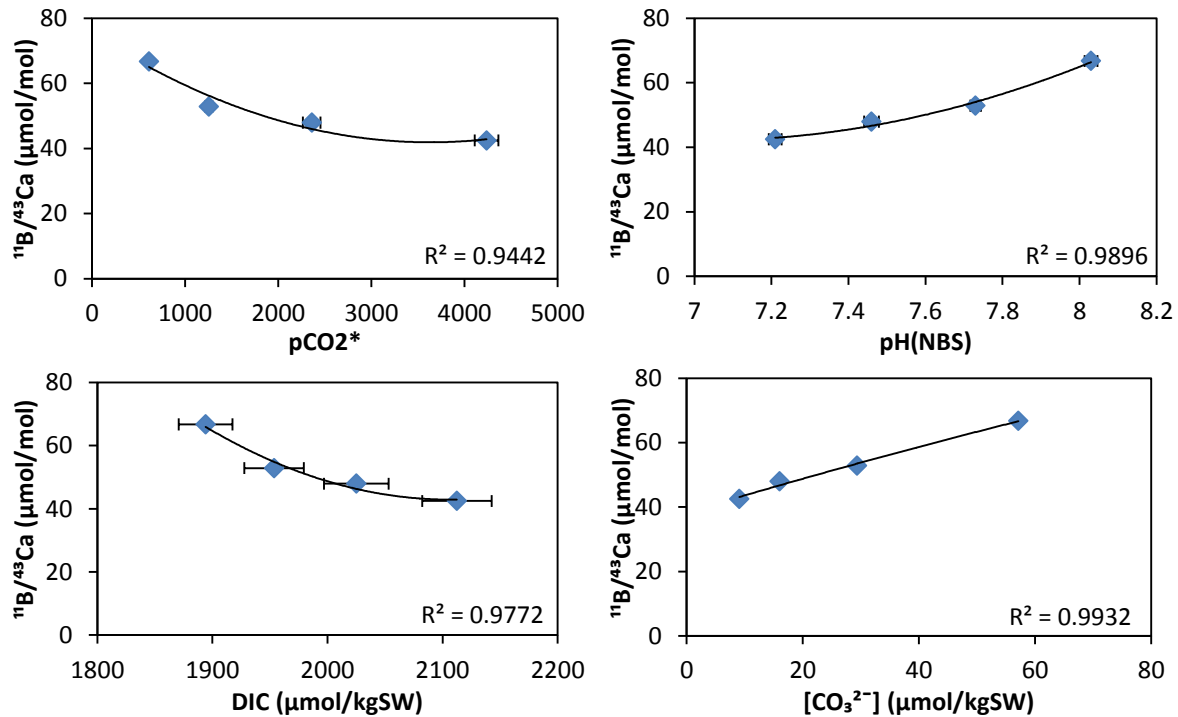


Figure 52 – B/Ca ratios as a function of pCO_2 , pH_{NBS} , DIC (C_T) and $[\text{CO}_3^{2-}]$. Vertical (n: 3) and horizontal (n: 53) error bars are given as the 95 % confidence interval except for $[\text{CO}_3^{2-}]$, which was not available.

Appendix 3: graphs for Me/Ca versus parameters of the carbonate system

Appendix 4: experimental conditions of salinity, temperature and pH over 1 year

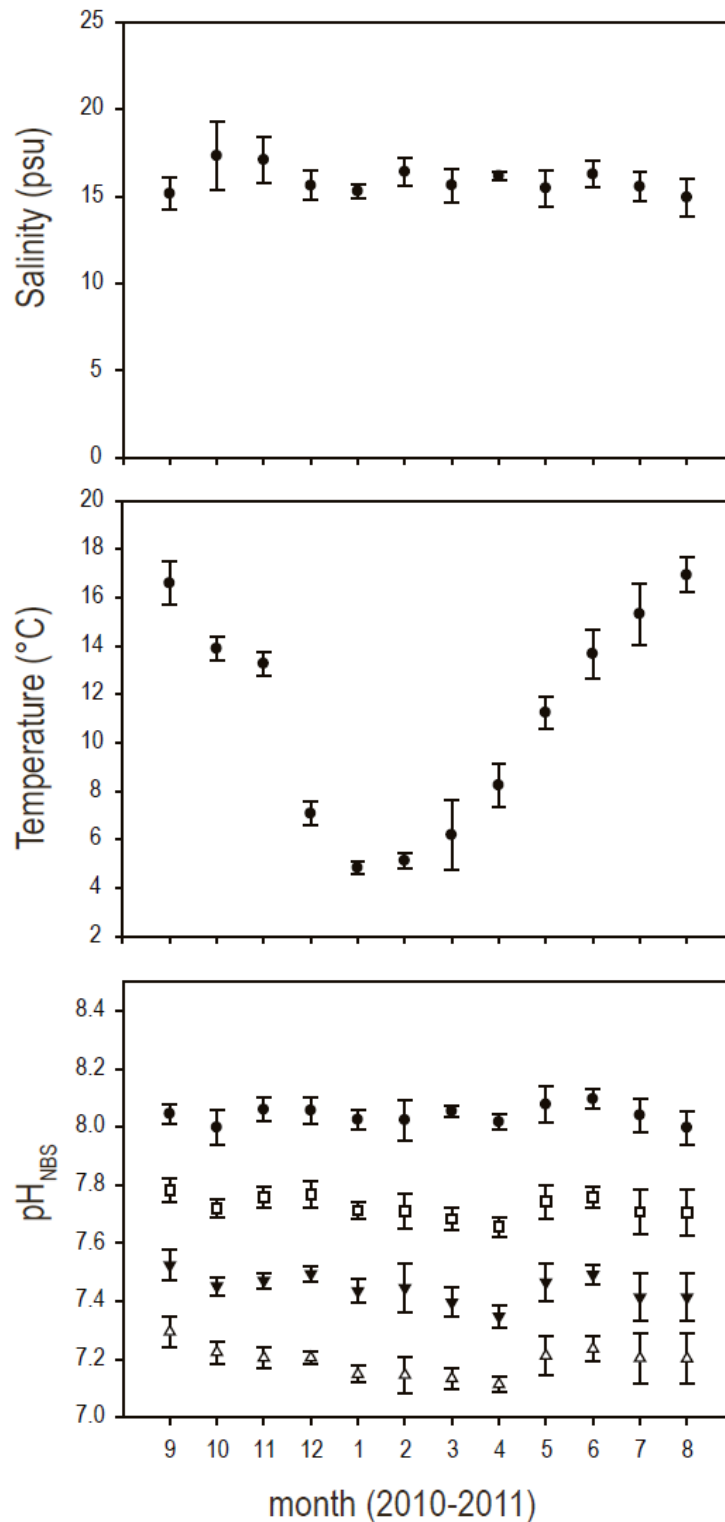


Figure 53 – variations of salinity, temperature and pH over the 1 year culturing experiment. Graphs were provided by Prof. Dr. F. Melzner